2023

Investigating the use of Ionic Liquids as a novel magnetic lubricant

Tim Evans
UCL
EngD in Molecular Modelling and Materials Science

Declaration

I, Tim Evans confirm that the work presented in my thesis is my own. Where information has been derived from other sources, I confirm that this has been indicated in the thesis

Abstract

The main body of this work explores ionic liquids (ILs) to be used as a magnetic lubricant and sealant in a vacuum pump. The problem has arisen due to upcoming legislation governed by the Stockholm Convention with respect to persistent organic pollutants; where the current lubricant falls into this category due to it's fluorinated composition and it's inability to decompose naturally. Other factors include the current lubricant's high viscosity and difficulty in removing and cleaning the parts of the pump where the lubricant has come into contact. Further to this, due to a gap in the current market it was hypothesized that a magnetic lubricant could enhance performance by using a magnetic field to hold the lubricant in the relevant parts of the pump, enabling less lubricant to be used, whilst also being used to create a seal and in turn enhance performance of the vacuum pump. In addition to this, a contribution to the IL modelling field with respect to XPS is completed, where novel dicationic ILs are modelled with respect to the C1s region using models derived and developed from existing methods.

12 core samples based on ionic liquids with paramagnetic anions derived from Fe^{3+} and Dy^{3+} and imidazolium or pyridinium-based cations are explored as lubricants. Key tests were performed to begin collecting data to allow for informed decisions on what samples may be more suitable for purpose. Viscosity measurements were performed using a Brookfield DV-III digital rheometer equipped with a small sample adapter at room temperature initially, followed by ramped measurements up to 80 °C and then followed by viscosity index (VI) calculations. VI calculations require a known density of the sample, this was completed by weighing 1 mL of the sample at room temperature, this was a fixed density where it is known density will decrease with a temperature increase. Thermal stability was measured using thermogravimetric analysis on a ramped rate moving from room temperature up to 450 °C at a rate of 10 °C per minute. Contact angles were measured on three different substrates namely steel aluminium and a fluoroelastomer comprised of hexafluoropropylene and vinylidene fluoride. The method used a Krüss DSA 25E contact angle goniometer with a standard automated syringe dosing unit, applying the touch on method where an average timed dynamic measurement was recorded.

Paramagnetism was measured using an Evans balance and friction behaviour. Specifically, the coefficient of friction was measured using a Bruker UMT Tribolab. This test made used of a ball of specified material applied at a specified force onto a steel plate which reciprocated at a specified Hz with a small amount of sample applied between the surfaces. Further to this, a surface profilometer was employed to analyse the wear scar left on the steel plate after the test had been completed using a Bruker DektakXT stylus profilometer. Friction behaviour also entails analysis of the sample after being subjected to friction testing to determine any chemical composition changes utilising X-Ray Photoelectron Spectroscopy (XPS) and infrared (IR) spectroscopy.

At this point, trends relating chemical composition to physical properties have began to be deduced; whereby in it's simplest form extending the alkyl chain component of the cation within the ionic liquid generally results in an increase in viscosity as well as a decrease in density. With regards to VI, increasing the alkyl chain length results in a decrease in VI. The same effect of alkyl chain length on contact angle can be seen whereby a longer alkyl component results in a decrease in contact angle for all surfaces investigated. The 12 core samples all displayed a paramagnetic response to the Evans balance with the Dysprosium samples showing a higher magnetic moment than the Iron-based samples, an expected result.

Work involving coefficient of friction experiments also found that the core samples gave lower COF values than the control lubricants, but XPS discovered the short chain ionic liquid samples were potentially less stable than their longer chain counterparts when compared to their original state based on changes to their spectra for before and after COF studies, IR spectroscopy also deduced subtle changes in composition.

The work finishes with one sample being scaled up, based on performances in previous tests and tested in a live pump with mixed results. Despite performing well as a lubricant relative to two control lubricants, compatibility issues arise resulting in problematic changes in chemical and physical composition of the scaled-up sample.

The remainder of the work covered troubleshooting the scaled-up sample by utilising the same previous analytical tools such as XPS and IR but also covered Mass Spectrometry (MS). This was used to determine potential impurities present in the used sample and inform on potential degradation pathways. This troubleshooting phase concluded that residual Fomblin (the control lubricant used previously) was causing contamination when analysing with XPS, further to this MS found peaks relating to a brand of antioxidants, known as Irganox which is likely to be from its use as an additive in Fomblin.

Furthermore, an unexpected result in this work was the magnetic properties of the samples were deemed not strong enough to fulfil their original objective; this resulted in further work being completed to remedy the issue.

Initially, inspired by ferrofluids it was hypothesised that perhaps an ionic liquid could be used as the carrier solvent for magnetic nanoparticles as an option to boost magnetism based on magnetite, Fe_3O_4 following a co-precipitation method. Confirmation of nanoparticle synthesis was completed using XRD with peaks matching a reference sample taken from ICSD. However, difficulties were experienced with relation to nanoparticle stability within the ionic liquid. Surfactants were briefly explored based on oleic acid and decyl, methyl-imidazolium bromide with no positive results. Novel in-situ methods using an ionic liquid as reaction media for the preparation of magnetite were explored with preliminary dynamic light scattering (DLS) measurements suggesting differences in size of nanoparticle relating to ionic liquid being used as the medium.

Further novelty was beginning to be explored with respect to a new type of poly(Ionic Liquid) based on a dysprosium anion. There were difficulties in characterizing the new material which leaves room for future work, however again the paramagnetic response despite being larger than the core samples explored was still not deemed strong enough for manipulation with a typical magnet.

In summary, this work has demonstrated that ionic liquids can be used as a lubricant in a vacuum pump, purely as a lubricant as opposed to a lubricant and sealant which was the aim of this project. The scaled up sample performed well

on performance of the pump however clearly it had degraded over the 2000 hours that it had run for. The inability to be manipulated with a standard magnet raised issues quickly with respect to utilising as a sealant within the pump. However, these issues enabled further work to be explored including nanoparticles and polymers and despite only being in the preliminary stages offers optimism that both objectives could perhaps be achieved.

This work offers further insight into how ionic liquids may perform in large scale experiments as opposed to bench top experiments in the laboratory. It has been seen that COF measurements may not give the full picture of how ionic liquids perform as lubricants as demonstrated by the unanticipated degradation when in the live test pump. But with respect to the test pump, this is a great contribution to the field where it is believed this type of experiment has not been reported in the literature to date.

Impact Statement

The work outlined in this thesis offers opportunities for further study within both academia and industry. The work has demonstrated new modelling methods for ionic liquids within XPS which could provide inspiration for further work on even more complicated ionic liquids. Further to this, towards the end of this work magnetic poly(ionic liquids) have been explored where, as stated, there is still a lot more work to be completed on this to characterise and develop into a key factor in a subject relating to ionic liquids; with a high likelihood of academic outputs be it publications, posters or presentations.

This project is sponsored by both the EPSRC and Edwards Vacuum, where the latter is an industry leader in vacuum pumps. Their aim was to produce a new lubricant to act as both a lubricant and sealant. Although the magnetic properties were not sufficient enough to allow the substance to be able to be used as a sealant; it has been demonstrated that the core samples in this work can be used as a lubricant. Using ionic liquids as lubricants is not a new discovery with the literature going back to 2001 for one of the first papers on the topic, but what differentiates this work is that an ionic liquid has been used as a lubricant in a real test pump. What is meant by real test pump is that papers reporting on ionic liquids as lubricants generally report values for the coefficient of friction taken from lab equipment but aren't applied to real environments. This work acts as a platform to demonstrate their applicability, and with this knowledge offers hope for lubricants throughout industry. For example, the motor industry is aiming to phaseout petrol and diesel vehicles and replace them with hybrids or fully electric vehicles. This irradicates the need for petrol and diesel but the engines operating inside the vehicle will still need to be lubricated to produce an efficient performance, therefore there is no reason why perhaps an ionic liquid cannot be used as a lubricant in this industry and replace the non-renewable lubricants also for an even greener environment.

UCL Research Paper Declaration Form

1. **For a research manuscript that has already been published** (if not yet published, please skip to section 2)

   a) **What is the title of the manuscript?**

   An X-ray photoelectron spectroscopy study of ionic liquids based on a bridged dicationic moiety

   b) **Please include a link to or doi for the work**

   https://doi.org/10.1177/17475198221092966

   c) **Where was the work published?**

   Journal of Chemical research

   d) **Who published the work?** (e.g. OUP)

   SAGE

   e) **When was the work published?**

   19/04/2022

   f) **List the manuscript's authors in the order they appear on the publication**

   Anham Zafar, Tim Evans, Robert G Palgrave and Imtiaz- ud-Din

   g) **Was the work peer reviewed?**

   Yes

   h) **Have you retained the copyright?**

   Open Access journal

   i) **Was an earlier form of the manuscript uploaded to a preprint server?** (e.g. medRxiv). If 'Yes', please give a link or doi)

   Yes

   https://discovery.ucl.ac.uk/id/eprint/10148186/

If ‘No’, please seek permission from the relevant publisher and check the box next to the below statement:

☐

*I acknowledge permission of the publisher named under **1d** to include in this thesis portions of the publication named as included in **1c**.*

2. **For a research manuscript prepared for publication but that has not yet been published** (if already published, please skip to section 3)

a) **What is the current title of the manuscript?**

Click or tap here to enter text.

b) **Has the manuscript been uploaded to a preprint server?** (e.g. medRxiv; if ‘Yes’, please give a link or doi)

Click or tap here to enter text.

c) **Where is the work intended to be published?** (e.g. journal names)

Click or tap here to enter text.

d) **List the manuscript’s authors in the intended authorship order**

Click or tap here to enter text.

e) **Stage of publication** (e.g. in submission)

Click or tap here to enter text.

3. **For multi-authored work, please give a statement of contribution covering all authors** (if single-author, please skip to section 4)

Experimental work carried out by Tim Evans and Anham Zafar, text in publication completed by Tim Evans and Anham Zafar

4. **In which chapter(s) of your thesis can this material be found?**

An XPS Study of Ionic Liquids based on a bridged dicationic moiety

5. **e-Signatures confirming that the information above is accurate** (this form should be co-signed by the supervisor/ senior author unless this is not appropriate, e.g. if the paper was a single-author work)

Tim Evans

T. Evans

Date:

27/01/2023

Supervisor/ Senior Author (where appropriate)

Robert Palgrave

R. Palgrave

Date

27/01/2023

Acknowledgments

Throughout my time studying for this body of work I have become great friends with many people throughout the chemistry department and further afield. Firstly Professor Robert Palgrave my main supervisor who has offered invaluable help and guidance throughout my time here, as well as everyone who has been a part or continues to be a part of the Palgrave research group.

Dr Paul Hellier, my secondary supervisor has also made this project possible through help and guidance in areas of engineering I am not so familiar with. Further to this, the work would not have been possible without my industry partners Edwards Vacuum and their staff Neil Turner, Mark Tomkins, Malcolm Gray, Paul Smith and Peter Lamb.

Without the risk of missing people out, I would like to thank everyone who has taken the time to have a drink with me during my time here, both alcoholic and non-alcoholic. I would also like to thank all the staff at UCL who keep the day-to-day operations running smoothly to make my life easier.

Contents

List of Figures

List of Schemes

List of Tables

Chapter 1

1.1 Background and setting of the scene

The aim of this body of work is to document the preparation and testing involved to formulate a new type of lubricant to be used in a vacuum pump.

Lubricants have been used throughout history, dating as far back as the 17th Century during ancient Egyptian times where olive oil was used as a lubricant to move large stones, it was then documented that they also used animal fats known as tallow to lubricate the axles of chariots.[1] The next milestone was in the 19th Century where the first oil well was successfully drilled in Pennsylvania 1859 leading to the dawn of the petroleum age, up until this point all lubricants were made primarily from vegetables or animal fats.

As well as lubricants, lubricant additives started to be added to general lubricants to improve properties such as oxidation inhibition, resisting corrosion as well as improving viscosity indexes and pour points. This began around the 1930s and 40s where the railway industry pumped money into the area in an effort to avoid engine failures.

Another milestone came in the 1950s where the first synthetic lubricants are developed, primarily for the use of aviation and aerospace industries, the first large scale commercially available synthetic oil came in 1972 known as AMSOIL Synthetic Motor Oil and was subjected to numerous tests to meet the industry performance standards of the time as set out by the American Petroleum Institute (API) as well as the Society of Automotive Engineers (SAE).[2]

Though before the commercialization, now well-known chemists by the names of Charles Friedel and his collaborator James Mason Crafts produced the first synthetic hydrocarbon oils in 1877. Years later in 1913, another chemist Friedrich Bergius developed a hydrogenation process for producing synthetic oil from coal dust and then again 12 years later Franz Fisher and Hanz Topsch developed a process for converting a mixture of carbon monoxide and hydrogen into liquid hydrocarbons.

A lubricant can be defined as a substance used to help reduce friction between surfaces in mutual contact, which in turn reduces the heat generated when the surfaces move. As well as this, the lubricant may also function as removing foreign particles, transmitting forces or cooling the surfaces.

The study of lubrication comes under the field of tribology, derived from Greek. It is the science and engineering of interacting surfaces in relative motion which covers friction, wear and lubrication. The term tribology was made widespread by Peter Jost in 1966 who included the term in his highly informative piece of work known as the 'Jost Report' which highlighted the cost of friction, wear and corrosion to the UK economy.[3]

As set out in the beginning, the aim of this project is to formulate a new type of lubricant to be used as both a lubricant and a sealant in a vacuum pump. Where a sealant can also be defined as a substance used to block a passage, for example a passage of fluid or gas through a surface, joint or opening in a material.

In order to make progress on this project foundations must be built i.e. the background on the current lubricant should first be understood. Previously, one type of lubricant would have been used for many different applications; though as the field has developed so has the complexity of the lubricant. The common types of lubricant derived from crude oil can be further categorized into 5 groups depending on their properties. As well as lubricants derived from synthetic oils, there are solid lubricants also known as dry lubricants, aqueous lubricants and finally biolubricants.

The current lubricant being used in the vacuum pump is a type of perfluoropolyether (PFPE), which is a type of synthetic oil where the believed structure can be seen in figure 1, as the actual structure is a trade secret.

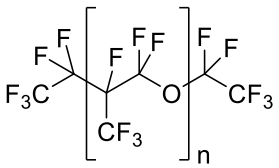

Figure 1 Hypothesized structure of the current PFPE type lubricant

This lubricant is highly functional with the manufacturer claiming properties such as: unmatched chemical and solvent resistance, good viscosity index, excellent thermal/electrical resistance, non-reactive with metal, plastic or rubber and a wide operating temperature range without the use of volatile organic chemicals.[4] These properties set the bar high for a suitable replacement though conversely there are a number of problems associated with the lubricant, the main being that the lubricant is derived from crude oil which we know is a non-renewable resource. Delving further, the viscosity of the lubricant is high and makes maintenance and cleaning of the equipment very difficult and finally, the equipment that the lubricant works on has improved vastly over time where no progress has been made on the lubricant where now staff members at Edwards Vacuum believe there must be a more suitable replacement to get better functionality.

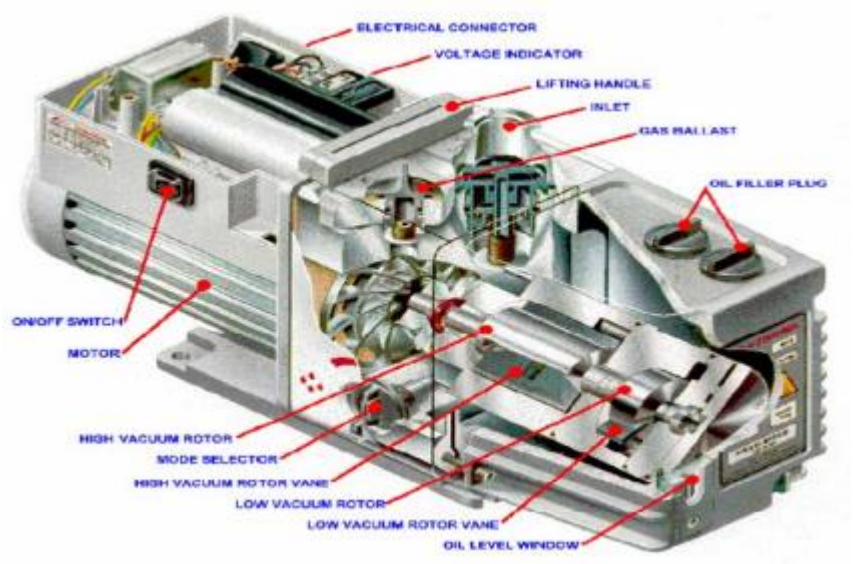

Figure 2 Schematic of the type of pump worked on in this project

In figure 2, an example rotary vane pump can be seen, this is the type of pump worked on in this project. It works by positive-displacement whereby vanes are mounted to a rotor which are driven by a motor and rotate inside a cavity. The lubricant will be present inside the motor, so that whilst the vanes are rotating there will also be lubricant present that creates a better seal between the vane and the cavity wall and effectively reduces pressure.

In order to plan for the project, the following performance criteria was derived and should be met by the new lubricant:

The lubricant must be chemically inert, especially to halogens, ozone, ammonia and hydrogen chloride

- The lubricant must not be impaired through the mechanical actions of bearings and gears
- All properties (viscosity, vapour pressure, specific heat capacity, thermal conductivity) should be maintained within 10% of their original values
- Thermal stability should be maintained at a value exceeding standard operating conditions of the vacuum pump
- Viscosity of the lubricant should not exceed 250 cSt
- Vapour pressure should be less than 0.001 pascals (Pa) at all temperatures up to 120 °C
- The lubricant should be sufficiently magnetic so that it can be induced to stay in place in a small gap between a rotating shaft and a concentric stator bore

The answer to this performance criteria is to use something known as an Ionic Liquid (IL).

An IL is a salt made up purely of positively and negatively charged ions where the ions themselves are often large, which as a result makes them poorly coordinating to make a low melting point liquid. Sometimes they are referred to as Room Temperature Ionic Liquids (RTILs) where, as the title suggests, means that they are a liquid at room temperature. Delving further they can also be categorized even more broadly to say that an IL is something that has a melting point below 100 °C. For the purpose of this body of work, the definition is going to be something that is a liquid at room temperature.

One term that is repeatedly used to describe ILs is ‘designer solvents’ not because they are a highly priced commodity but due to their facile ability to be manipulated using different anions and cations.[5] Being able to change the anion/cation combinations results in ILs with different properties and allows for tailoring of the IL to specific requirements. A review of IL literature will follow later in this body of work, competing solutions will now be briefly explored.

As the current lubricant is derived from crude oil, the most obvious starting point for a replacement lubricant could come in the form of a biolubricant. Biolubricants are usually made from plants such as palm or soybean, but can also be made from synthetic esters and petroleum oils that satisfy established biodegradability and toxicity criteria.[6] They possess many advantages over traditional crude oil based lubricants such as high lubricity, a high viscosity index (meaning minimal changes in viscosity as temperature is increased), high flash point and low evaporative losses. Though on the other hand, biolubricants in their natural form have low oxidative stabilities meaning it is likely they will oxidize whilst in use, or even polymerize, as well as other physical issues such as an unpleasant smell and potential for poor compatibility with paints or sealants within the equipment.

Another competing solution could be the use of additives. Lubricant additives are organic or inorganic compounds dissolved or suspended as solids in oil. They typically range between 0.1-30% of the oil volume depending on the machine.[7] There are 3 basic roles that they employ which are to enhance existing base oil properties, suppress undesirable base oil properties or to impart new properties on base oils. These properties could be viscosity improvers, anti-wear/extreme pressure additives or even corrosion inhibitors. Though ultimately, these additives are all added to a base oil which would mean tweaking rather than fully replacing the current lubricant which is where the problem lies; though to delve further, perhaps additives could be employed in the research process.

The use of an IL as a lubricant is better than the other two competing solutions because the lubricant itself can be prepared from more accessible starting materials or rather, materials that satisfy toxicity and environmental degradation legislation which is important from a commercial and ethical point of view when clients are looking for an alternative lubricant that is not going to harm the environment. As stated previously ILs allow their properties to be fine-tuned through the careful manipulation of different anions and cations, perhaps acting as inherent additives. To re-iterate, the aim of this project is to prepare a novel magnetic lubricant based on an IL which possesses the same or better properties than the standard (control) lubricant.

But why is magnetism important? The theory behind this is that a magnetic lubricant can be manipulated around the necessary parts of the machinery, or the machinery could be magnetized allowing the IL to be attracted to the necessary area and therefore allow less of the lubricant to be used resulting in a more cost and waste effective lubricant. Furthermore, as also set out in the beginning of this thesis is that the lubricant is also to act as a sealant. A magnetic lubricant could also be used as a sealant by being held in place with a magnet. Magnetic ILs are not the only way to achieve a magnetic lubricant, there are also other competing solutions known as ferrofluids (FFs) and magnetorheological fluids (MRFs).

A ferrofluid is a colloidal liquid that is made up of nanoscale ferromagnetic particles that are suspended in a carrier fluid i.e. nanoparticles dissolved in a solvent. This is different from an IL which was defined in the beginning of this thesis as being solely positively and negatively charged ions that *result* in a liquid. An FF is similar to an MRF though the difference is that in the MRF the size of the particles are larger, on the micrometer scale rather than nanoscale. Furthermore, another subtle difference is that FFs are often coated with a surfactant to inhibit aggregation and are generally suspended by Brownian motion, whereas in an MRF the particles are too heavy for Brownian motion to allow them to remain suspended.

Advantages of an IL over FFs and MRFs are that the ILs can be optically transparent with high colour purity, as well as the inherent properties of ILs in general; the key factor in ILs being their wide liquid range. FFs and MRFs require a carrier solvent which is likely to be volatile and therefore not be able to withstand the demanding working conditions of an operating vacuum pump.

The aims of this project can then be condensed to the following key points:

- Synthesize a range of novel magnetic ionic liquids
- Assess suitability through physical and chemical testing
- Tweak properties of the ionic liquid until optimum performance has been achieved

1.2 Ionic Liquids in the literature

1.2.1 Background and Origins of Ionic Liquids

As stated previously, an IL is made up solely of positively and negatively charged ions that result in a liquid. Though initially, they were known as low melting point salts; but before even that, work by Friedel and Crafts which was published in a French scientific journal in 1877 found that when a small amount of anhydrous aluminium chloride was added to amyl chloride a liquid was obtained.[8] Though it wasn't until some chemists in Japan built on this work to find that the oil previously synthesized consisted of an alkylated aromatic ring cation and a chloroaluminate anion, therefore demonstrating that it was in fact an ionic liquid.[9]

Though 1888 can be argued as the key year for the development of ILs and their history. In this year, Gabriel reported the discovery of a protic ionic liquid, ethanol-ammonium nitrate which had a melting point between 52 and 55 °C, possibly the first example of an organic salt which had a melting point below 100 °C.[10] However, another date is often cited as being the most important in IL history; that being 1914 with work by Paul Walden where in the paper the physical properties of ethylammonium nitrate were discussed, which has a melting point of 14 °C.[11]

The field of ILs did not appear to gain traction until the 1980s with work by Nanjundiah *et al* or Wilkes *et al* who studied the electrochemical properties between $AlCl_3$ and *N*-butylpyridinium chloride and the study of dialkylimidazolium chloroaluminate 'melts' respectively.[12, 13] With a further breakthrough in 1992, where Wilkes *et al* prepared air and water stable imidazolium based ILs which paved the way for which could be now categorized as 'industry standard' ILs.[14]

The chemistry of the IL is made up of a positively charged cation and a negatively charged anion, where typically the cation is an organic structure based on imidazolium, pyridinium, or quaternary ammonium or phosphonium; whereas the anion is usually an inorganic moiety such as tetrafluoroborate, hexafluorophosphate or bis(trifluoromethane)sulfonamide. Generic structures of cations and anions can be seen below in figure 2.

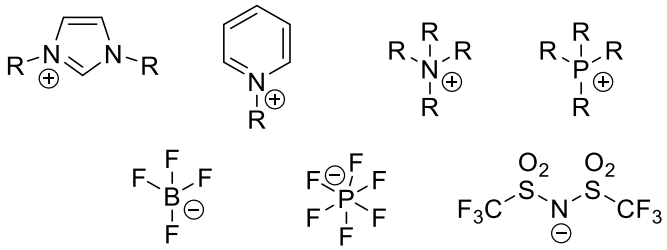

Figure 3 Common generic cations and anions of ionic liquids

In figure 3, the R represents a generic alkyl chain, with one of the most common ILs being an imidazolium cation with a methyl and butyl group bonded to each of the nitrogen atoms; combined with, for example, tetrafluoroborate. This can be seen below in figure 3.

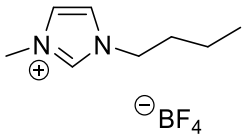

Figure 4 1-Butyl, 3-Methyl Imidazolium Tetrafluoroborate, one of the most common ILs

The nomenclature of this IL, a de facto industry standard, has many different shorthand abbreviations for the cation. Long hand would be 1-Butyl-3-Methyl Imidazolium, though shorthand there is a numbering system which would convert to C_4C_1Im with the numbers representing the length of the alkyl chain, or lettering which would be BMIm with the B standing for butyl and M for methyl. Both methods have flaws, for example no mention of functional groups which may or may not be present, but for the purpose of this report the numbering system will be used as it is perhaps more intuitive.

As stated towards the beginning of this report, ILs possess the title of ‘designer solvents’. This is most easily demonstrated through two examples. With the same cation, say C_4C_1Im, one could choose any known anion to pair this with though if tetrafluoroborate was used the resulting IL would be hydrophilic; though if hexafluorophosphate was used the resulting IL would be hydrophobic. The next section will describe the evolution of synthetic methods from the literature, and how different cations and anions are prepared.

Figure 5 A hydrophilic IL containing BF_4 and hydrophobic IL containing PF_6

1.2.2 Synthetic Methods

As stated in the previous section, the date widely regarded as the beginning of IL synthesis was in 1914 when Paul Walden prepared ethylammonium nitrate. This was achieved through the neutralization of ethylamine with concentrated nitric acid to reach the IL. The method can be seen below in scheme 1.

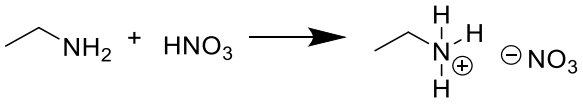

Scheme 1 Paul Walden's preparation of ethylammonium nitrate

The field was largely quiet after that until in 1975 where there was another paper published; this time by Chum *et al* who assessed the electrochemical properties of a mixture of aluminium chloride and ethylpyridinium bromide, which would be regarded as an IL. Though in this paper there is no mention on how the 'room temperature molten salt' was achieved.[15]

Slightly further on in the IL synthesis timeline, again as mentioned previously, was the work by Nanjundiah *et al* and Wilkes *et al*. The Nanjundiah group in 1982 studied electrochemical properties of iron in an aluminium chloride-butylpyridinium chloride ionic liquid. There is no detailed description on how the ionic liquid was prepared other than that 'a mixture of aluminium chloride and n-butylpyridinium chloride mixtures of compositional variation ranging from 2:1 to 0.75:1 (mol ratio of $AlCl_3$:BuPyCl) exist as liquids at essentially ambient temperatures'.

The paper published by the Wilkes group in 1982 detailed how the IL was prepared. The IL was based around dialkylimidazolium chloroaluminate melts; here the stereotypical structure of an IL is beginning to take shape with an organic cation and inorganic anion. The reaction scheme can be seen below in scheme 2. A glovebox was used for the synthesis under a dry argon

atmosphere as the research group believed that the aluminium chloride based ‘melts’ would be just as moisture sensitive as aluminium chloride.

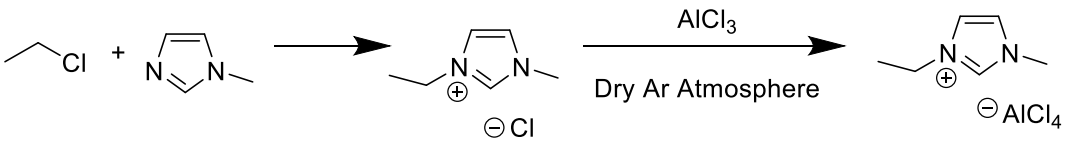

Scheme 2 Wilkes' Group preparation of dialkylimidazolium chloroaluminate melts

The Wilkes group then published a further paper in 1992 which resulted in air and water stable imidazolium based ILs. This paper featured the now common tetrafluoroborate anion coupled with a 1-ethyl-3-methyl imidazolium cation which was recorded as having a melting point of 15 °C. Other ILs in the paper included variations on the anion such as nitrite and nitrate. The ILs reported in the paper were synthesized on the bench top with no special precautions taken such as a glovebox, where a metathesis reaction of the halide salt with the appropriate silver salt was completed in methanol. An example reaction scheme from the paper can be seen below in scheme 3.

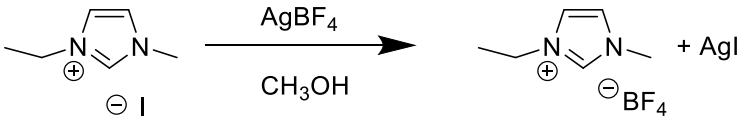

Scheme 3 One of the first preparations of air and water stable imidazolium based ILs

This paper paved the way in terms of IL synthesis, where the method can be rationally broken down into 2 steps. First there is a Menshutkin step which is a conversion of a tertiary amine into a quaternary ammonium salt by reacting with an alkyl halide. Named after Nikolai Menshutkin who described the procedure in 1890, though the step is not limited to nitrogen it also applies to phosphonium or sulphonium nucleophiles also. The second step in the process is known as the Finkelstein reaction, named after Hans Finkelstein who discovered the reaction in 1910 which is a nucleophilic substitution reaction involving the exchange of one halide anion for another. More often than not referred to as the anion exchange step. In terms of IL synthesis, this applied to replacing the halide anion from the salt formed in the first step with another such as PF_6 which results in another halide salt being expelled. The two steps can be seen below in scheme 4.

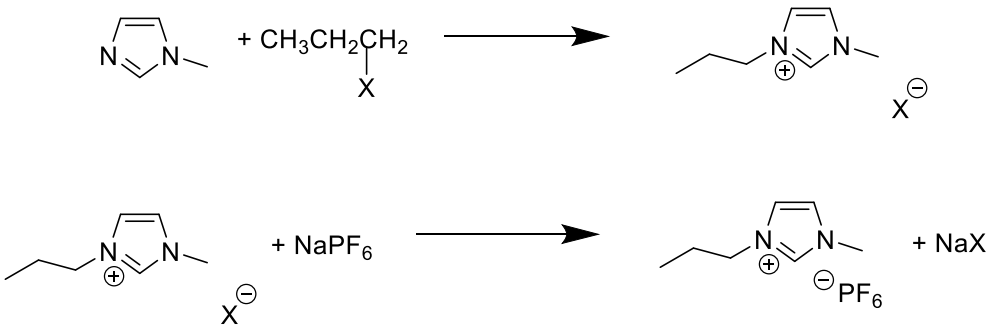

Scheme 4 An accepted method for the preparation of common ILs

However, as straightforward as the general synthesis appears there are a number of problems that are associated with the process. The key points to note include residual halide contamination, long reaction times and usually a large excess of the alkyl halide and/or the organic solvent used as a reaction medium.

Residual halide contamination occurs because the first step in the synthesis process usually uses an alkyl halide as the alkylating agent in the quaternisation process. Despite good yields there is often halide contamination left over. In a paper by Plechkova *et al*, the influence of halide contamination was investigated and reported that contamination could radically alter the physical properties of the IL in question.[16] This paper than suggested that perhaps a reaction pathway should be found that did not make use of haloalkanes; this pathway was then discovered by de Souza *et al* in 2002 who reported the direct synthesis of 1,3-disubstituted imidazolium tetrafluoroborate ILs using a one pot procedure which can be seen below in scheme 5.[17]

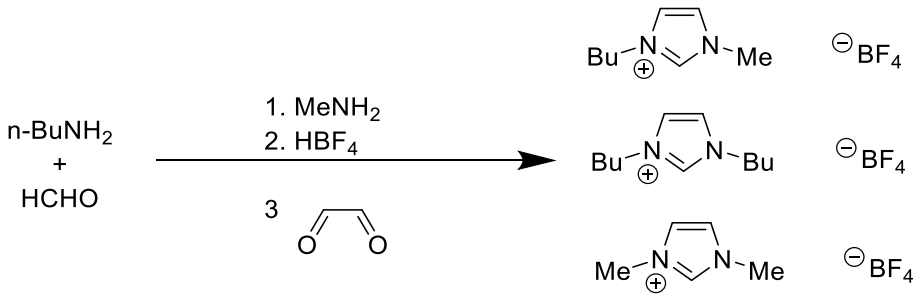

Scheme 5 One pot synthesis of imidazolium based ILs, following a halogen-free based method

For the halide-free synthetic method described in scheme 5, another drawback of the process is still that the reaction time is long at 12 hours. One of the first chemists within the IL field to have a go at addressing this issue was Varma and Namboodiri back in 2001.[18] In this paper they described a solvent free synthesis of imidazolium-based halide salts which are liquid at room temperature using a microwave. This eliminates the relatively high energy requirements and time duration to achieve an acceptable yield. The time duration is on the scale of seconds with the longest reaction time being 90 seconds, they also compare their yields with typical yields using traditional methods where generally their yields for the microwave synthesis are the same or higher. Though they are only completing the first step of the reaction, alkylating an imidazolium-based cation with various chloro, bromo and iodo-alkanes.

One drawback on this one pot procedure is that it produces a mix of three products which are difficult to separate; furthermore the yield is quite low at 66%. Other methods of halide free syntheses can be categorized into three distinct groups depending on the method: synthesis via *N*-heterocyclic carbenes, phosphorus-based reactions with imidazoles and sulphur-based reactions with imidazoles.[19]

1.2.3 Magnetic Ionic Liquids

Magnetism can be broken down into three main types; there is paramagnetism which is a material that becomes magnetized in a magnetic field but disappears when the field is removed. There is ferromagnetism which refers to materials that retain their magnetic properties even when the magnetic field has been removed as well as antiferromagnetism which has spins aligned in a regular pattern with neighbouring spins pointing in opposite directions but above the Néel temperature becomes paramagnetic. Further to this there is also ferrimagnetism which is similar to antiferromagnetism whereby there are distributions of opposing magnetic moments but ferrimagnetism is generally seen on an unequal magnitude resulting in spontaneous magnetization. Finally, there is diamagnetism which refers to a material that is weakly repelled by a magnetic field. Paramagnetism is what this work is interested in. Paramagnetism occurs in an IL through careful manipulation of the anion. This was first achieved by Hayashi *et al* in 2004 who synthesized an IL with an

$[FeCl_4]^-$ anion.[20] Further work was then completed in 2006 where factors influencing the magnetic response were investigated.[21] Paramagnetism in the IL occurs from the 5 unpaired d-electrons in the transition metal based anion. The unpaired electrons are attracted by a magnetic field due to the electrons' magnetic dipole moment, magnetism in the 2004 paper was confirmed using the super conducting quantum interference device (SQUID) method which is a very sensitive magnetometer used to measure subtle magnetic fields. The paper goes on to say that the lLs display 'a beautiful response to the magnetic field'.

Additionally, in 2008 Del Sesto *et al* reported on a series of ILs containing different anions which all showed paramagnetic behaviour. The anions investigated were based on Fe^{3+}, Co^{2+}, Mn^{2+} and Gd^{3+} as well as phosphonium based cations and the 'traditional' imidazolium.[22]

Additionally, lanthanides can also be utilized to demonstrate a paramagnetic response, using a dysprosium-based anion in its +3 oxidation state. This corresponds to 5 unpaired f-electrons and demonstrates a higher magnetic moment value in the region of around 10 Bohr magnetons compared with around 5 Bohr magnetons for an iron-based anion with the same number of unpaired electrons. The reason for the higher magnetic moment is because the orbital angular momentum for the f orbitals contributes much more to the magnetism compared to d orbitals meaning it is not just the number of unpaired electrons but also the total number of electrons in the f orbital altogether. As it turns out, there are 5 unpaired f electrons but also 4 paired electrons meaning that it is not only the spin that contributes to the paramagnetism but also the angular momentum.

The first paper to report on dysprosium based ILs was by Malick *et al* who synthesized ILs based on a dysprosium thiocyanate and are described as '(super)paramagnetic liquids at room temperature'.[23] 10 years later, in a report made my Cheng *et al*, fluorescigenic magnetofluids were reported.[24] These were based on gadolinium and terbium as well as dysprosium where they all showed responses to neodymium magnets (neodymium magnets are the strongest type of permanent magnet commercially available), and displayed

temperature-dependent paramagnetic susceptibility with small deviations from the Curie law at low temperatures.

Due to the close to infinite possibilities ILs possess, there are other ways of boosting an IL's magnetic properties, a detailed report on these will follow in subsequent sections but they will be briefly explored now. One option is to introduce nanoparticles into the IL system, these could be dispersed in the IL in a similar vein to a ferrofluid, or they could be introduced to the IL through chemical bonding.

Another option is to look into poly(ionic liquids), or more specifically poly(magnetic ionic liquids). This would entail preparing a monomer incorporating a magnetic anion and subsequently polymerizing the monomer to create a polymer backbone connected with multiple magnetic anions, with a view to all of the magnetic anions working together.

With this brief review on magnetism, it is anticipated the work will initially explore paramagnetic anions based on Fe^{3+} and Dy^{3+} and rely on further methods such as nanoparticles or polymers if the magnetic response is not deemed strong enough. Further to this, particularly for nanoparticles the introduction of these could also have negative effects on other properties of the sample which would have to be rectified.

1.2.4 X-Ray Photoelectron Spectroscopy

X-Ray Photoelectron Spectroscopy (XPS) is a surface analysis technique that involves irradiating the chosen sample in a vacuum with photons and then measuring the kinetic energy of the electrons emitted. This process relies on the photoelectric effect where photons penetrate the surface of the sample and the energy of the photoemitted electrons is analyzed. Only the electrons that originate from within the uppermost few nanometers of the sample can leave the surface without suffering energy losses meaning that the technique is surface sensitive.[25] The process can be described using an equation derived by Einstein which can be seen below.

$$KE = h\nu - BE \quad (1)$$

Where KE = Kinetic Energy

$h\nu$ = energy of the incident photon

BE = Binding Energy

The photon energy is a controlled variable, and the kinetic energy is measured in the XPS spectrometer, from this the binding energy can be derived using the above mentioned equation. For each element there is a characteristic binding energy used to identify it (excluding hydrogen) which shows as a peak in the spectrum. Using this information, changes in oxidation state or chemical environment give rise to small variations in binding energy which then correspond to changes in position of the peak in the spectrum. As well as peak shifts, sizes of the peak can also be used to determine concentration of the given element, relative to other components.

XPS is completed in an ultra-high vacuum environment, where typically it is only solid samples which are analysed. Due to ILs possessing a wide liquid range and negligible volatility this enables them to be analysed without evaporating.

XPS allows for spotting potential tribochemical reactions which may or may not have occurred during lubrication tests due to the inherent surface sensitivity present with the technique. The first paper to utilize this method came in 2002 by Liu, in this paper it was deduced that a boundary film had formed mainly consisting of FeF_2 or FeF_3.[26] This type of deduction would have come from first completing a survey scan which shows peaks at different binding energies, which in itself correspond to elements in different oxidation states. From this, likely decomposition products can be proposed. Furthermore, the survey scan can be completed before any lubrication studies have been completed. This way the prepared IL lubricant samples can be analysed for purity, another use for XPS with ILs. As well as checking for purity, another side of the same coin can be analysed; that being a modelling aspect of ILs.

Modelling with ILs first arose in the literature around 2011 with a paper by Men *et al.*[27] Since then more and more papers have been published applying

different fitting models to various types of IL structures.[28-31] This work can go hand in hand with the study of tribochemical reactions, as it is likely if an IL lubricant starts to, for example, decompose during testing the XP spectra will look different. The carbon 1s region is what has been studied extensively and is highly important with regards to ILs and XPS. If the lubricant has begun to decompose then the original fitting model is likely to no longer fit allowing for facile deductions to be made. When talking about decomposition, or a tribochemical reaction at the surface, these are deduced by a shift in peak position or extra peaks present in the post-lubrication test spectra.

This analysis technique of scanning the worn surface or the IL sample after being subject to lubrication studies has now become a standard procedure in IL tribology, with a vast quantity of papers now available.[32-38] In the work that follows, it is hoped that a significant contribution to this field will be made.

1.2.5 Ionic Liquids as a Lubricant

The widely reported properties of ILs include negligible volatility, wide liquid range, non-volatility with high thermal and chemical stability; as well as high conductivity and wide electrochemical window. It is the former properties that make ILs an ideal candidate as a replacement lubricant.

The first paper to report an IL as a novel lubricant came in 2001 by Ye *et al*.[39] In this paper, a 'novel versatile lubricant' is described. Two ILs are investigated, C_1C_6Im BF_4 and C_2C_6Im BF_4 on a range of friction pairs including steel with itself, with aluminium, with copper and with ceramics to name a few. Their work reports that the two ILs show excellent friction reduction, antiwear performance and high load carrying capacity. To assess lubricity, in this paper they use an Optimol SRV which is a type of oscillating friction and wear tester, and include two control samples being phosphazene and PFPE. Interestingly, the C_2C_6Im BF_4 lubricant performed better, deduced by having a smaller coefficient of friction (COF) value than the two control lubricants over varying loads. With this being the first paper to report on ILs as lubricants, they also go on to hypothesize the reasoning for this significant performance and suggest the ILs adsorb onto the sliding surface and form effective boundary films to reduce friction and wear. This hypothesis is backed up with XPS data displaying the B

1s spectra with peaks relating to B_2O_3 and BN, naturally over time more work has been completed relating to XPS which will follow in this report.

The following year another report on ILs as lubricants was published by the same authors.[26] Here they complete similar testing though also use a CZM vacuum friction tester which allows the workers to analyse the lLs' negligible volatility and wide liquid range whilst also assessing their lubricating properties. The same control lubricants are used where the vacuum friction tests also show that the 2 ILs perform considerably better with COF values half that of the PFPE lubricant. Further work is also carried out with XPS to analyse the wear scars left behind after testing where they build on their previous XPS work and attain that as well as Boron related surface protective films, metal (Fe) fluoride-based species are present possibly due to the degradation of the BF_4 anion in the IL samples and producing anti scratch components.

In a paper published in 2009, this time by Qu *et al*, ammonium-based ILs were investigated as lubricants and compared to both their imidazolium-based counterparts as well as a 'conventional and fully formulated engine oil'.[40] The lubrication performance is discussed where steel paired with various aluminium alloys were investigated. The ammonium-based IL is made up of 3 octyl carbon chains and the imidazolium with a decyl and methyl group, both with an bistrifluoromethane (NTf_2) anion. This was interesting as it is a hydrophobic fluorine containing anion as opposed to the hydrophilic BF_4. The paper reports that generally, the ammonium-based IL outperformed the control group on all of the different friction pairs and temperatures. Yet the imidazolium-based IL performed well on two out of the three alloys. The underperforming alloy was Al 6061, this poor performance was ascribed to tribocorrosion, as opposed to a surface protective tribofilm previously reported. This paper then demonstrated that not only the anion but also the cation influences the lubricating properties of the IL.

In one of the first review papers published with work corresponding to ILs in tribology, general trends have been deduced.[41] It can be seen that, generally, the coefficient of friction decreases as the length of the alkyl chain increases on the cation part of the IL, at this point in the literature thought to be because of

the increase in viscosity and therefore working in the hydrodynamic region where the lubricating surfaces are fully supported by the lubricant. This type of mechanism is also known as the Bowden-Tabor model In which density-packed adsorption of the lubricant molecule on friction surfaces is essential.[42] This phenomena can be seen below in figure 6, taken from the review article.

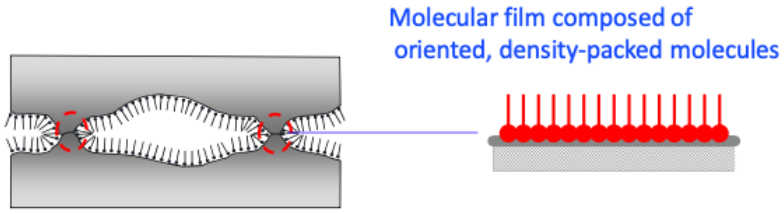

Figure 6 Bowden-Tabor model taken from the review article mentioned in text, demonstrating IL adsorption on the surface

There are various methods of determining coefficients of friction, wear volumes and wear scars. In the literature reported thus far an SRV instrument has been reported. SRV stands for Schwingung (oscillating), Reibung (friction), Verschleiß (wear); the SRV measures the physical interactions between a lubricant and two specimens in a loaded contact. The upper specimen oscillates in a linear path on the lower stationary specimen at a specified frequency, stroke length, load, temperature and test duration. This is very similar to the UMT Tribolab, which stands for Universal Mechanical Tester and is quoted as being a highly versatile tribometer and argued to be the most widely used tribometer on the market. Both of these pieces of equipment can then perform industry standard tests, where two of the key tests are D5707 and D4172. The former is used to determine coefficients of friction and wear that is run for a fixed time at a moderate load whereas the latter is a four-ball wear test method. The purpose of this test is to determine the wear preventive characteristics of the lubricant whereby a steel ball is rotated against three other stationary balls which have been lubricated under a specified load, speed, temperature and time. The premise is that the better the lubricant is, the smaller the wear scar will be on the three stationary balls. In this thesis, due to equipment restraints the reciprocating test was used however a better option would have been to complete a ball on disc test which would better recreate the constant motion of the rotary vane pump as opposed to reciprocation.

In a paper published by Kondo *et al*, the lubricity and corrosiveness of seven commercially available ILs are investigated.[43] The paper investigated piperidinium, imidazolium and phosphonium cations with three fluorine containing anions and three fluorine free anions. Friction and wear tests were completed on an SRV machine with surface analysis completed by SEM-EDX (scanning electron microscopy followed by energy dispersive x-ray analysis) and XPS.

Each IL was subjected to wear testing in both air and a dry nitrogen atmosphere, as well as varying temperatures from 50 to 200 °C. For the halogen containing ILs, good lubricity was displayed, where it is argued because of the formation of an iron fluoride boundary layer on the sliding surface, however corrosion was also observed on the surfaces in contact with the IL. However, under the dry nitrogen atmosphere, the halogen containing ILs showed an increase in lubricity and a reduction in corrosiveness. This was believed to be down to the formation of the iron fluoride boundary layer being unable to hydrolyse the iron halide to the corrosive hydrogen halide.

Furthermore, for the halogen free ILs, they performed poorly in comparison with higher coefficients of friction; yet no remarkable corrosion was observed on the sliding contacts upon post-test analysis.

From this paper, and the literature reported thus far it can be seen that fluorine containing ILs offer better lubricity though at the expense of increased corrosion due to hydrolysis of tribofilms formed during testing. What will now follow is an investigation into halogen-free ILs in relation to tribology.

In a paper published by Minami *et al* in 2012, the tribological properties of halogen free ILs are studied.[44] The paper described the cyano group as a ‘pseudo-halogen’ whereby they behave chemically similar to halogens. Building on this they prepare two cyano based anions, tricyanomethanide and tetracyanoborate as well as tributylborane and an additive tributylmethylphosphonium dimethylphosphate. This then leaves the paper with six halogen-free ILs and one typical NTf_2-based IL for control purposes.

Wear testing was completed at 20 and 50 °C with wear analysis completed with AES (Auger electron microscopy) and XPS. In their conclusions, it is clear that

the halogen free ILs showed inferior tribological performance in comparison to the halogen containing control sample. However, the corrosion caused by the halogen containing control sample was confirmed as a major drawback. As stated in their introduction, the cyanogroups acting as pseudo-halogens did still tribochemically react with the rubbed surfaces to yield boron oxides as confirmed by XPS.

In a progressive paper published in 2014, ILs derived from amino acids (AAILs) were studied as halogen-free lubricants on steel/steel, steel/copper and steel/aluminium.[45] The cations were made up of tetrabutyl ammoniums with varying anions based on Serine, Threonine, Valine, Leucine and Lysine. As well as friction and wear testing, physical properties such as viscosities (including viscosity indexes) and thermogravimetric analysis (TGA) which is used to determine decomposition temperatures. The viscosities of the AAILs are substantially higher with values ranging from 1007.15 – 2991.50 mm^2 s^{-1} at 40 °C, compared with 27.2 and 41.89 for typical imidazolium cations with a BF_4 and NTf_2 anion. The viscosity indexes reported are considerably lower than that of the control ILs also, meaning that the viscosity of the amino acid derived ILs varies greatly with temperature, which is considered a negative attribute due to the likelihood of varying temperatures in real life scenarios.

In relation to TGA, the paper reports the onset decomposition temperature, for which the AAILs all have lower decomposition temperatures also with values ranging from 145.5 - 172.6 °C compared with values above 300 °C for the control ILs.

Hydrolysis stability and corrosiveness was also investigated. To ascertain hydrolysis stability each AAIL was stirred with the same quantity of water at 80 °C for several hours with the pH-value of the solution being checked at regular 30 minute intervals, with the control samples containing halogens used for comparison. The IL containing BF_4 quickly hydrolysed to an acidic solution due to the presence of HF after 30 minutes demonstrating the instability of the IL however the NTf_2 containing IL and all of the AAILs showed no change in pH-value. Corrosiveness was tested using a copper strip, in which each AAIL and control IL had a piece of the copper strip submersed for 72 hours at 100 °C. For

all of the AAILs there was no colour change or signs of corrosion; whereas the two control ILs showed copper strips that had significantly changed indicating severe corrosion.

For friction and wear tests, the NTf_2 containing IL was used as the control as well as a commercial oil known as PAO40. The loads applied during the tests included a 200N load and two 100N loads, each for 30 minutes. For each of the substrate pairs, the AAILs showed a lower COF value and lower wear volumes. As well as this, due to their halogen free character, XPS analysis suggested that the lubrication mechanism was attributed to the formation of a fast physical adsorption film as opposed to the traditional tribochemical reaction to form a film, which is then typically hydrolysed from moisture in the air causing corrosion. The difference here being a physical adsorption film is providing lubrication through physical separation of the two components in the friction test, which would be more beneficial than a tribochemical reaction. This is because in order for a tribochemically reacted film to form requires one or more components to decompose/react. This could be the lubricant decomposing and reacting with the nascent surfaces exposed, this would be detrimental in the long run because slowly the lubricant that you loaded with will become less and less and lubrication of all moving parts will become restricted due to smaller amounts of the lubricant being present.

In a paper previously mentioned in this report by Totolin *et al*, more halogen free ILs are investigated as potential lubricants.[37] However, in this paper hybrid mixtures are investigated, with a phosphonium phosphate IL used as an additive in imidazolium alkylborane based ILs. The phosphonium phosphate IL appeared to enhance both the thermo-oxidative stability when placed in an oven at 100 °C for 1, 3 and 7 days; and the tribological performance. The tribological performance was evaluated on a steel/steel contact followed by chemical analysis of the worn surface by XPS. From this, they state that there is clear evidence of iron phosphide based tribofilms from the phosphonium phosphate IL.

Naturally this paper touches on the effects of additives which have not yet been covered. An exploration of this area will follow further in this report. Bringing it

back to halogen free ILs, in a more recent paper, 2021, Chen *et al* also investigated this topic, this time in relation to TC4 a type of titanium light alloy.[46]

Two phosphonium based ILs were explored, both with the same cation but different anions, one based on sulphonate (DOSS) and the other composed of ammonium dibutyl dithiophosphate (DABD). Their work showed that the DOSS based IL had better tribological performance than the other when investigated for silicon nitride/titanium friction pair, this was achieved again by a beneficial tribochemically formed protective film that formed during the friction test.

Additives have been briefly touched on throughout this report, and a brief exploration of additives in relation to IL based lubricants will now follow.

In a paper by Kamimura *et al,* traditional additives were explored.[33] The additives were based on fatty alcohols and acids, phosphorus and sulphur compounds and organic metal compounds. There were some solubility issues when trying to disperse the additives though they did appear to improve tribological performance when compared to the IL without any additives dispersed.

What is more novel in fact is using an IL itself as an additive, this was first completed by Qu in 2012.[47] In this paper, the reverse was studied, dispersing an IL based additive in traditional hydrocarbon lubricating oils and two commercially available poly alpha olefin (PAO) based engine oils. The additive was a phosphonium phosphate type IL and was complimented for its oil-miscibility and non-corrosiveness, where initial characterization and testing suggested that there was substantial potential for using this additive, especially in the commercially available engine oils.

Similar work has been carried forward with a plethora of papers being published investigating different IL based additives for different hydrocarbon-based oils.[36, 38, 48-50] What could be interesting is a hybrid type lubricant utilizing a promising halogen free based IL, modified further with other IL based additives to achieve a universally applicable lubricant. This would be interesting as it is known that halogens cause corrosion with respect to ionic liquids as lubricants and a recurring theme is, for example, the production of HF from fluorine containing anions. Yet a halogen free IL irradicates this issue but the drawback from

halogen free, especially fluorine-free is that these often offer the best lubricity results. Working to the assumption the new halogen free based IL is offering promising results in ambient conditions for example room temperature experiments under low loads in the laboratory, new IL based additives could be added (under the premise they will be compatible) to further tailor their applications for example extremes of temperature or higher loads. This could contribute favourably to the objectives outlined in this project because the pump here requires the lubricant to operate at high temperatures and pressures.

In a recent study, 2019, the effects of a magnetic IL were investigated on a steel/steel pair at varying temperatures and compared with a more traditional commercially available magnetic fluid.[51] The magnetic fluid which is a mixture of dioctyl sebacate and magnetite (Fe_3O_4) nanoparticles can be considered a ferrofluid. The magnetic IL is based on a typical imidazolium cation and a dysprosium-based anion.

The tribological properties were assessed at four temperatures ranging from 25 – 150 °C, and two loads, 100 and 200 N. Post tribological assessment analysis was completed using scanning electron microscopy, energy dispersive X-ray analysis and XPS.

From the data collected in their work, the magnetic IL outperforms the commercially available magnetic fluid. This again is attributed to the formation of an effective boundary lubrication film, believed to be composed of Dy_2O_3, FeS, $FeSO_4$ and nitrogen containing organics, compared with the magnetic fluid which is only able to form a lubricating film at higher temperatures. Another drawback from the use of the nanoparticles is that the authors found they began to accumulate in the wear zone thereby enhancing abrasive wear of the steel/steel sliding contact.

From this review, it is believed that there is sufficient scope to suggest the applicability of a new type of magnetic lubricant and sealant. There is an abundance of literature describing ionic liquids and their applications as lubricants and lubricant additives. With ionic liquids as lubricants, there is now over 20 years of knowledge in the literature which continues to grow. The most recent work relevant to this project as stated goes back to 2019, comparing a

magnetic ionic liquid to a ferrofluid with respect to lubrication. This work is aimed at exploring magnetic ionic liquids further with respect to lubrication. Further to this, the lubricant also needs to act as a sealant, which has not been explored before in the literature offering further novelty to this work. What will follow is experimental work aiming to achieve this goal.

Chapter 2

2.1 Experimental Methods and Materials

2.1.1 Materials

All chemicals were used as bought from Sigma Aldrich with no further purification techniques, with purity as stated.

Methyl Imidazole 99%, pyridine 99%, 3-methyl pyridine 99%, chlorobutane 99%, chloroctane 99%, chlorodecane 98%, bromobutane 99%, bromodecane 98%, 1,2-dibromoethane 98%, 1,5-dibromopentane 97%, 1,10-dibromodecane 97%, iron (III) chloride hexahydrate 97%, silver nitrate 99%, dysprosium nitrate hexahydrate 99.9% trace metals basis, vinyl Imidazole 99%, AIBN 0.2 M solution in toluene. Solvents included acetonitrile 99.5% and water were used as acquired along with deuterated dimethyl sulfoxide and deuterated chloroform for NMR experiments.

Control lubricants Fomblin and Leybonol were both provided by Edwards Vacuum.

For contact angle measurements, steel with ra ~1.5 coupon, aluminium 1.5 mm thick mill finish plate and 0.5 mm thick rubber sheet grade A vinylidene fluoride hexafluoropropylene, known by its brand name Viton, were used.

For friction tests, carbon steel coupon 5.5 cm x 4.2 cm with Ra ~ 1.5, coupled with either 10 mm diameter aluminium polished ball bearing or 10 mm diameter 52100 steel ball bearing with Ra ~ 0.1 um.

2.1.2 Equipment

^{1}H NMR and ^{13}C NMR were recorded at 500/400 MHz, 125/100 MHz and 470/376 MHz on Bruker Avance 500/400 spectrometers. All spectra are referenced to $(CD_3)_2SO$ residual solvent peaks (^{1}H NMR δ = 2.50 ppm; ^{13}C NMR δ = 39.52 ppm).

Raman spectroscopy was completed using a Renishaw In-Via spectrometer with a laser wavelength of 514.5 nm (green).

Infrared (IR) spectra were recorded on a spectrometer as neat using a Bruker Alpha spectrometer.

Thermogravimetric analysis (TGA) measurements were recorded on a TA instruments TGA 5500. Unless stated otherwise, measurements began at room temperature and ramped at 10 °C per minute up to 450 °C in air.

Viscosities were measured using a Brookfield DV-III programmable rheometer with an SC-27 spindle and an additional small sample adapter, with water jacket and external water bath for temperature regulation. Viscosities were recorded once a stable value had been reached.

Contact angles were measured using a Krüss DSA 25E contact angle goniometer with a standard automated syringe dosing unit.

Magnetic susceptibility was measured using a Sherwood Scientific magnetic susceptibility balance (MSB) mark 1 with a magnetic field strength of 3.5 kGauss.

Bruker UMT Tribolab was used to measure COF values using a specified 10 mm ball on reciprocating steel coupon plate with a stroke length of 4 mm and varying frequencies, applied forces and durations and 3 – 4 drops of sample roughly equating to 1.5 – 2 mL.

Surface profiles were measured using a Bruker DektakXT stylus profilometer.

XP spectra were recorded using a K-alpha spectrometer equipped with a monochromated, micro-focused, Al K-Alpha X-ray source (1486.6 eV), a quartz crystal monochromator set in a 250-mm Rowland circle, hybrid optics, multichannel plate, hemispherical analyzer and 128-channel sensitive detector.

Powdered X-ray diffraction (XRD) was measured using a STOE Stadi P diffractometer (with STOE Dectris Mythen 1K detector), that operates with Mo K-alpha radiation (λ = 7.0930 Å) with Debye-Scherrer geometry in foil transmission mode

2.1.3 Experimental Setup and Procedures

Detailed syntheses can be found in the Appendix but briefly, equimolar haloalkane and methyl imidazole were mixed overnight at 90 °C after which ^{1}H NMR was taken using deuterated DMSO as the solvent to ascertain reaction progress. Once complete the reaction mixture was cooled and either equimolar iron (III) chloride hexahydrate was added followed by removal of water to yield

the IL or alternatively, equimolar silver nitrate was added in acetonitrile where a yellow precipitate was observed. Followed by filtration and addition of dysprosium nitrate hexahydrate where the mixture was left to stir for 2 hours followed by removal of solvent to yield the IL.

Viscosity indexes were measured in the same way as room temperature, only a water bath with built in circulator was used to pump heated water through the water jacket built into the small sample adapter. As stated in the results section the temperature was only able to reach 80 °C, where internal temperature of the viscometer was displayed to ensure the correct temperature had been reached.

Contact angles were measured by loading a syringe with the specified sample and dispensing 2 µL of each specified sample at a dispense rate of 0.05 µL/s onto different substrates. Each substrate, steel, aluminium and rubber sheet was cleaned with acetone and allowed to dry before being used. A video recording was then taken with a trigger point to start the measurement once the touch on method had been used to acquire the droplet. Each measurement was taken 3 times.

Data analysis of contact angles were completed using FTA32 video 2.1 software, where the baseline of the droplet was set in the software and measured using a non-spherical fit. The measurement published is a timed average as the droplet spreads.

Thermal Stability measurements were taken by weighing 10 mg of specified sample and then heating from room temperature (the tests never began at higher than 30 °C) at a ramp rate of 10 °C per minute up to 450 °C in air. Isothermal measurements were taken similarly by heating to the specified temperature at 10 °C per min and then holding at the constant specified temperature for 1 hour in air. Data was then exported to a csv file and opened in Origin 2019 64bit for analysis and plotting of the data.

Magnetism measurements were completed by initially weighing 0.2 g of the sample and recording the weight of a magnetic susceptibility tube, as well as noting the calibration constant of the Evans balance to be used. The range knob was set to ‘x 1’ and the zero knob was adjusted until the display read 000. The empty tube was inserted into the machine and the reading was taken (R_0). The

empty tube was then filled with 0.2 g of the sample that was measured previous being careful to avoid spillages and then re-weighed. This filled tube was then placed into the balance and a new reading was taken (R). Once complete the length of the sample in the Evans tube was measured with a micrometer and then emptied. A new clean Evans tube was used for each measurement.

Tests to measure coefficient of friction (COF) were completed using a Bruker UMT Tribolab utilising a ball on reciprocating plate test. The independent variables under control were duration of test, force load and reciprocating velocity. Initial tests were completed under a force load of 400 N, at 20 Hz for 900 seconds with a stroke length of 4 mm and data points recorded roughly every 0.02 seconds using roughly 2 mL of sample per test. As well as test settings, the initial tests used an aluminium ball and a steel plate as previously described in the materials section. The steel plate was first cleaned with acetone before being subjected to testing, and was repeatedly cleaned between tests with each test being completed on a different part of the coupon. New aluminium balls were used for each test, where each test was repeated twice.

To produce Stribeck curves, further test settings were applied. This time the load was decreased to a constant 5 N, with reciprocating speeds increasing from 0.1 to 0.5 to 1 Hz and then from 2 Hz increasing by 2 Hz at each step up until and including 20 Hz. Each step lasted 180 seconds with a stroke length of 4 mm and data acquired at roughly every 0.02 seconds using roughly 2 mL of sample per test. All measurements were completed at room temperature, as in, there were no heating or cooling elements involved in data acquisition. Control tests were performed on Fomblin and Leybonol where stated for Stribeck curves, the initial tests used Fomblin as a control as well as a dry test with no lubricant present.

The COF values reported are timed averages for both methods of testing, per se the first test is an average spread over the full 15 minutes whereas the COF values reported to produce Stribeck curves were timed averages at each step. Parameters recorded for each step include Fx, Fz both in N, LVDT, LV and Z in mm, Y in rev, V2 in RPM, Ff in N, as well as calculated COF.

Stribeck data was again collected using a steel coupon as detailed previously, and was cleaned with acetone between measurements along with a fresh steel ball (described previously) every time also. Only one run was completed for each sample.

Surface profiles were measured in 2D and 3D after the high load friction tests were completed. The 2D surface profile was measured roughly in the middle of the wear scar going across the shortest distance. These were measured using a hills and valleys profile on a standard scan type for a duration of 30 seconds, the stylus force was 10 mg with a radius of 2 μm and a stylus scan range of 65.5 μm and a scan resolution which varied between 0.3 and 0.4 μm. 3D profiles were measured in the way but with a rectangle area specified with X and Y axis profiles produced with lower resolution.

Chapter 3

3.1 Results and Discussion

3.1.1 An XPS Study of Ionic Liquids based on a bridged dicationic moiety

The most prominent fields in which XPS can be utilized include metal alloys, solid state chemistry, and polymers.[52-54] But due to the inherent non-volatility and wide liquid range of ionic liquids, this allows them to also be analysed in an ultra-high vacuum (UHV) based technique such as XPS.

As stated earlier in this report, XPS is a leading technique for the surface analysis of organic and inorganic compounds that provides information regarding surface composition and chemistry. Furthermore, many ILs experience little or no detectable beam damage in lab-based XPS instruments, this is due to the dynamic nature of the liquid surface which then produces spectra that possess core line signals that are intense, sharp and reproducible.[55] Furthermore, due to the electrically conducting nature of ILs, substantial differential charging is also prevented though more viscous ILs do still suffer from charging.

An important aim of XPS analysis is to deconvolute complex core line spectra and then accurately identify and quantify the different chemical environments that are present. However, this is made difficult due to XPS core line signals appearing complex because an element can appear in several chemical states within a sample. In a bid to deconvolute these complex spectra, which are made more difficult when measuring small molecules and the presence of surface contamination, the development of models of the C1s spectra have been devised. However this approach is more widely documented for inorganic non-molecular materials than for organic molecules such as ILs.[56] For chemical environments seen in organic molecules, the binding energy (BE) chemical shifts are typically smaller than the full width at half maximum (FWHM) of core photoemission lines, and therefore to overcome this fitting models are used.[57-59]

In an IL, there are multiple environments of carbon. The easiest example of different environments would be aromatic environments originating from an imidazolium-based cation versus carbons in an aliphatic chain bonded to the imidazolium cation. Each of these carbon environments would appear at slightly

different BE's, and the complexity of the XP spectra is due to the covalent bonding and delocalization of charge within the cation as well as different length aliphatic components and even different functional groups. Furthermore, physical properties of the IL can also affect the XP spectra. For example, a more viscous sample can lead to surface charging leading to a different XP spectra.[60] It is for these key points that an accurate, robust and reliable fitting model for ILs is required to get precise information.

In this work the aim is to adapt and assess current models used for monocationic ILs and apply them for use with dicationic ILs (DcILs).[25, 28, 61] Below in table 1, the names of the DcILs to be assessed can be seen, whilst also being displayed in figure 6 to see their chemical structures.

Table 1 Names of dicationic ILs (DcILs) to be studied

DcIL	Name
1	1,1,-(ethane-1,2-diyl)-bis(3-methylpyridinium) dibromide
2	1,1,-(pentane-1,5-diyl)-bis(3-methylpyridinium) dibromide
3	1,1,-(decane-1,10-diyl)-bis(3-methylpyridinium) dibromide
4	1,1,-(ethane-1,2-diyl)-bis(pyridinium) dibromide
5	1,1,-(pentane-1,5-diyl)-bis(pyridinium) dibromide
6	1,1,-(decane-1,10-diyl)-bis(pyridinium) dibromide

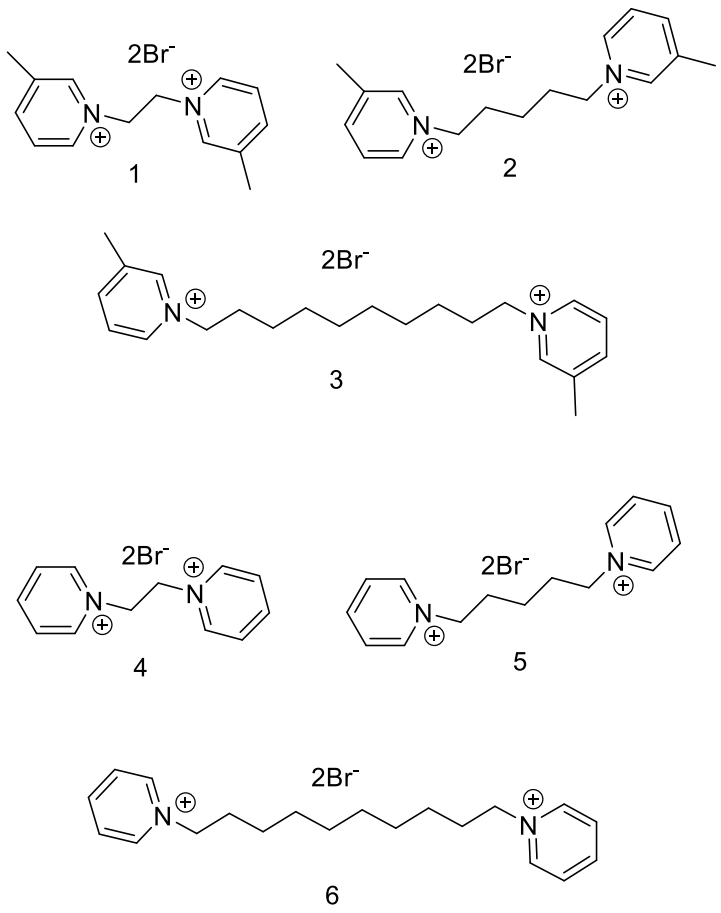

Figure 7 DcILs to be modelled, 1-3 based on 3-methyl pyridine and 4-6 based on pyridine

From figure 7 it can be seen that two series of DcILs have been prepared and analysed based on pyridinium cations with bridge lengths of 2, 5 and 10 carbon atoms long. In these synthesized DcILs, only the cation contains carbon therefore the C1s photoelectron spectra only has contributions from this component whereas typical spectra would show two discrete photoemission envelopes for carbon, one from the cation and one from the anion. Furthermore, survey spectra from all the samples are shown to contain only the elements expected.

The C1s spectrum was asymmetric in all samples studied and appears to be comprised of different components which forms the basis of this work, to accurately model the different carbon environments present in the cation. Definition of the BE scale (often described as charge correction) is usually completed using C1s however because the samples under analysis contain carbon this makes definition difficult. Therefore the body of this work focuses on understanding the spectra shape in terms of molecular structure as opposed to

absolute binding energies. Furthermore, charge compensation has been used to reduce charging whilst the spectra have not been adjusted therefore the absolute binding energies presented in this work should not be used alone to characterize the carbon environments; however, the relative binding energies of each component are a valid tool for understanding the chemical environments.

As stated, the DcILs analysed in this section are based upon pyridinium cations. Pyridinium cations have been demonstrated in the literature to display better thermal stabilities and higher viscosities than their imidazolium counterparts.[62, 63] In addition to this they are also known for their lubricity properties both as additives and as a base oil.[64] For this reason, this section of work aims to establish fitting models for pyridinium based DcILs, in a bid to use XPS modelling to help characterize potential degradation of DcILs when exposed to lubrication studies.

As a starting point it is known that a 3-component model has already been deduced for pyridinium based ILs by Men et al.[30] Further to this, a 4 component model is widely accepted for imidazolium based ILs.[25, 56, 65]

With the model, there are parameters present to create the model. A Shirley background is used, and full width half maximums (FWHMs) are kept constant between each component present in the model. Further to this, when each component has been defined the ratios must be kept constant to relate the model to the molecular structure. As well as this, the line shapes of the peaks present in the model are a mix of Gaussian 70% Lorentzian 30%.

In a typical imidazolium cation, there are 4 components contributing to the signal, C_A is the carbon in the aromatic ring bonded between the two nitrogen atoms. C_B is accepted as the other two carbon atoms in the aromatic ring bonded to each other and a single nitrogen; the third component C_C is accepted as the two aliphatic carbon atoms bonded to the nitrogen atoms in the aromatic ring and finally C_D which is the aliphatic component made up of the remaining carbon atoms in the alkyl chain which are bonded to the carbon atom which is bonded to the nitrogen. This method can be seen in figure 7 with a generic C_4C_1Im cation.

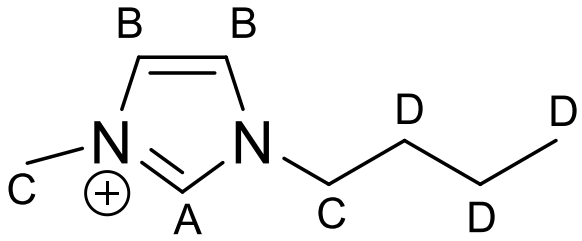

Figure 8 Accepted modelling method for imidazolium based cations, with different components with different labelling

Based on this accepted model, it was first attempted to derive a fitting model utilizing 4 components for the bridged DcILs which can be seen in figure 8. However, after doing this and fitting the components, it lead to components C and D appearing at BE that were almost exactly identical.

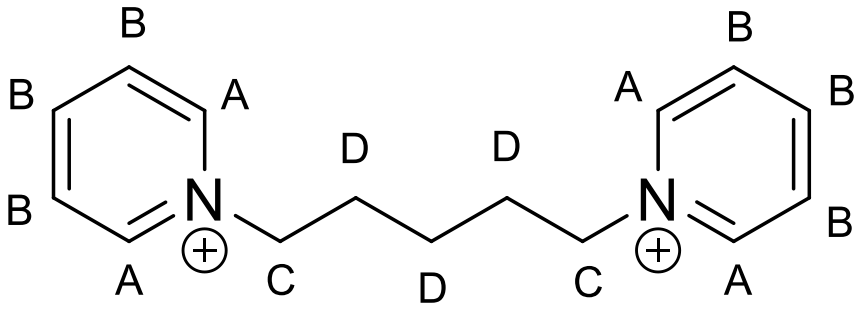

Figure 9 Initial attempt at the modelling of bridged pyridinium based dicationic species

To remedy this, bearing in mind that a model with more components will always result in a better fit, it was decided to combine C and D to give a three-component model which can now be seen in figure 9.

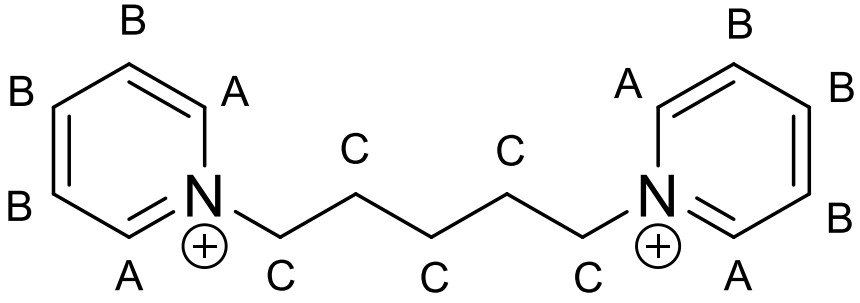

Figure 10 Derived model with a simplified 3 component model

From the figure above, the different environments are still labelled closely to the accepted imidazolium model. This being environment A which are the aromatic carbons bonded to nitrogen, environment B being the remaining aromatic

carbons in the pyridinium rings and component C which is the alkyl component acting as the bridge between the two pyridinium rings.

The first 3 DcILs can be seen below in figure 11, their model was constructed using a Shirley background and a line shape following the 70% Gaussian 30% Lorentzian (GL30). As well as this, the full width half maximum values were fixed equally. The components of the model were fitted with relative intensity as taken from the molecular structure. When fitting the components, they were constrained themselves to appear at specific binding energies relative to the structure that they were in. For example component A is an aromatic carbon bonded to nitrogen causing it to be constrained at a higher binding energy, whereas component C is an aliphatic carbon which will appear at a much lower binding energy and cannot appear higher than A. With this, the components were fitted as above and an obvious trend can be seen; increasing the length of the alkyl bridge causes the BE for the C component to shift to a lower value relative to the other components. This trend can also be seen for the last 3 DcILs in figure 12, however the last 3 do not possess the methyl group at position 3 in the pyridinium ring though from the data presented it can be concluded that it has accurately been described as a C_C component.

When comparing the methyl substituted pyridinium rings to their non-methyl substituted counterparts it can be seen that the aliphatic component appears much closer to the aromatic carbons in the model compared with their non-methyl pyridinium counterparts. This could be due to the inductive effect caused from methylation pushing electrons into the aromatic pyridine ring but position 3 is also where electrophilic reactions are likely to occur. Electrophilic reactions at position 3 offers 3 canonical forms where the positive charge is spread over positions 2, 4 and 6. Positions 2 and 6 are important because these are either side of the electronegative N atom in the pyridine ring. The electronegative N atom already has a positive charge due to alkylation, this build up of positive charge therefore increases the attraction between the remaining components and thus leading to an increase in binding energy for the C component.

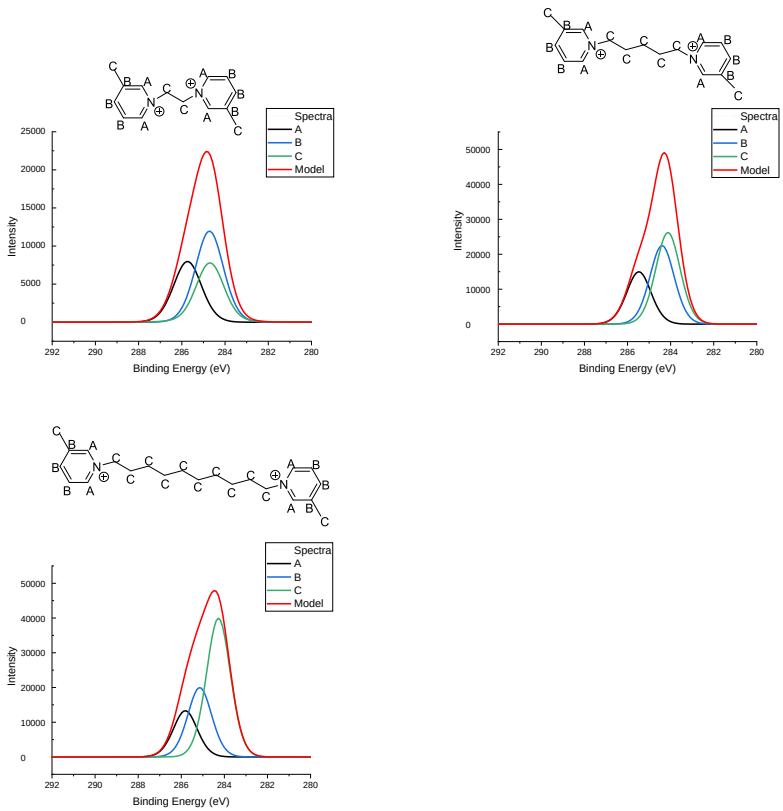

Figure 11 3-Methyl Pyridinium based bridged dicationic spectra, showing how spectra changes with elongation of the bridge component

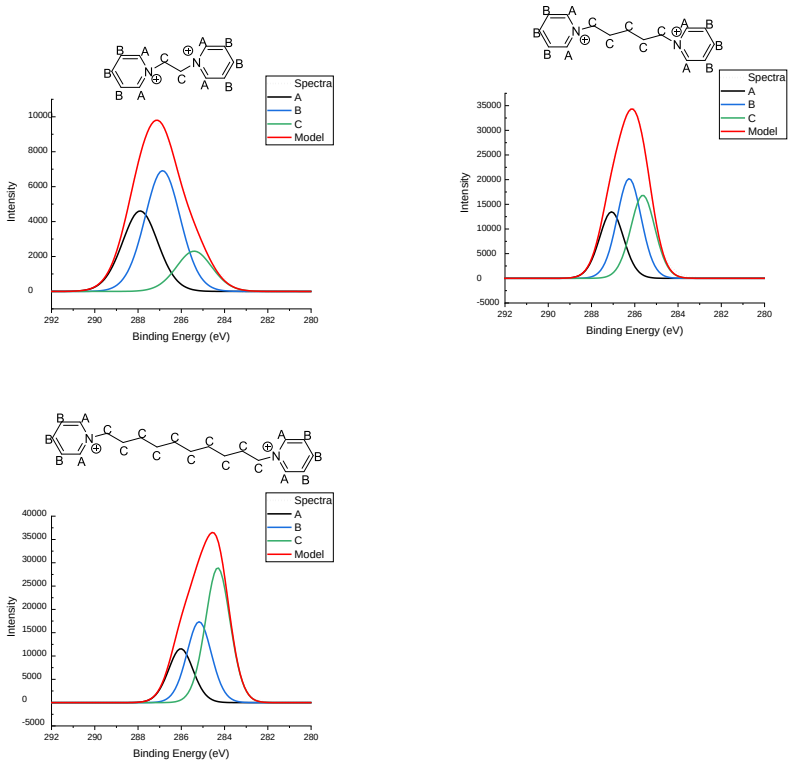

Figure 12 Pyridinium bridged dicationic ILs spectra, showing how spectra changes with elongation of bridge component

3.1.2 12 Core Samples Overview

The basis of this report is to synthesize a new lubricant based on ILs. To achieve this, 12 core samples have been synthesized and characterized, which will serve as the first port of call when assessing properties, spotting trends and deducing next steps. The names and chemical structures can be seen below in table 2.

Table 2 12 Core samples to be assessed

Name	Cation	Anion
MIL1	$C_4C_1Im^+$	$FeCl_4^-$
MIL2	$C_8C_1Im^+$	$FeCl_4^-$
MIL3	$C_{10}C_1Im^+$	$FeCl_4^-$
MIL4	$C_4C_1Im^+$	$FeCl_3Br^-$
MIL5	$C_{10}C_1Im^+$	$FeCl_3Br^-$
MIL6	$C_{10}Py^+$	$FeCl_3Br^-$
MIL7	3-methyl-$C_{10}Py^+$	$FeCl_3Br^-$
MIL8	3[$C_4C_1Im^+$]	$Dy(NO_3)_6^{3-}$
MIL9	3[$C_{10}C_1Im^+$]	$Dy(NO_3)_6^{3-}$
MIL10	3[C_4Py^+]	$Dy(NO_3)_6^{3-}$
MIL11	3[$C_{10}Py^+$]	$Dy(NO_3)_6^{3-}$
MIL12	3[3-methyl-$C_{10}Py^+$]	$Dy(NO_3)_6^{3-}$

The first 3 samples, MIL1-3, were prepared following a procedure set out by Hayashi *et al* in their seminal paper of 2004.[20] Where methyl imidazole was first alkylated with a chlorinated haloalkane, here being chloro-butane, octane and decane to create the corresponding imidazolium cation intermediates with a single chloride as the anion. In the paper, two methods are described for the anion exchange step where it was opted to add $FeCl_3.6H_2O$ for an endothermic reaction as opposed to adding $FeCl_3$ alone and receiving an exothermic reaction.

Following a similar procedure, MILs 4 and 5 were prepared only this time using a bromoalkane which then results in an $FeCl_3Br$ anion. This was completed with the foresight of seeing if there would be changes in properties when the anion has been changed, with the same cation. Furthermore, as the reaction times

are slightly shorter when using brominated alkanes as opposed to chlorinated, it was elected to prepare further samples. This resulted in pyridinium-based cations with an $FeCl_3Br$ anion, MILs 5 and 6. The reasoning for preparing pyridinium-based cations was that a larger cation may be more stable due to electronic effects of the pyridinium ring as opposed to the smaller (and relatively more strained than the pyridinium ring) but still aromatic imidazolium counter part. In preparing MILs 6 and 7, shorter chain versions utilizing bromobutane resulted in solids and therefore could not be analysed further.

Dysprosium based anions were investigated, though these samples (MILs 8-12) have slightly different structures. The main difference being that because Dysprosium has a stronger paramagnetic response which will be explored later but the dysprosium nitrate anion has an overall 3^- charge.[23] Which then means it requires 3 equivalents of the cation to balance the charge. The same principles as before were also applied to achieve an array of samples with comparable and contrasting structures and therefore properties, for example short and long chain alkyl substituents.

All 12 core samples have been characterized using proton and carbon NMR as well as Raman spectroscopy for the Fe containing MILs and Infrared spectroscopy for the dysprosium-based MILs.

Naturally, paramagnetic samples cannot be characterized using proton and carbon NMR; this is because proton and carbon NMR relies on an external magnetic field. ^1H and ^{13}C can be detected in a magnetic field as they only have 2 spin states, they can either align with the magnetic field known as the ground state and is the lowest energy; or they can absorb energy and align against the magnetic field known as resonance. This energy is then detected when the nuclei returns to its ground state and a spectrum is produced with intensity of the peak plotted against frequency, known as the chemical shift

To build on this further, the distribution of electrons around the nucleus also affects how the nuclei are affected by the external magnetic field. When the magnetic field is applied, the electrons surrounding the nucleus will produce a small electric current which in itself produces a magnetic field that opposes the magnetic field that is being applied externally. This results in the ‘shielding’

phenomena whereby a shielded nucleus will have a smaller chemical shift as opposed to a deshielded nucleus. A shielded nucleus is caused by electron donating groups and a deshielded nucleus is caused by electron withdrawing groups; with the MIL samples, upon quaternisation the electron density of the cation is reduced as the lone pair of electrons is now involved in covalent bonding. This results in a deshielded cation and hence the cation is shifted further downfield to a higher chemical shift

Because of this, with respect to the paramagnetic nature of the MIL, the anions (spread throughout the sample) will align with the external magnetic field applied, this will cause different fluctuations in the strength of the magnetic field felt causing different relaxation times (time taken for nuclei to return to their ground state) causing broad and potentially indecipherable spectra. Therefore it meant this analysis was completed after the first step, once the initial cation was prepared. Proton NMR was the most useful tool as it enabled the reaction progress to be monitored, for example it is possible in the spectra to see when there is left over methyl imidazole or pyridine as there will be peaks that correspond to that organic molecule, furthermore it can easily be deduced when the reaction is complete as all of the starting material has ‘disappeared’ from the spectra resulting in new peaks shifted further downfield. This shift in peak downfield for the cation is a result of electrons being used up in bonding to make the cation, and therefore deshielding the nucleus and being more susceptible to the magnetic field i.e. shifted further down the spectrum.

This means only the cation has been characterized, and even if paramagnetic samples could be analysed in an NMR spectrometer, the spectra would likely look the same as there is no difference in the cation upon completing the second step, the anion exchange. This is because there are no protons in either the iron or dysprosium-based anion. Therefore other methods of characterization are required.

For the iron-based anions there are two different compositions $FeCl_4$ and $FeCl_3Br$. These can then adopt different symmetries around the iron centre, Tetrahedral (Td) and C3v. Raman spectroscopy is used to distinguish between these 2 types of anion; however halide exchange could happen. This could then

lead to a mixture of $FeCl_2Br_2$ and $FeCl_4$ or other combinations that add up to the correct overall stoichiometry which Raman will help to decipher. It is based on an inelastic scattering process involving an energy transfer between incident light and illuminated target molecules. A small fraction of the incident light is shifted from its starting wavelength to various different wavelengths depending on the interaction with the vibrational frequencies of the illuminated molecule. The molecules vibrational energy levels determine the size of the shift and the number of different peaks depends on the symmetry of the molecule.

Figure 13 below is the resulting spectra.

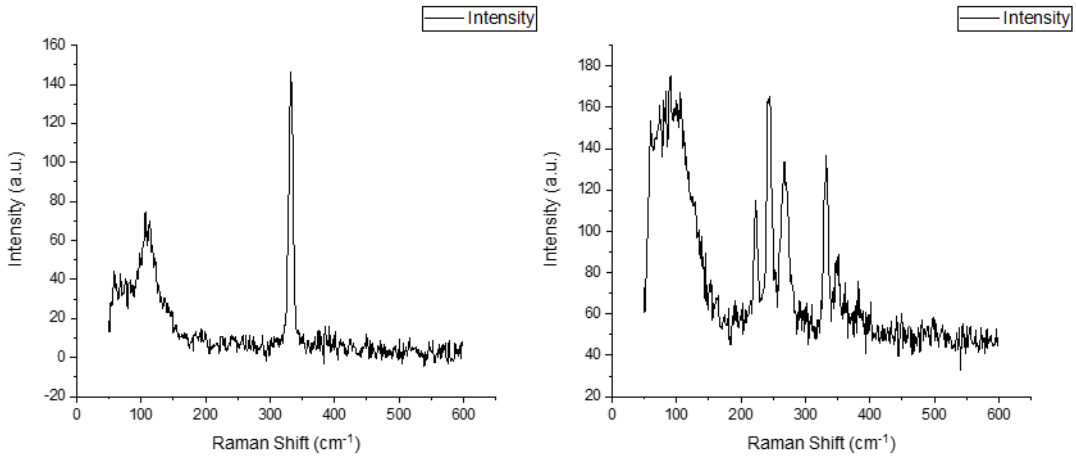

Figure 13 Raman spectra for $FeCl_4$ (left) and $FeCl_3Br$ (right)

As can be seen in the spectra, there are notable differences. The spectrum on the left is that of $FeCl_4$ which shows only 1 large singular peak at 333 cm^{-1}. This arises from the anion adopting a tetrahedral shape, or point group as they are often referred. This peak is in accordance with the literature and is caused by an iron chloride bond stretch. [20, 21, 66] The spectrum on the right is that of $FeCl_3Br$, note here that there is an obvious increase in the number of peaks present, shown at 221, 243, 267 and 332 cm^{-1}. This is caused by a reduction in symmetry of the molecule where the point group here is known as C_{3v}. This is also in accordance with that of the literature where the peaks at 221, 243 and 267 cm^{-1} were assigned to stretching of the iron bromide bonds and the peak at 332 cm^{-1} assigned again to the iron chloride bond.[67-69] There is also obvious noise present at around 100 cm^{-1} which is thought to be caused by the filters present in the instrument when measuring the spectra, there is also similar

noise present in the left spectrum but as the instrument was used on different days for each spectrum this could be the reason they are present in unequal intensities.

3.1.3 12 Core Sample Property Evaluation

The 12 samples previously discussed form the basis of this work, a description and discussion of tests and measurements undertaken will now follow, with the aim of gaining a deeper understanding of the properties and therefore suitability of said samples as a lubricant.

3.1.3.1 Viscosity Investigations

As set out in the beginning of this thesis, the objective is to prepare a lubricant that does not have a viscosity that exceeds 250 cSt. With this, it is also known that the current lubricant in use, Fomblin, has a very high viscosity which makes it difficult to handle; meaning the overall aim is a combination of not exceeding 250 cSt but also to have a viscosity that is less than that of Fomblin. Viscosity is a measure of a fluid's resistance to flow. This is an important property for a lubricant as it needs to be thick enough (high viscosity) to lubricate the operating machinery yet still runny enough (low viscosity) to easily manoeuvre around the equipment. This concept will be explained further in this report with respect to the Stribeck curve and the three modes of lubrication namely boundary, mixed and hydrodynamic.

If the lubricant is too viscous it is likely to impair the performance of the machinery as moving parts will turn sluggish whilst trying to pass through the lubricant; yet at the other end of the scale if the lubricant has an excessively low viscosity, there will be too much friction again due to moving parts coming into direct contact and potentially causing damage.

Viscosities were measured using a Brookfield DV-III programmable rheometer, the machine works by driving a spindle which is immersed in the test sample through a calibrated spring. The viscous drag of the fluid against the spindle is measured by the spring deflection. The spring deflection is then measured with a rotary transducer and the range of viscosities which the rheometer can measure is determined by the rotational speed of the spindle; as well as the size and shape of the spindle, the container that the spindle is rotating in and the full scale torque of the calibrated spring.

There are two types of viscosity measurement dynamic which is also known as absolute viscosity, and kinematic viscosity. Dynamic viscosity is a measure of

internal resistance and is the tangential force per unit area required to move one horizontal plane with respect to another plane, at a unit velocity, when maintaining a unit distance apart in the fluid. Kinematic viscosity is the ratio of dynamic viscosity to density and is a quantity in which no force is involved. It is obtained by dividing the dynamic viscosity of a fluid by the density of the fluid that is being measured.[70] Moving forward in this report, dynamic viscosity measurements will be presented.

Table 3 Measured viscosities of the 12 core samples, including 2 controls

Sample	Cation	Anion	Viscosity /mPas
MIL1	$C_4C_1Im^+$	$FeCl_4^-$	46 +/-0.7
MIL2	$C_8C_1Im^+$	$FeCl_4^-$	84 +/- 1
MIL3	$C_{10}C_1Im^+$	$FeCl_4^-$	150 +/- 2
MIL4	$C_4C_1Im^+$	$FeCl_3Br^-$	36 +/- 0.5
MIL5	$C_{10}C_1Im^+$	$FeCl_3Br^-$	95 +/- 1
MIL6	$C_{10}Py^+$	$FeCl_3Br^-$	142 +/- 2
MIL7	3-methyl-$C_{10}Py^+$	$FeCl_3Br^-$	145 +/- 3
MIL8	3[$C_4C_1Im^+$]	$Dy(NO_3)_6^{3-}$	104 +/- 2
MIL9	3[$C_{10}C_1Im^+$]	$Dy(NO_3)_6^{3-}$	358 +/- 5
MIL10	3[C_4Py^+]	$Dy(NO_3)_6^{3-}$	47 +/- 0.7
MIL11	3[$C_{10}Py^+$]	$Dy(NO_3)_6^{3-}$	706 +/- 11
MIL12	3[3-methyl-$C_{10}Py^+$]	$Dy(NO_3)_6^{3-}$	105 +/- 1.5
Fomblin			463 +/- 7
Leybonol			258 +/- 4

As can be seen in table 3, each of the sample lubricants have different viscosities. These differences can be translated to their respective structures; the easiest trend can be spotted moving from MIL1 to MIL3 where the alkyl chain on the imidazolium ring is being incrementally increased from 4 to 8 to 10 carbons long. The resulting effect of this is an increase in viscosity, this can also be seen moving from MIL4 to MIL5 where the carbon chain is increased from 4 to 10. Furthermore, as demonstrated by the data, the anion also influences viscosity whereby MIL1 and 4 have the same cation but a different anion similarly MIL3 and MIL5 have the same difference. Here, the viscosity is lower

in the $FeCl_3Br$ anions compared with the $FeCl_4$ anions. Possible reasons for this are that the larger $FeCl_3Br$ anion could result in a weaker force of attraction between the two components and therefore an overall reduction in viscosity. Delving further, the $FeCl_3Br$ anion is an anion with lower symmetry; therefore reducing the packing efficiency of the anion which would also result in a lower viscosity. Increasing the alkyl chain with regards to an imidazolium cation has been studied extensively in the literature, one of the first being published in 2001 where a chain length of 4 to 6 and then 8 was investigated.[71] As also demonstrated by the data obtained in this study, the influence of different anions has also been shown, this too has been studied in the literature with one of the first papers to discuss this phenomena being published in 2004 by Tokuda *et al.*[72] In this paper, 6 ILs are investigated based on a C_4C_1Im anion with different fluorinated anions and the viscosities compared. PF_6 is compared with BF_4 with the former having a larger viscosity than the latter, similarly for $(C_2F_5SO_2)_2N$ and $(CF_3SO_2)_2N$ with the former also having a larger viscosity, and finally CF_3SO_3 and CF_3CO_2 with the former again having a larger viscosity.

For MIL6 and MIL7, these are based on a pyridinium cation and $FeCl_3Br$ anion with the subtle difference being a methyl group substituted at position 3 on the pyridine ring for MIL7. The methyl group was introduced in an attempt to reduce viscosity and explore the influence, with the hypothesis being the methyl group would reduce symmetry in the cation and therefore reduce the viscosity. Symmetry in ILs was discussed in a paper by Greeson *et al* who investigated symmetric and asymmetric imidazolium-based cations.[73] Their findings relating to viscosity were that the asymmetric cations had a reduced viscosity when compared to their symmetric counterparts. This conclusion was based on an asymmetric imidazolium cation based on the formula C_nC_1Im with n increasing by 2 from 2 up until 12, and a symmetric cation based on the formula $(C_n)_2Im$ with n increasing by 2 from 2 up until 12. The effect of reduction in viscosity became more pronounced as the value of n increased. Relating this back to MIL6 and MIL7, their viscosities are relatively similar compared to others in the series with viscosities of 142 and 145 mPas respectively. Perhaps increasing the length of the alkyl chain at position 3 would offer another option of tailoring

the viscosity, with more pronounced effects resulting from greater extension of the alkyl chain.

For the series of MILs 8-12, these have an unorthodox structure whereby there are 3 positively charged cations required to balance the 3^- charge on the anion. This then has a dramatic effect on the viscosity changes that result when modifying the cation. Similar trends can be drawn in comparison with the singly charged MILs, that being an increase in alkyl chain length on the cation resulting in an overall increase in viscosity. This can be seen when comparing MIL8 and MIL9 as well as MIL10 and MIL11, as can be seen by the data the numerical differences are far more substantial. Furthermore, a methyl group was introduced into MIL12 in a similar vein to previous, that being to reduce cation symmetry. When comparing this with MIL11, the effect the reduction in symmetry has on the viscosity is also large, reducing the viscosity to a value comparable to MIL8 which has a short alkyl chain of 4. Due to the unique nature of this work, there is little viscosity data in the literature to compare and contrast with results found in this body of work. In a paper published in 2017, a range of hydrophobic MILs are synthesized with the possible applications described as being used as an extraction solvent in liquid-liquid extraction and general reaction media.[74] In their paper, the cation is phosphonium based with a plethora of different anions; in terms of viscosity work an image is published showing an inverted sample vial containing the MIL whereby the reader can judge the samples to be very viscous.

As set out in the beginning of this work, the operating temperature of the vacuum pump could be up to 85 °C. However each end of the pump has a temperature difference of roughly 15 °C. This is caused because at one end is the motor rotating the shafts and the other end has a higher temperature due to the compression of gas. As is common knowledge, the viscosity of liquids generally decrease as temperature is increased. Because of this, a viscosity index is devised. A viscosity index is an arbitrary, unitless measure of a liquid's change in viscosity relative to temperature change. Where the lower the viscosity index the more the liquid is affected by changes in temperature, this method of characterization is commonly seen in industry, especially engineering departments using different fuels.

So far, dynamic viscosity measurements have been measured with units of milli pascal seconds; in order to calculate a viscosity index the kinematic viscosity must be used. To convert dynamic viscosity to kinematic viscosity we must divide by the density of the fluid being measured. This can be seen below in table 4.

Table 4 Table showing density and calculated Kinematic Viscosity

Sample	Dynamic viscosity /mPas	Density /gcm^{-3}	Kinematic Viscosity /cSt
MIL1	46 +/-0.7	1.489	31
MIL2	84 +/- 1	1.317	64
MIL3	150 +/- 2	1.254	120
MIL4	36 +/- 0.5	1.512	24
MIL5	95 +/- 1	1.335	71
MIL6	142 +/- 2	1.357	105
MIL7	145 +/- 3	1.407	103
MIL8	104 +/- 2	1.436	72.4
MIL9	358 +/- 5	1.410	254
MIL10	47 +/- 0.7	1.434	33
MIL11	706 +/- 11	1.336	528
MIL12	105 +/- 1.5	1.322	79.4
Fomblin	463 +/- 7	2.229	208
Leybonol	258 +/- 4	1.063	243

As can be seen in table 4, densities of the MIL samples vary. In a similar vein to viscosity, these changes can be attributed to the molecular structure of the MIL. For example, for MIL1-3 the alkyl chain is being increased in length which appears to be inversely proportional to density where they appear to decrease. This is also the same for MIL 4-5, 8-9 and 10-11. Densities were acquired by weighing the mass of a 1 mL syringe before then filling the syringe with 1 mL of the sample at room temperature and re-weighing the mass. The difference in values equated to the density of the sample. It could be deduced that due to the bulkier substituents, for example the longer alkyl chains, due to reduced

packing efficiency less of the sample can fit in the 1 mL of space leading to a reduction in density.

Moving back to the viscosity index, below in figure 13 there are graphs of the change in viscosity relating to temperature. To calculate the viscosity index the following equations are used:

$$VI = 100\frac{L-U}{L-H} \; if \; VI \leq 100 \tag{2}$$

$$VI = 100 + \frac{\left(e^{\frac{\log H - \log U}{\log Y}}\right)^{-1}}{0.00715} \; if \; VI \; > 100 \tag{3}$$

Where:

U = kinematic viscosity of test oil at 40 °C

Y = kinematic viscosity of test oil at 100 °C

L and H values differ depending on calculation where tabulated values can be found in ASTM D2270, for ease of use VI's have been calculated using an online calculator which follows ISO 2909 and ASTM D2270.[75]

The viscosity index (VI) is a unitless measure of how a fluid's viscosity changes with temperature; where the lower the VI, the more the viscosity is affected by changes in temperature and a higher VI demonstrating the opposite effect whereby the viscosity of the fluid is unaffected with changes in temperature. When the VI was initially introduced for characterization, the scale was measured from 0 to 100, however it is now widely accepted for some fluids do have a very high VI that being a value above 110. Below in table 5 the classifications can be seen.

Table 5 Classification for viscosity index values

VI	Classification
<35	Low
35 – 80	Medium
80 – 110	High
>110	Very high

Below in figure 14, graphs of viscosity and temperature can be seen. Due to apparatus issues, the upper temperature that the viscosity could be reliably measured was 80 °C. As can be seen from the VI equation, this requires an upper viscosity measurement at 100 °C, to achieve this, the graphs have then been extrapolated to this temperature value and the corresponding viscosity acquired. Furthermore, as stated previous, these measurements are for the dynamic viscosity, meaning they again need to be converted to their kinematic values by dividing by their density. It must be noted that a fixed density value has been used which was measured at room temperature and not with density values that vary with temperature. The final values for the measured 40 °C kinematic viscosity and theoretical 100 °C kinematic viscosity can then be seen in tables 6 and 7.

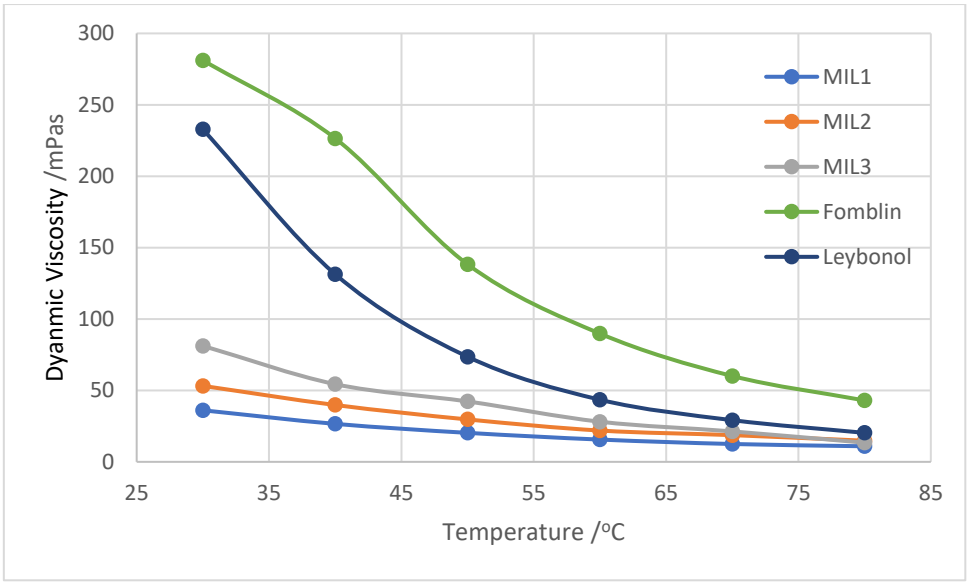

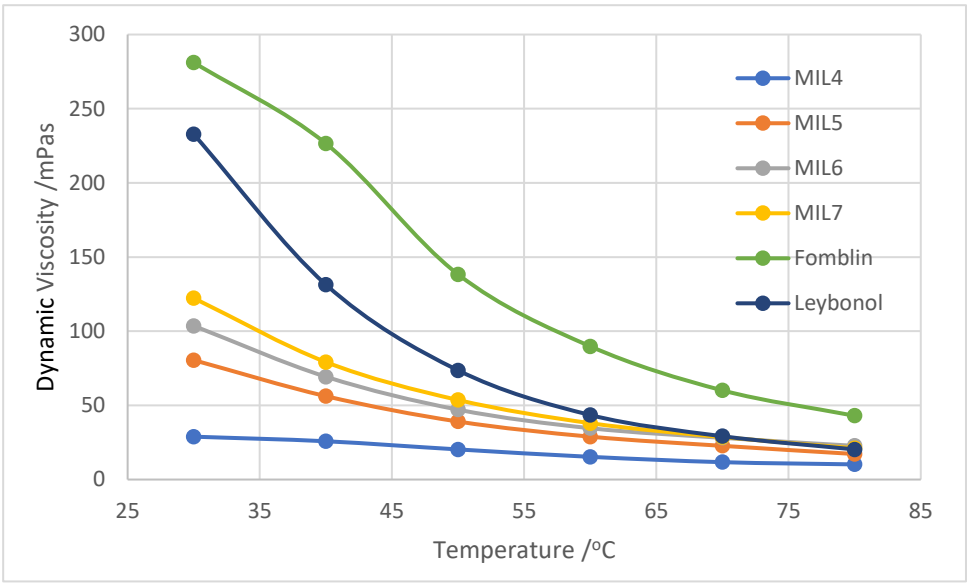

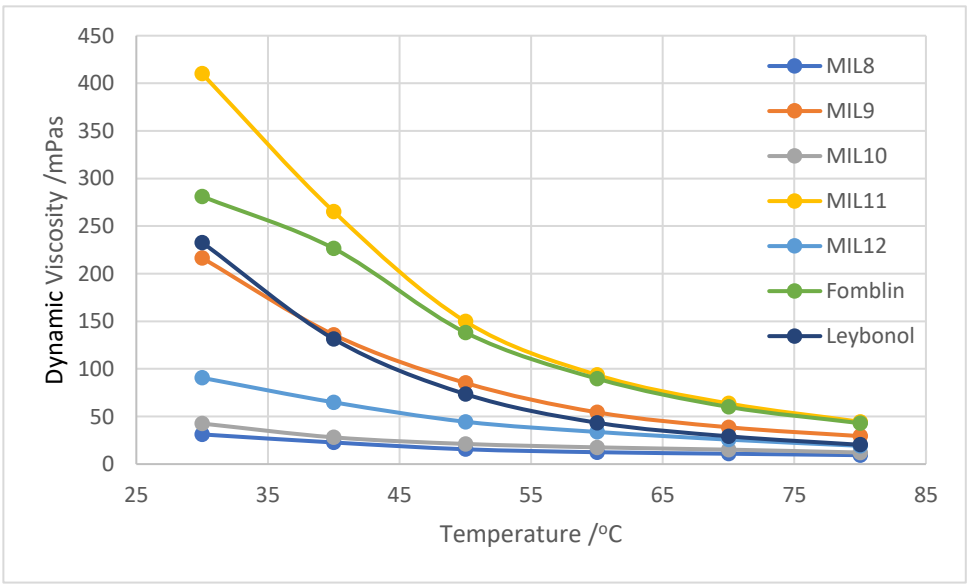

Figure 14 Graphs showing viscosity change as temperature is increased up to 80 °C for all MIL samples plus controls

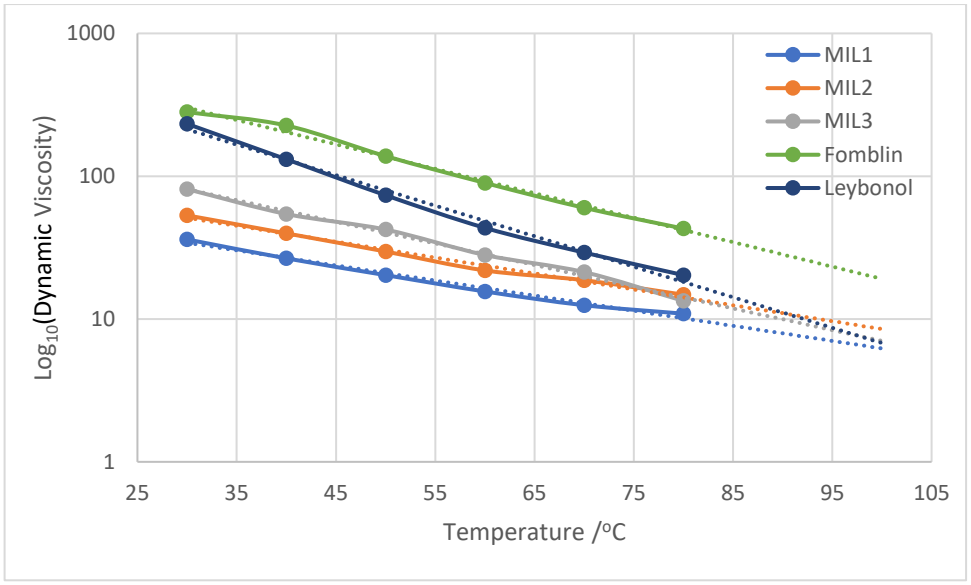

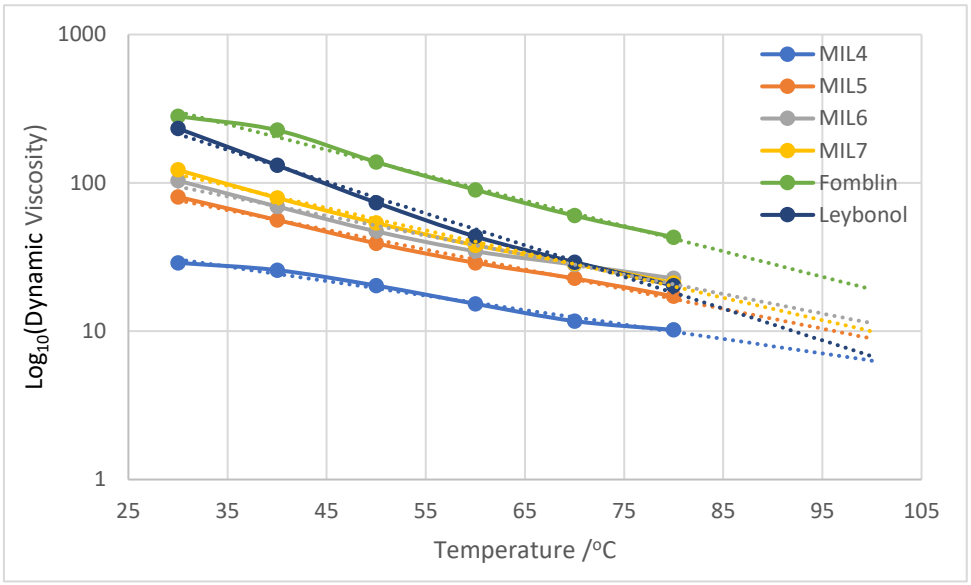

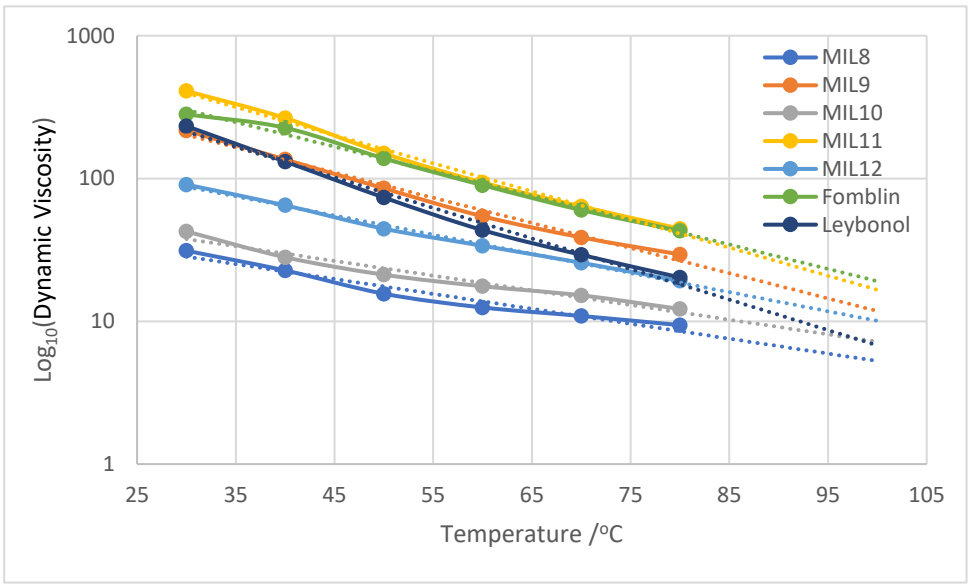

Figure 15 Graphs showing extrapolated data to show theoretical viscosity at 100 degrees

Table 6 Calculation of theoretic Dynamic and Kinematic Viscosity

Sample	Equation of trendline	Theoretical Dynamic Viscosity at 100 °C	Theoretical Kinematic Viscosity at 100 °C
MIL1	$y = 70.922e^{-0.024x}$	6.434	4.321
MIL2	$y = 110.21e^{-0.026x}$	8.185	6.215
MIL3	$y = 231.18e^{-0.035x}$	6.981	5.566
MIL4	$y = 59.817e^{-0.022x}$	6.628	4.383
MIL5	$y = 191.82e^{-0.031x}$	8.641	6.472
MIL6	$y = 234.1e^{-0.03x}$	11.655	8.588
MIL7	$y = 324.28e^{-0.035x}$	9.792	6.959
MIL8	$y = 58.41e^{-0.024x}$	5.298	3.689
MIL9	$y = 682.94e^{-0.041x}$	11.318	8.027
MIL10	$y = 76.716e^{-0.024x}$	6.959	4.852
MIL11	$y = 1541.8e^{-0.045x}$	17.127	12.819
MIL12	$y = 221.06e^{-0.031x}$	9.958	7.532
Fomblin	$y = 985.48e^{-0.039x}$	19.948	8.949
Leybonol	$y = 933.81e^{-0.049x}$	6.953	6.541

Table 7 Conversion of dynamic viscosity at 40°C to kinematic viscosity

Sample	Measured Dynamic Viscosity at 40 °C	Kinematic Viscosity at 40 °C
MIL1	26.6 +/- 0.4	17.8
MIL2	39.8 +/- 0.6	30.2
MIL3	54.4 +/- 0.8	43.4
MIL4	25.8 +/- 0.4	17.1
MIL5	56.2 +/- 0.8	42.1
MIL6	69.3 +/- 1	51.1
MIL7	79.2 +/- 1	56.3
MIL8	22.7 +/- 0.3	15.8
MIL9	135.9 +/- 2	96.38
MIL10	28.1 +/- 0.4	19.6
MIL11	265.2 +/- 4	198.5
MIL12	64.9 +/- 1	49.1
Fomblin	226.5 +/- 3	101.6
Leybonol	131.4 +/- 2	123.6

Table 8 Calculated Viscosity Index values

Sample	Viscosity Index	Alkyl chain Length
MIL1	138	4
MIL2	151	8
MIL3	80	10
MIL4	138	4
MIL5	84	10
MIL6	127	10
MIL7	79	1+10
MIL8	157	4
MIL9	43	10
MIL10	191	4
MIL11	51	10
MIL12	134	1+10
Fomblin	57	n/a
Leybonol	7	n/a

As stated in the introduction to viscosity indexes, the classifications can be seen as low, medium, high and very high in table 5 above. In table 8 the final viscosity index values have been determined.

In table 8 above, a trend can be seen relating MIL structure and VI. As is known in the literature, increasing the alkyl chain length on the imidazolium cations increased the viscosity but now this results in a decrease in value for VI. The cause of this can be seen in the viscosity/temperature graphs from figure 13, at 80 °C all of the samples have a dynamic viscosity value below 50 but at 40 °C the dynamic viscosity values vary greatly. Due to this large variation the VI equation results in a very low VI index for the initial higher viscosity samples.

In table 8, Fomblin (the control lubricant which is currently in use by the vacuum pump system) can be seen as having a value of 57 whereas in the literature Fomblin is quoted as having a range from 60 – 350 depending on the grade being used.[76] Leybonol is another control lubricant that can be used, there is no direct data yet when entering viscosity values found on various product

manufacturers websites a value of 3 is produced. All of the samples in the table above with the exception of MIL 9 and 11 have a viscosity index value greater than the two control lubricants. The lowest values are for MIL9 and 11, yet when using the classification table they fall into the same category as Fomblin. This demonstrates that the MILs are showing early signs that a promising new lubricant could be utilized using MILs.

3.1.3.2 Contact Angle on varying substrates

Contact angles are measured because different lubricants interact with surfaces in different ways. In order to form an effective boundary layer the lubricant must 'wet' the surface Wetting the surfaces means the lubricant spreads out in a uniform fashion once in contact with the surface. This can be assessed by measuring the contact angle of the droplet formed on the surface.

Contact angle, θ, is a quantitative measurement which is defined geometrically as the angle formed by a liquid at the three-phase boundary where a liquid, gas and solid intersect. It is described by the Young equation.

$$Y_{sv} = Y_{sl} + Y_{lv}cos\theta_Y \quad (4)$$

The Interfacial tensions Y_{sv}, Y_{sl} and Y_{lv} form the equilibrium contact angle of wetting which is sometimes referred to as the Young contact angle θ_Y.

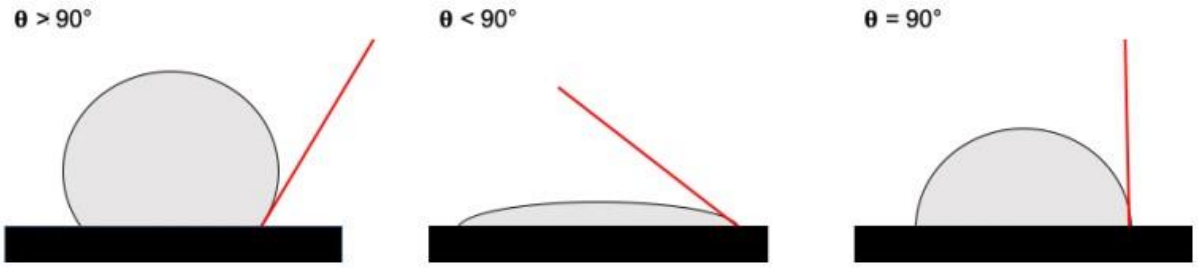

Figure 16 Schematic of different contact angles, left showing poor wetting and middle showing good wetting of the surface

From the figure, a low contact angle indicates the liquid wets the surface well (spreading on the surface), with a value of zero indicating complete wetting. While a high contact angle shows poor wettability (not spreading on the surface).

There are two methods available for measuring the contact angle, static and dynamic. Static angles are measured when the droplet is standing on the surface and not moving; whereas dynamic angles are measured whilst the liquid droplet is moving (spreading) on the surface. They are sometimes referred to as advancing or receding angles.

In this work, the dynamic measurement will be used to analyse the lubricants wettability on three key surfaces which will be steel, aluminium and Viton as detailed in the experimental as vinylidene fluoride hexafluoropropylene.

Viton is a brand name that is used as a polymer-type sealant in vacuum seals. It is hoped that all MIL samples will match or better the control samples which would signify good wetting of the surface; whereby in theory would mean a good boundary film would be present to prevent friction and wear. A good boundary film here meaning a physical barrier where the lubricant can adsorb onto the surface at a sufficient thickness to provide hydrodynamic lubrication which is where the two surfaces are fully supported by the lubricant.

Table 9 Average contact angle measured for each substrate

Sample	Substrate average contact angle /°		
	Aluminium	Steel	Vinylidene Fluoride Hexafluoropropylene
MIL1	64 +/- 1	67 +/- 1	69 +/- 1
MIL2	40 +/- 1	47 +/- 3	61 +/- 2
MIL3	34 +/- 3	24 +/- 4	49 +/- 4
MIL4	50 +/- 1	65 +/- 3	80 +/- 3
MIL5	50 +/- 4	49 +/- 3	59 +/- 2
MIL6	44 +/- 4	36 +/- 5	64 +/- 2
MIL7	40 +/- 2	46 +/- 4	62 +/- 2
MIL8	48 +/- 4	60 +/- 3	79 +/- 2
MIL9	43 +/- 6	40 +/- 7	43 +/- 3
MIL10	71 +/- 2	66 +/- 4	80 +/- 2
MIL11	39 +/- 5	42 +/- 6	47 +/- 3
MIL12	26 +/- 4	38 +/- 5	43 +/- 4
Fomblin	24 +/- 5	29 +/- 6	29 +/- 5
Leybonol	29 +/- 3	24 +/- 5	35 +/- 3

The largest contact angle values for each sample can be seen on vinylidene fluoride hexafluoropropylene, with mixed results seen for aluminium and steel. Furthermore, when relating MIL structure to contact angle value it can be seen, for example, MIL1, 2 and 3 that increasing the alkyl chain length decreases the contact angle value across all 3 substrates. This is similar for MIL4 and 5, 8 and 9, and 10 and 11. The introduction of a methyl group to MIL7 and MIL12 appears to have mixed results when compared with their non methylated counter parts 6 and 11 respectively.

These trends relating alkyl chain length to contact angle could also be closely related to viscosity, where the incremental increases in viscosity also correlate with decreases in contact angle value, for example MILs 1-3, 4 and 5, 8 and 9 and 10 and 11. Furthermore Fomblin, Leybonol and MILs 9 and 11 showed the

highest viscosity values, with Fomblin and Leybonol also showing the lowest contact angles across all three substrates. When introducing MIL9 and 11 into this trend, the results are mixed. If comparing them to the entire table they do not possess the lowest contact angles, but if comparing to the MILs with similar structures they do. This suggests there are fundamental differences in physical properties that inherently cause differences. In the MIL samples, generally the higher viscosity samples possess a lower density than their similarly structured counterparts as discussed earlier in this report. This could then relate to the contact angles measured whereby a more dense fluid is likely to be unable to resist physically spreading on the substrate.

In addition to this, the experiments were completed at room temperature which is a limitation of this test. This is because it is known the vacuum pump that will be used will operate at temperatures up to 85 °C, which as demonstrated in previous work in this thesis shows an increase in temperature causes a decrease in viscosity. It is then believed that this would also correlate with a decrease in contact angle caused by the sample having a high enough thermal energy to overcome the forces of cohesion within the sample causing a greater spreading effect on the substrate being tested.

A paper published in 2018 investigated contact angles of different ionic liquids at varying temperatures.[77] The paper studies three different cations, an imidazolium, phosphonium and ammonium all with the same bis(trifluoromethane) anion. In the paper, contact angles are measured at 25, 40 and 100 °C with the data reported showing mixed results. The ammonium-based IL showed a slight increase in contact angle from 25 to 40 °C, but then reduced to its lowest value at 100 °C, the phosphonium based IL also showed an increase from 25 to 40 °C and remained constant at 100 °C. Finally, the imidazolium-based IL showed an increase in contact angle after each elevation in temperature. Though interestingly, their viscosity data shows the expected decrease in viscosity as the temperature is increased from 25 to 40 to 100 °C suggesting that the cationic structure is influencing the contact angle measurements. As well as contact angle, they also measured surface tension where at each increase in temperature, 25 to 40 to 100 °C they all showed a slight decrease in value.

Similarly, in a paper by Bhattacharjee and Khan in 2019 they investigated the effect of alkyl chain length on the wetting behaviour of imidazolium based ILs.[78] This paper is based on molecular dynamics (MD) simulations based on 2 imidazolium tetrafluoroborate ILs, one as a C_1C_1Im and the other as a C_3C_1Im BF_4 on a graphite surface. After allowing the system to equilibrate they then studied some properties, the first being the effect of drop size, here they increased the number of ion pairs in their system and studied the contact angle. Their findings showed that increasing the size of the droplet appears to increase the size of the contact angle. Further work on this explored the evolution of the contact angle with respect to time for different sized droplets, here they found that the high initial contact angle of the droplet slowly reduced to an equilibrium value, similar to the results found in this work. In this paper, they also study the effect of an increase in temperature with respect to contact angle; For a droplet of fixed size, increasing the temperature from 300 to 350 K appears to reduce the contact angle for both ILs being studied with generally lower angles seen for the longer C_3C_1Im IL. This backs up the data reported here whereby increasing the alkyl chain length decreases the contact angle, however angles have not been measured at increased temperatures above that of room.

3.1.3.3 Thermal Stability

Thermal stability is how stable the lubricant will be when operating under elevated temperatures. This is an important aspect of a lubricant as equipment that is constantly in motion is likely to heat up; therefore meaning it is imperative the lubricant does not fail and cause damage to vital machinery. This parameter will be assessed using thermogravimetric analysis (TGA) which acts as an accelerated test to determine at which point the lubricant will fail. It is likely the upper operating temperature of the equipment the lubricant will be a part of will not reach above 90 °C, so the lubricant needs to remain unchanged at that point, unchanged meaning no reduction in mass percentage which would be indicative of thermal degradation of the ionic liquid's cation, anion or both.

TGA is a type of thermal analysis where a known mass of a sample is monitored over time as the temperature changes (increases in this case). This is completed by using a thermogravimetric analyser where a stable sample would show no or minimal reduction in mass as the temperature increases. It is a widely known phenomenon that ionic liquids have a wide liquid range and are generally stable up to around 300 °C, so it is anticipated that the core samples prepared should be stable up to this point.

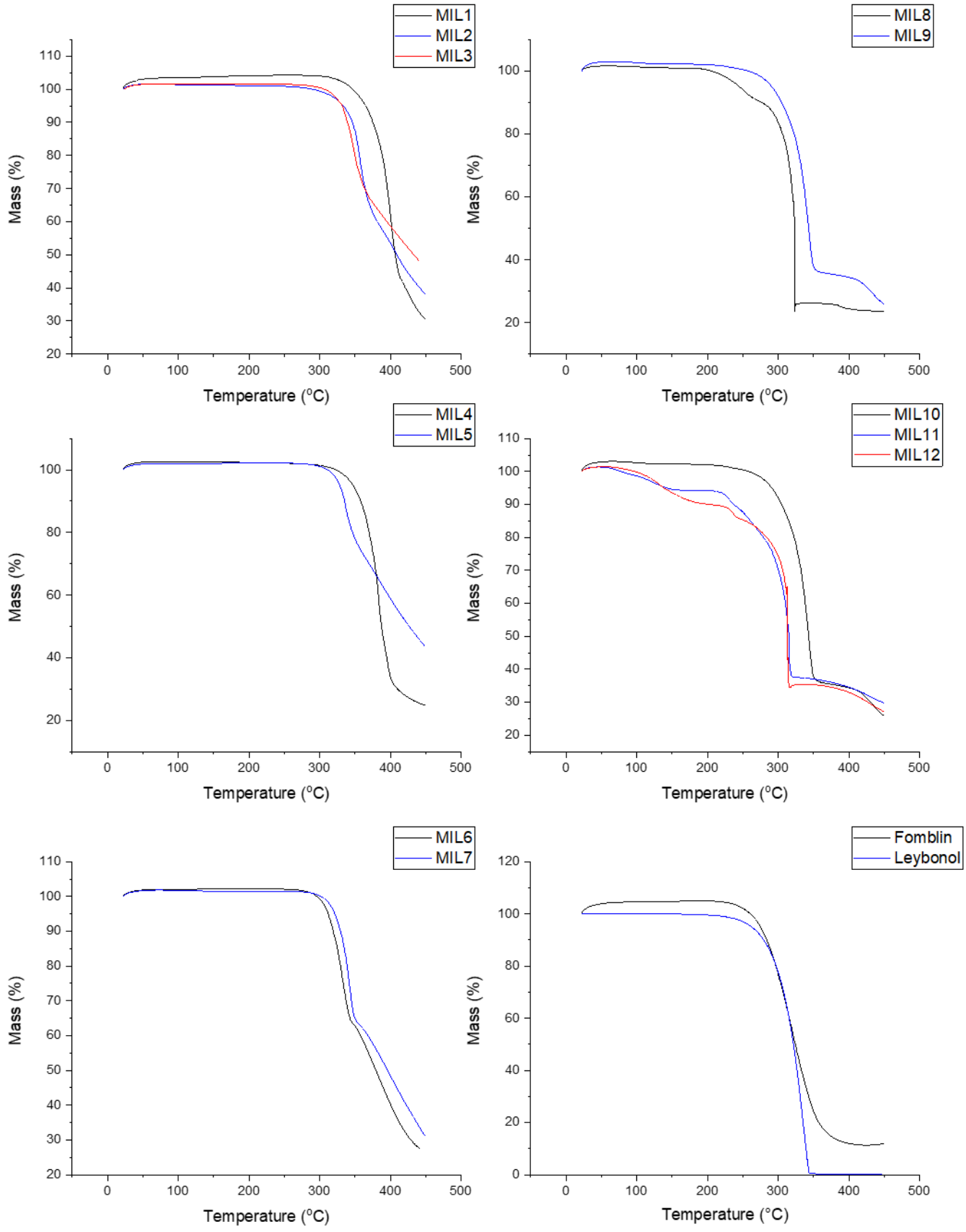

Figure 17 TGA Curves of all MIL samples and 2 control lubricants, showing different decomposition temperatures all based on the same 10 °C per minute ramp up from room temperature to 450 °C

As stated previously, it is widely known that ILs are thermally stable due to their non-volatile nature. In figure 17, TGA curves are shown for each MIL as well as Fomblin and Leybonol which are the control experiments.

The main point in this experiment is to ensure the samples are thermally stable at 85 °C as this is the upper operating temperature of the pump that the samples will be lubricating; whereby the graphs show that all samples are stable at that temperature.

In the figure, it can be seen that all of the samples appear to have an onset decomposition temperature around 300 °C, with slight variations which could be attributed to chemical structure. For example, MIL1, 2 and 3 have an increase in alkyl chain length where the mass percentage of the shortest alkyl chain appears to decrease the most and the longest alkyl chain appearing to decrease the least. This is a similar trend for 4 and 5, 6 and 7, and 8 and 9.

Furthermore, the dysprosium samples which consist of 3 equivalents of cation for each anion appear to be affected more by temperature. For the $FeCl_4$ and $FeCl_3Br$ anions the onset of decomposition clearly begins above 300 °C whereas for the dysprosium samples it appears to begin sooner. This is especially noticeable for MILs 10, 11 and 12, these samples are based on a pyridinium cation as opposed to imidazolium. This is a result which was not anticipated as the pyridinium cation was selected for it's potential to be generally more stable due to an aromatic structure that is larger than its imidazolium counterpart. However, these results suggest that perhaps the dysprosium-based anion is decomposing as opposed to the cation.

There is little thermal stability data in the literature with regards to Dysprosium hexanitrate as an anion. But one paper that does study this property is by Pierson *et al* from 2017.[74] In this paper, a phosphonium cation is paired with various hexafluoroacetylacetonate anions; where each of the anions have a different metal centre including cobalt, manganese, nickel, dysprosium, gadolinium and neodymium. Though the MILs synthesized and discussed in this paper are more traditional in the respect that each anion and cation has a single charge as opposed to the Dy^{3+} in this work.

With regards to thermal stability, this was assessed using gas chromatography to reveal the onset temperature of either volatilization or decomposition. This was achieved by immobilizing a film on the inner wall of a fused silica capillary tube, followed by slow heating in the gas chromatography oven where an ultra-sensitive flame ionization detector was used to detect the MIL as it volatilized/decomposed. In the samples analysed, the dysprosium sample began to decompose at around 225 °C, similar to the gadolinium and nickel-based MILs in their study.

Relating that temperature to the decomposition temperatures found in this work, the imidazolium-based dysprosium MILs have a higher decomposition temperature than 225 °C but the pyridinium based dysprosium anions have an onset much lower than 225 °C though with the bulk appearing to decompose at that temperature. Thus, suggesting the structure of the anion and cation can influence the decomposition temperatures.

Furthermore, thermal stability is a widely reported property when discussing the IL due to their wide liquid range. Thermal stability is also a key component when the IL is being used as a lubricant, what will follow is some data from the literature with regards to structure, lubrication and thermal stability.

As stated in the introduction, phosphonium and ammonium cations are also utilized as well as more traditional imidazolium and to some extent pyridinium. One of the first papers to report on thermal stability came in 2000 by the McEwen group.[79] In this paper, they explore extensively various imidazolium based ILs; the onset of thermal decomposition ranges from around 280 up to 470 °C with their conclusions being that the stability of imidazolium based ILs increases with increased alkyl substitution as long as linear alkyl groups are used. A more extensive investigation came in a review article published in 2013 by Stevens *et al* who included phosphonium and sulphonium as well as investigating the decomposition mechanisms.[80] As for thermal decomposition, their work also backs up the hypothesis that increasing the length of the alkyl component decreases thermal stability, this was seen for the imidazolium based ILs. With respect to ammonium and phosphonium ILs the latter were seen as more thermally stable than their tetraalkyl ammonium counterparts; sulphonium

based ILs both cyclic and linear were then also found to be less stable than quaternary ammonium ILs.

When the paper discusses decomposition pathways, numerous theories are discussed. The first being a general anion thermal degradation particularly for inorganic anions containing sulphonyl groups which degrade to form sulphur dioxide. Another likely decomposition mechanism is described as the reverse menshutkin reaction, ultimately allowing the IL to rearrange to produce 2 stable components for example a neutral imidazole compound and inorganic salt. Other thermal rearrangement reactions are discussed with alkene formation discussed as a potential mechanism where it is hypothesized these are more likely to occur in ILs with longer alkyl components. But generally, all the analysis methods used have made use of some type of mass spectrometry coupled method to 'unambiguously reveal the cleavage of the N-C bond as a main degradation process'.

More recently, Reeves *et al* investigated the tribological performance of environmentally friendly ILs in high temperature applications.[81] In this paper a large number of ILs were analysed; in their thermal analysis measurements two approaches were taken. This first was the more typical test called the dynamic decomposition test whereby the samples were heated at an increasing constant rate to determine the temperature at which the decomposition begins (as indicated by mass loss) and finishes. This is the same method as presented in this work, though their second method is known as an isothermal decomposition measurement. Here the lubricants were held at 100 °C below and then 50 °C below their decomposition onset temperatures. In the former test, all results were as expected with decomposition temperatures above 300 °C, however the isothermal tests yielded more interesting results where all of the lubricants began to slowly decompose at even 100 °C. These tests were completed over an 8 hour period and are more interesting in that, as anticipated in a similar vein in this work, the lubricant is likely to be subject to high operating temperatures and therefore it is necessary to know how the lubricant may react in prolonged time periods. Earlier in this work it has already been demonstrated the effect of viscosity with regards to heat and thermal stability; furthermore, the isothermal tests in this paper all show that the decomposition process actually begins

sooner than the original decomposition temperature acquired using the dynamic method. This is important as the results presented thus far show the stereotypical properties of the MIL samples showing thermal stability up to 300 °C however, perhaps this value could be lower if an isothermal method had been completed at 85 °C to more accurately represent the pump in operation, and to further enhance the test it could be held at 85 °C for a specified amount of time, for example a minimum of 8 hours but ideally as long as deemed possible, perhaps on the scale of weeks. Further tests in this thesis look at holding the scaled up sample at 100 °C for one hour, an isothermal TGA curve is produced where to briefly discuss here there is roughly 10% weight loss observed which can be attributed to water loss since it occurs at the very beginning of the test followed by a flat constant line for the remainder of the test suggesting satisfactory thermal stability.

3.1.3.4 Magnetism

As set out in the project aims, magnetism is an essential property in order for the lubricant to also act as a sealant. The three types of magnetism have been discussed earlier in this report, what will follow is the method of measuring this property.

Magnetism, or magnetic susceptibility, will be measured using an Evans balance developed by Dennis Evans in 1973.[82] The balance works by having 2 permanent magnets mounted back to back and supported by a suspension strip. When the sample tube is inserted in between the two magnets a deflection is detected by an optical transducer. A current is then passed through a coil which is attached to one of the magnets in order to counteract the initial deflection. The force that the sample exerts onto the magnet is then proportional to the current applied to the coil to counter act the force, thus allowing for a reading to be taken.

The Evans balance can be used to determine the mass magnetic susceptibility Xg using the following equation:

$$Xg = \frac{L}{m}[C(R - R_0)] \times 10^{-9} \quad (5)$$

Where L = sample length in centimetres

m = sample mass in grams

C = balance calibration constant (unique to each balance)

R = the measurement taken when the sample is inside the tube

R_0 = the measurement taken when the tube contains no sample

This gives a value of Xg in centimetre-gram-second (cgs) units of erg G^{-1} g^{-1}. This can then be converted into the molar susceptibility Xm by multiplying by the relative molecular mass (RMM) of the corresponding sample:

$$Xm = Xg \times RMM \quad (6)$$

This gives an Xm value in units of erg G^{-1} mol^{-1} but can also be represented as cm^3 mol^{-1}. However, a correction must now be made as all compounds have pairs of electrons which will be weakly repelled from the magnetic field therefore

meaning a diamagnetic correction must be made. This is completed by adding up the diamagnetic contributions of all the atoms in the molecule by using a paper published by Bain and Berry which contains the data.[83] This then produces the following equation which is a correction:

$$Xm^{corr} = Xm - Xm^{dia} \quad (7)$$

The final step is then to calculate the effective magnetic moment, μ, using the curie law:

$$\mu = 2.84[Xm^{corr}T]^{0.5} \quad (8)$$

where T = temperature in kelvin.

Once the effective magnetic moment has been calculated, this can then be put into the spin only formula where it is assumed only spin contribution is contributing to the magnetic moment:

$$\mu = [n(n+2)]^{0.5} \quad (9)$$

This is a valuable equation as it reveals the number of unpaired electrons present in the sample and can be used as another method of confirming the structures that have been synthesized, for example the iron containing samples have iron in it's +3 oxidation state, resulting in 5 unpaired electrons assuming they are in high spin configuration which is a reasonable assumption as halogens such as chlorine and bromine lead to high spin complexes therefore meaning a value of 5 should be the output from the spin only formula. Results can be found in table 10 below.

Table 10 Calculated magnetic moment values and values for n from the spin only formula where applicable

Ionic Liquid	μ /erg G^{-1}	Expected μ /erg G^{-1}	n (calculated from spin only formula)
MIL1	5.70	5.92	5.61
MIL2	5.94	5.92	5.02
MIL3	5.74	5.92	4.82
MIL4	5.67	5.92	4.76
MIL5	6.12	5.92	5.19
MIL6	6.18	5.92	5.26
MIL7	5.58	5.92	4.66
MIL8	9.71	10.65	-
MIL9	9.77	10.65	-
MIL10	10.21	10.65	-
MIL11	9.96	10.65	-
MIL12	11.14	10.65	-

As can be seen in table 10, the magnetic moment has been calculated for all 12 core samples. The expected magnetic moment for the iron-based MILs is 5.92 and 10.65 for the dysprosium-based MILs, the experimental values vary between samples but could be accredited to difficulty in physically manipulating and preparing samples. For example, with the iron-based MILs, the spin only formula can be used as a way of confirming structure as the value of n should be 5; equating to 5 unpaired electrons. Reasons for deviations from this value could be dilution resulting in a value lower than 5 which can be seen for MILs 3, 4 and 7. However in general, the results found for the iron based MILs agree with those of the experimental literature.[73]

For the dysprosium-based samples, there is more fluctuation in the magnetic susceptibility results. Dysprosium was used to further boost magnetism and by comparison with their iron based counterparts this has held true with expected and actual magnetic moments having larger values agreeing with that of the literature.[84] However there is no way of using the spin only formula as

dysprosium makes use of 5 unpaired f electrons as well as contributions from the orbital angular momentum. From the dysprosium samples there are only 2 samples with values close to the expected value from the literature, MIL 10 and 12, the others all have values below. This could be down to difficulty handling the samples causing physical errors, for example the high viscosity samples being difficult to handle and transfer to the Evans tube to be measured or even impurities present in the preparation of the MILs.

As mentioned previously in this thesis, the obvious competitor to an MIL as a sealant is a ferrofluid. In a paper by Iacovita *et al*, the magnetism of different sized nanoparticles are investigated in various ferrofluids.[85] Traditionally the magnetic moment is reported in Bohr magnetons which is the magnitude of the magnetic dipole moment of an electron orbiting an atom, to convert the values of the samples in this report into Bohr magnetons, Avogadro's constant, the relative molecular mass and the value of 1 emu/g must be taken into account. The results can be seen below in table 11.

Table 11 Conversion of magnetic moment into Bohr magneton

Sample	Magnetic Moment /erg G^{-1}	Bohr Magneton /emu g^{-1}
MIL1	5.70	94.56
MIL2	5.94	84.49
MIL3	5.74	76.14
MIL4	5.67	83.12
MIL5	6.12	73.42
MIL6	6.18	74.67
MIL7	5.58	65.42
MIL8	9.71	54.74
MIL9	9.77	44.69
MIL10	10.21	60.46
MIL11	9.96	46.54
MIL12	11.14	50.29

When relating chemical structure of the MIL samples to the Bohr Magneton data, it can be deduced that increasing the molecular weight reduces the Bohr Magneton value. This is to be expected since the conversion takes into account the RMM of the sample. The reason for converting these values was to then compare with a typical value for a ferrofluid. In the paper by Iacovita *et al* magnetic hysteresis loops are performed for the large and small Fe_3O_4 magnetite nanoparticles with values of 75 and 82 Bohr Magnetons.

Even when using the lower value of 75 to compare with the MILs in this report, only 4 samples have a value higher, those being MILs 1-4, with MILs 1-3 possessing lower molecular weight $FeCl_4$ as opposed to $FeCl_3Br$ or $Dy(NO_3)_6$. However, even with the samples that show values higher than the lowest ferrofluid value, when completing a visual test with a laboratory grade magnet at best there is only a small visual change where the meniscus of the liquid moves towards the magnet; whereas with the ferrofluid there is obvious attraction with manipulations easily being executed with the magnet.

Further to this, a commercial ferrofluid was acquired and subjected to the Evans balance method of quantifying the magnetic moment in erg G^{-1}. There was an assumption made for this method, this being that the carrier solvent was not taken into account for the RMM of the sample so it was assumed the ferrofluid consisted only of Fe_3O_4 which will cause a large overestimate. For the rest of the calculation, this gave a value for the magnetic moment as 34.4 erg G^{-1}. With this value it can be seen that it is still over 3 times larger than the highest magnetic moment acquired for the MILs in this work, however due to the assumptions made as stated the value could be lower if the concentration of Fe_3O_4 in solvent was known. Taking this value further, when converting it for Bohr Magneton data, which again takes into account RMM we get a much larger value of 830 emu/g for the ferrofluid. Although again this number is extremely large in comparison to the values reported in table 11 with assumptions made for chemical composition the data does demonstrate that the MILs have much lower magnetic susceptibility which can be demonstrated as stated previously with manipulations using a handheld magnet.

This is a major drawback of the MIL samples being tested so far, the anticipated result and the actual result do not align. Meaning that the MILs prepared do not show a sufficient magnetic response to a magnet where the anticipated result was easy manipulation of the ionic liquid with a standard magnet. The process of the IL acting as a sealant was to hold the IL in place with a magnet to create a seal to effectively reduce the pressure in the vacuum.

With this work so far, it is clear that the MIL samples are unlikely to be able to function as a sealant through the use of a magnet. More work needs to be completed in this area, which will follow later in this report to boost the magnetism and start behaving like the traditional ferrofluid consisting of purely magnetic nanoparticles and solvent where the resulting liquid can be easily manipulated using a standard grade magnet.

3.1.4 Lubricity Evaluation and Analysis

3.1.4.1 The Coefficient of Friction and related studies

As the main focus of this project is to produce a lubricant, testing is required to analyse this property. The easiest method to characterize lubricity is to measure the coefficient of friction (COF).

The COF is a dimensionless scalar value which describes the ratio of the force of friction between two bodies and the force pressing them together, a key factor in this is that the COF value is relative to the materials in use.[86] The COF has two distinct parameters which are the coefficient of static friction and the coefficient of dynamic friction. Static friction is the friction between two or more solid objects that are not moving relative to each other and are in a rest position; whereas dynamic friction comes into effect when the mating surfaces are in motion. The latter will be investigated in these tests using the following formula:

$$\mu = \frac{Frictional\ force\ (F)}{Normal\ Force\ (N)} \quad (10)$$

To take this experiment further, it is possible to prepare Stribeck curves which are graphs that show how the COF changes with respect to changes in velocity on the testing rig. All of this data will be measured using a UMT Tribolab with an aluminium ball pressed against a reciprocating steel plate, with the lubricants sandwiched in-between. A basic figure showing the set up can be seen below in figure 18 with the aluminium ball and steel plate represented in black, and the sample lubricant in yellow. Typically, a reciprocating test (which was used in this work) or a pin on disc test can be used to determine COF values. In this work, due to equipment limitations the reciprocating test was used; however in future work perhaps a pin on disc may have better resembled the pump the lubricant is going to be used in due to a constant motion of the rotary vanes turning. However, reciprocating tests can still offer valuable data to compare samples and gain an understanding of how they might perform.

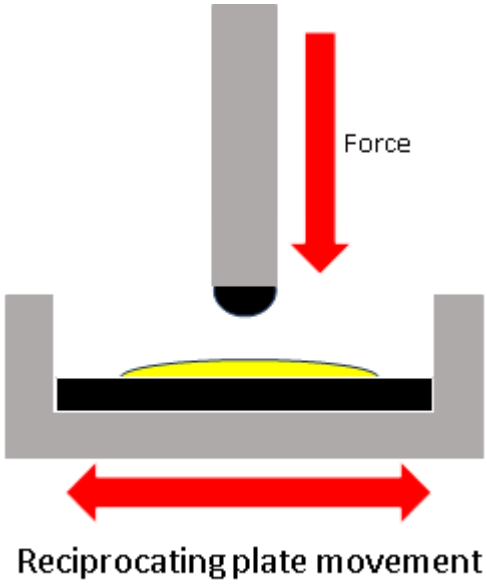

Figure 18 Diagram of the cross section of the UMT Tribolab used to measure COF values, showing the ball represented in black on the grey cylinder pressing down at a specified force whilst the steel plate represented in black sitting in the grey container reciprocates back and forth at a specified Hz. The test sample is represented in yellow and is placed between the two contacts

Initially, the UMT Tribolab was set up using test criteria based on an ASTM D2783 standard test method which is used for extreme-pressure properties of lubrication fluids. This used a force load of 400N set with a reciprocating plate at 20 Hz, with the test running for 15 minutes at room temperature, where the test was repeated three times. An average COF was determined and can be seen below in table 12.

Table 12 Initial mean COF values measured

MIL	Mean COF
Dry	0.2879 +/- 0.031
MIL1	0.1666 +/- 0.005
MIL2	0.1428 +/- 0.003
MIL3	0.1489 +/- 0.003
MIL4	0.1743 +/- 0.011
MIL5	0.1537 +/- 0.003
MIL6	0.1532 +/- 0.007
MIL7	0.1550 +/- 0.003
MIL8	0.1516 +/- 0.006
MIL9	0.1444 +/- 0.005
MIL10	0.1507 +/- 0.006
MIL11	0.1527 +/- 0.005
MIL12	0.1524 +/- 0.006
Fomblin	0.2196 +/- 0.010
Leybonol	N/A

There were two controls used in this method, one being Fomblin (Leybonol was unavailable at the time of testing) and the other being a dry sample where no lubricant was used. A low COF value indicates a good performance, with a low value being relative to the control sample being used. As expected, the dry sample showed the highest COF value as there was no lubricant present to reduce the friction caused by the two surfaces rubbing together; the next highest value was for the Fomblin with values of 0.2879 and 0.2196 respectively.

All of the MIL samples produced values lower than the two values previously mentioned. When analysing MILs 1-3 it can be seen that increasing the alkyl component on the imidazolium cation reduces the COF value, this is also true for MILs 4 and 5 where a decrease in value also correlates with an increase in chain length for the alkyl component. When comparing these two sets of MILs, it

could be suggested that the $FeCl_4$ anion performs better than the $FeCl_3Br$ as it has lower values for each comparative pair i.e. MIL1 versus MIL4 and MIL3 versus MIL5.

MIL6 and 7 are both based on the pyridinium cation but 7 has a substituted methyl group at position 3 on the pyridinium ring, this has a negligible effect on viscosity values and here there is also a negligible effect with very similar values for the mean COF.

The dysprosium samples possess large variations in their viscosity values, yet when being evaluated for a COF value the numbers do not vary substantially. For example, MIL 8 and 9 have dynamic viscosity values of 104 and 358 respectively yet their mean COF values are 0.1516 and 0.1444. As is known, the dysprosium MILs have 3 equivalents of cation per anion but MILs 8 and 9 have the same cations as 1 and 3, and 4 and 5. When comparing these values collectively the dysprosium MILs give slightly lower values for COF suggesting they are the most desirable samples thus far. The COF values for MILs 10, 11 and 12 also show mixed results, the lowest value COF here is for MIL10 which is the short chain pyridinium cation versus long chain and methyl substituted long chain cations. The dynamic viscosity values vary greatly here with values of 47, 706 and 105 respectively but given the magnitude of variation here there appears to be little effect on COF values with them all being on a similar scale.

Overall the lowest values in this test were for MILs 2, 9 and 3 in descending order.

Using a surface profilometer, also provided by the Henry Royce Institute, analysis of the wear scar left on the steel plate was completed after the COF values were determined. This provided further information on how the samples were performing, where a shallower wear scar depth would be suggestive of a better performing lubricant. The results can be seen in table 13.

Table 13 Measured wear scar depth using a surface profilometer

MIL	Estimated Deepest Point /micrometres
Dry	39.27
MIL1	34.89
MIL2	33.42
MIL3	38.32
MIL4	38.93
MIL5	37.14
MIL6	33.78
MIL7	41.67
MIL8	37.68
MIL9	35.51
MIL10	33.51
MIL11	37.36
MIL12	38.14
Fomblin	37.56
Leybonol	N/A

From the results in table 13, the wear scar depth reported is the estimated deepest point in the scar. The values vary from 33 up to 42 micrometres with potentially misleading data; for example, the dry sample wear scar depth is reported as 39.27 micrometres though one would expect this to have the deepest wear scar as there is no lubricant reducing friction, especially since that test had previously recorded the highest mean COF. However this is not the case, the deepest wear scar point is reported for MIL7. Furthermore, Fomblin, one of the control lubricants has a wear scar depth of 37.56 micrometres, this is lower than some other values of wear scar depth despite having the second highest value for mean COF. The lowest COF values came for MILs 2, 9 and 3 but the wear scar depth data only correlates with MIL2 which did achieve the shallowest wear scar however again for MILs 9 and 3 their wear scar depth values are mixed.

In figure 19, 3D maps have been produced showing a detailed view of the wear scar for each sample, in addition to this in figure 20, 2D maps of a cross section of the wear scar have also been produced for each sample.

Using all of this data, it can be seen that there is a definite groove in the plate, with material being worn away and deposited around the outside of the wear scar. The 2D maps of the cross section perhaps give a better indicator of wear, using the reasoning that the flatter the bottom of the wear scar could correlate with more wear on the spherical ball. This is because in an ideal situation, there would be no wear but since there is, it should be a non-flat scar whereby the flatness of the bottom of the wear scar suggests more vigorous wear on the ball being used to produce the data. An example of an ideal wear scar cross section can be seen in MILs 6 and 7 with well rounded scars vaguely resembling a spherical ball, whereas the MILs 4 and 11 show the extreme wear with very flat bottoms suggesting the aluminium ball being used in the test has been heavily worn along with the coupon, with a flat bottom arising from heavy abrasive wear.

However, the 2D map may not be telling the whole story, one limitation of the 2D map versus the 3D map is that the 2D map is only scanning one line of the wear scar so they may not be scanning the deepest point unlike the 3D map which operates under a grid function. Though one drawback on the 3D map is that the colour coordination can be difficult to interpret on a low quality image however when teamed with the 2D cross section, thorough analysis can be completed.

Dry, Fomblin

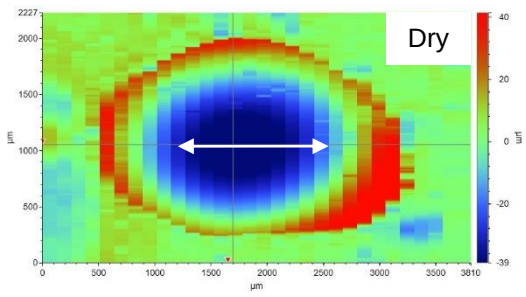

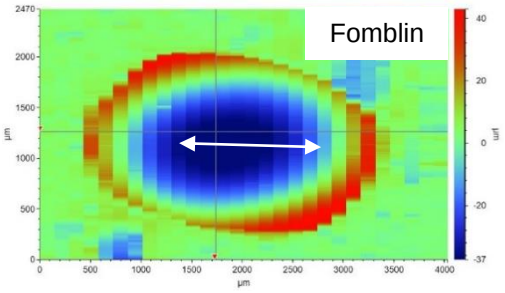

MIL1-3

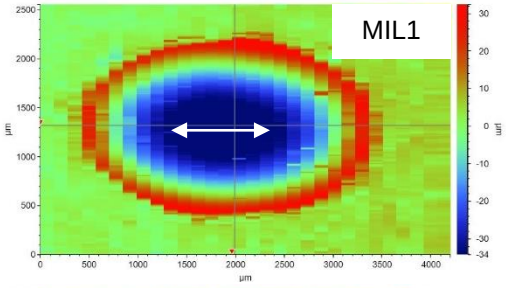

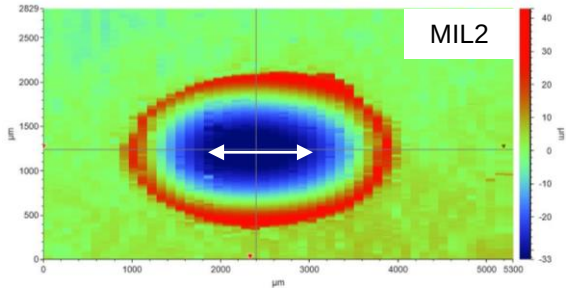

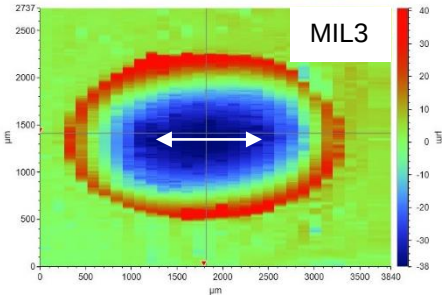

MIL4-5

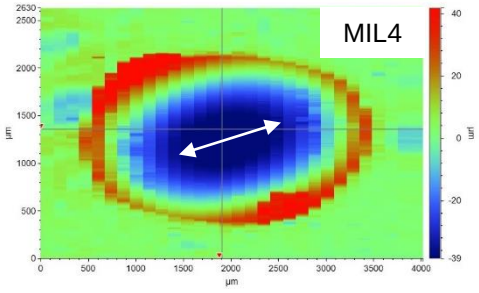

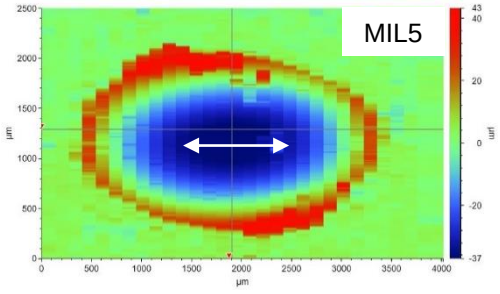

MIL6-7

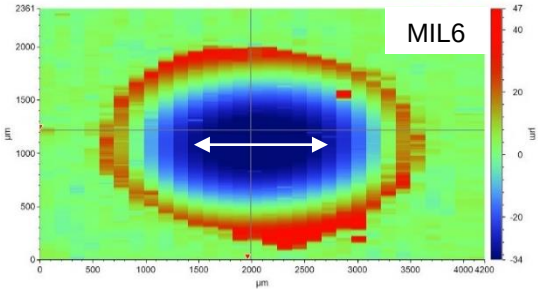

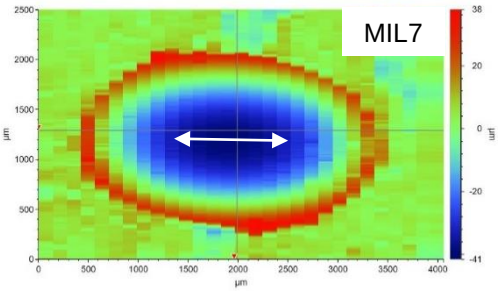

MIL8-9

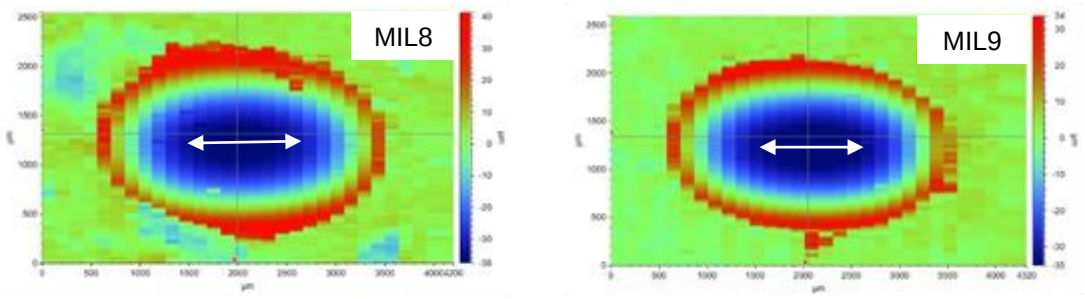

MIL10-12

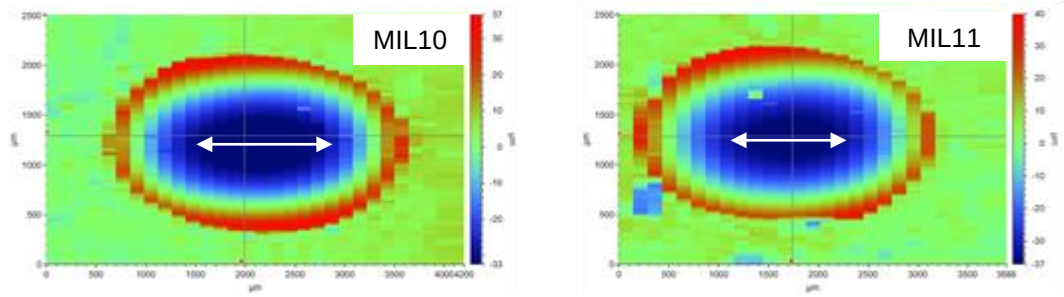

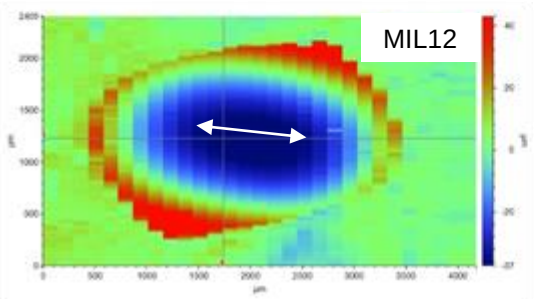

Figure 19 3D maps of the wear scar created on initial COF measurements, with white double headed arrow showing direction of reciprocation

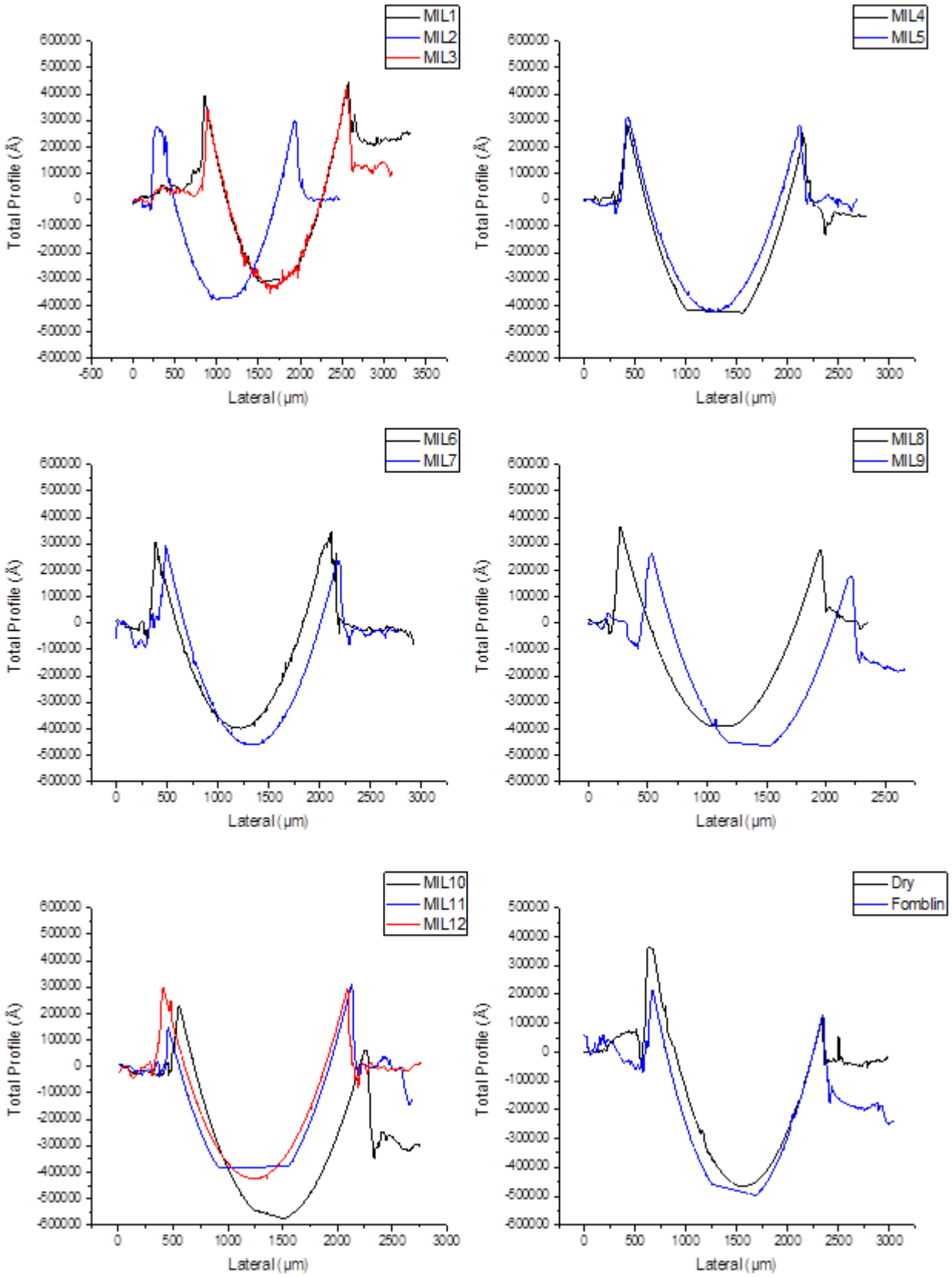

Figure 20 2D diagrams of the wear scar created during calculation of initial COF values, taken as a cross section of the shortest distance across the wear scar, not across the length of the wear scar where reciprocation took place

To build on this work, following further discussion it became apparent that the test settings applied were too aggressive. This was because the wear scars were very prominent with the 2D and 3D wear scars. Both methods showed a considerable amount of the test surface being displaced at either end of the wear scar where the reciprocating motion was taking place; irrespective of lubricant sample being used. Even for Fomblin and Leybonol, deep grooves were seen suggesting initial load forces were too strong, and the softer aluminium ball was also being abrasively worn. Examples of these heavily worn wear scars can be seen below in figure 21.

Figure 21 Steel coupon showing aggressively worn wear scars, resulting from initial test settings

Taking inspiration from a recent publication using the same instrument, new settings were applied to acquire COF values; as well as produce a Stribeck curve for each sample to gain a deeper understanding on the lubricating properties.[36]

The new settings made use of ramped measurements; starting at 0.1 Hz up to 20 Hz under a constant load of 5N and each step lasting 3 minutes. As anticipated, the COF value varies with the speed of reciprocation, where selected results can be seen below in table 14.

Table 14 Mean COF values at specified Hz, using new test settings

Sample	Mean COF at specified Hz						
	0.1	0.5	1	6	10	16	20
MIL1	0.2264	0.2011	0.2046	0.1278	0.1203	0.0995	0.0870
MIL2	0.2332	0.1537	0.1371	0.1109	0.1015	0.0924	0.0812
MIL3	0.2585	0.1762	0.1488	0.1003	0.0886	0.0833	0.0789
MIL4	0.1847	0.1651	0.1717	0.1160	0.1063	0.0979	0.0904
MIL5	0.1434	0.1366	0.1411	0.1056	0.1024	0.0973	0.0857
MIL6	0.1538	0.1415	0.1540	0.0898	0.0863	0.0900	0.0846
MIL7	0.1420	0.1522	0.1521	0.1037	0.0890	0.0852	0.0846
MIL8	0.4390	0.2566	0.2245	0.1262	0.1079	0.0999	0.0923
MIL9	0.1677	0.1311	0.1215	0.1012	0.0973	0.0925	0.0866
MIL10	0.4157	0.2220	0.1867	0.1019	0.0869	0.0868	0.0919
MIL11	0.2646	0.1354	0.1241	0.0980	0.0944	0.0890	0.0847
MIL12	0.1926	0.1437	0.1302	0.1042	0.0952	0.0915	0.0901
Fomblin	0.1789	0.1770	0.1674	0.1614	0.1582	0.1400	0.1187
Leybonol	0.1776	0.1627	0.1504	0.1354	0.1334	0.1189	0.0988

In table 14, selected COF values have been selected at specified reciprocating speeds. Below in figure 22, Stribeck curves have been produced following a conversion of firstly Hz into RPM by multiplying by 60. In this work, because of the reciprocating motion of the test, first to convert RPM into radians per second RPM is multiplied by 2π/60, and then again this value is multiplied by the stroke length which was 4 mm on the UMT tribolab to get a linear velocity of mm/s.

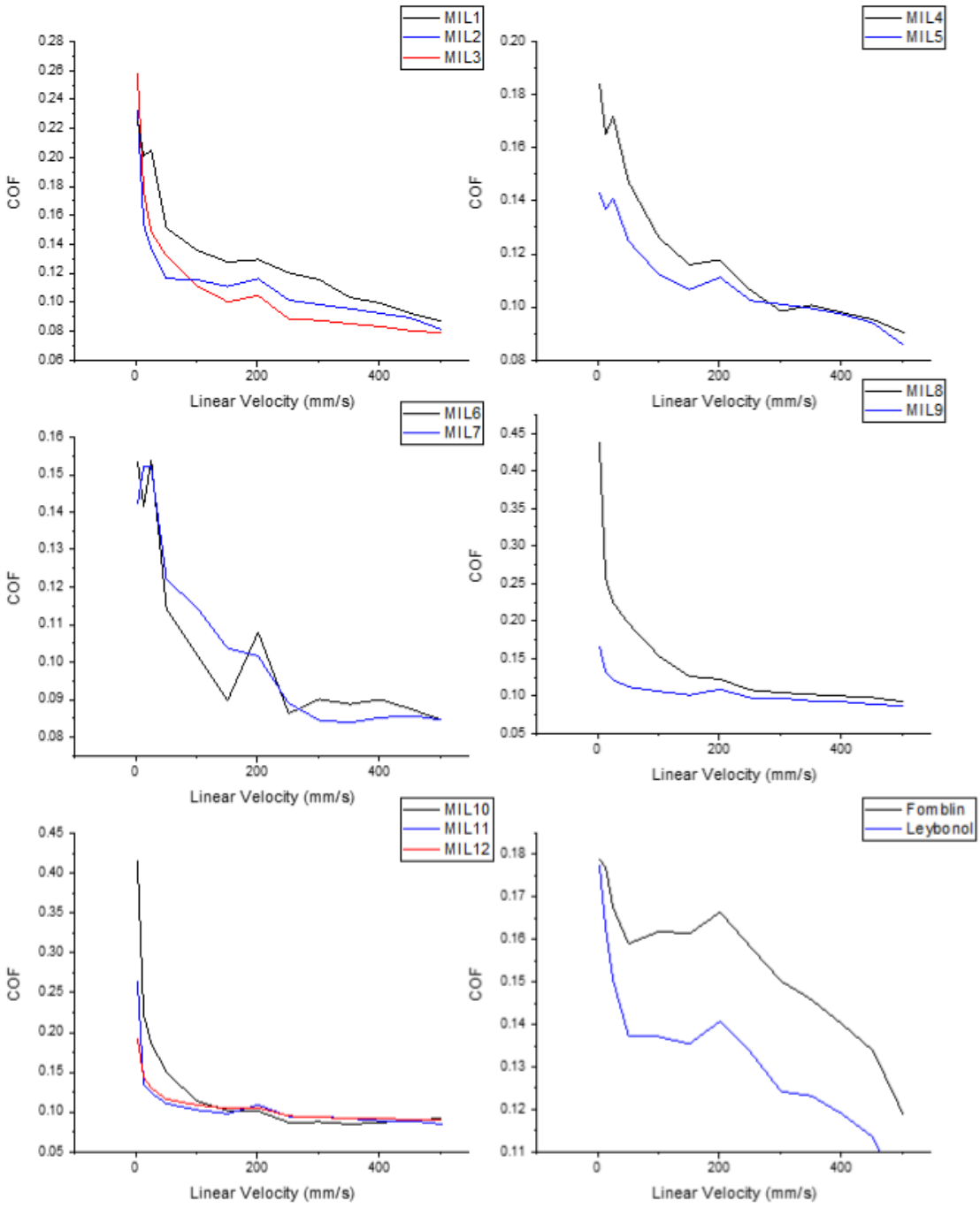

Figure 22 Stribeck curves produced for each sample on the updated test settings, featuring a 5N load force and reciprocation from 0.1 Hz to 20 Hz

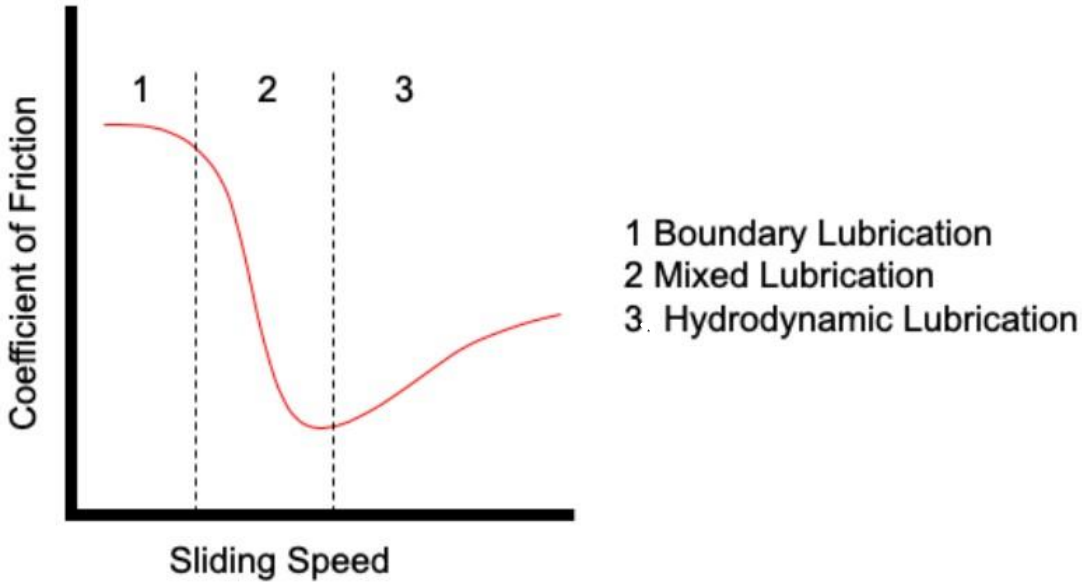

Figure 23 Typical Stribeck curve with regions depicted by 1, 2 and 3

In figure 23, a typical Stribeck curve can be seen. In the figure, the y-axis is denoted as the COF but there are two options for the x-axis. This can be sliding speed (also known as velocity) as shown in the figure, or it can be a calculation involving speed multiplied by viscosity all divided by the load force being used in the experiment. Furthermore, the curve can be split into three regions based on the type of lubrication that is occurring. Initially, at a high COF in region 1 this is known as boundary lubrication. At this point, the two surfaces that are looking to be lubricated are in contact resulting in a high coefficient of friction. As the curve progresses into region 2 known as mixed lubrication, the COF begins to decrease. This happens because there is now a lubricant present allowing for better lubrication, however, as the name of the region suggests there is a mixed component occurring meaning that there is some separation between the two contact points but also still a small amount of asperities in contact. In region 3 of the Stribeck curve, the COF value begins to increase again. In this region the two contacts are fully supported by the lubricant with zero asperities in contact, because of this it might be hypothesized that the COF value should reach a steady state however in practice there are still factors influencing the COF. The main factor being the viscosity of the lubricant being tested, whereby a lubricant with a high viscosity will result in an increase in the COF compared with a lubricant with a lower viscosity.

Typically, Stribeck curves are acquired using a pin on disc tribometer; whereby two variables are fixed (load and viscosity) and the third component, velocity, is varied over a suitable range so that the contact interface goes through all the regions expected on a Stribeck curve. In the pin on disc tribometer this is easily achieved as the speed at which the disc rotates can be varied. However due to limitations on equipment available, in this work the Stribeck curve was acquired using a reciprocating mode, which meant it can be difficult to develop enough velocity over a long enough stroke length before reversal to reach region 3 of the curve; below in figure 24 is an example of Stribeck curves acquired using a reciprocating test.[87]

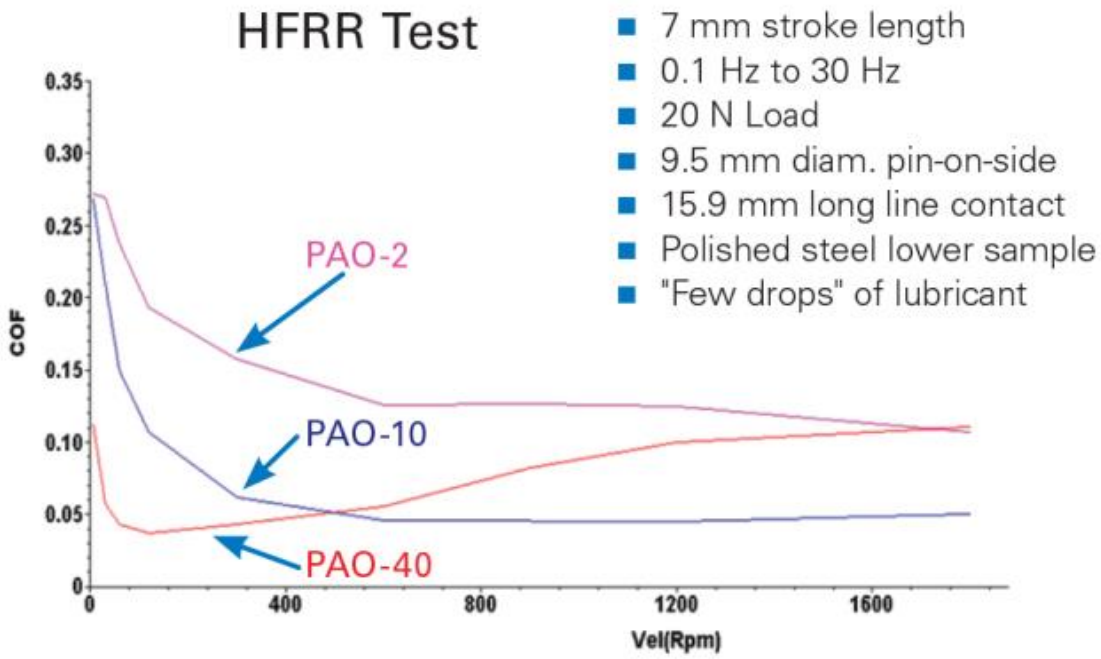

Figure 24 Example Stribeck curves using the same test method as this work, taken from the reference in text[87]

In the figure, three curves can be seen with PAO referring to poly alpha olefin and the number referring to the viscosity in cSt at 100 degrees along with test settings using to acquire the curves in a high frequency reciprocating rig (HFRR) test. The load force used is 20 N whereas in the experimental work completed in this work the force used was 5N, as stated previously the experimental curves can be seen above in figure 20.

In the figure, a curve has been produced for each of the MIL samples and each of the controls. It can be seen that generally the Stribeck curves produced using the UMT Tribolab look similar to the example given in figure 22. At the onset of

the test all of the MIL samples show a high COF value for boundary lubrication followed by a decline typical of mixed lubrication until a take-off point is reached, the take-off point being the point on the graph where there is a notable change in COF value, believed to arise due to the transition from mixed lubrication into hydrodynamic. But after this point, unlike a stereotypical curve the COF value continues to either decrease or plateau in the region, whereas in conventional terms the COF value would actually begin to increase and then level out due to the two surfaces being supported fully by the lubricant with the viscosity of the lubricant becoming the main factor. The increase in COF value is related to the viscosity where a high viscosity sample would see a greater rise in COF before levelling out when compared with a lower viscosity sample.

The control samples, which are known as well performing lubricants possess curves which do not differ much in COF though a vague stereotypical curve can still be seen despite the minor fluctuations in COF (when compared with the MIL samples which have a wider range of COF values at each step).

When interpreting the ionic liquid curves, it can be seen that for MILs 1-3 when the curves begin to plateau the effect on alkyl chain length appears to be more evident; with the increase in alkyl chain length resulting in an overall lower COF. Work which has already been proved with the standard test method.

Furthermore, this phenomenon can also be seen for the other MILs. For example, with MILs 4 and 5 the COF has small fluctuations but generally continually decreases until the test is done. With MILs 8 and 9, after a high initial COF for MIL 8 they both appear to reach a steady COF value with the higher speeds showing a more constant COF value, still with MIL 9 (the long chain counterpart) having a lower value. For MILs 10-12 again after high initial COF values once the test has progressed they all show a stable line with small differences in COF value.

The curves produced for MILs 6 and 7 are more erratic, there is still a take off point but perhaps the test should have been reproduced, although in a similar vein to the control lubricants because the range of COF values are relatively close together it results in a larger fluctuation to the curve perhaps giving the impression the work is worse than it is.

All of the samples show a take-off point at a speed of 480 RPM, below in table 15 the values have been tabulated. The most obvious differences which can be seen in both the curves and the table values is that the control samples show a much higher value of COF relative to the ionic liquids. This take off point is important because it acts as the barrier between mixed and hydrodynamic lubrication. As stated previously, for hydrodynamic lubrication where the load is fully supported by the lubricant, the value of COF is then governed by physical properties of the lubricant with the most important being the viscosity.

Table 15 COF values at the take off point from the Stribeck curves at 480 RPM

MIL	COF Value at 480 RPM
MIL1	0.1046 +/- 0.0064
MIL2	0.1162 +/- 0.0054
MIL3	0.1295 +/- 0.0095
MIL4	0.1178 +/- 0.0071
MIL5	0.1112 +/- 0.0052
MIL6	0.1080 +/- 0.0112
MIL7	0.1016 +/- 0.0068
MIL8	0.1223 +/- 0.0073
MIL9	0.1088 +/- 0.0054
MIL10	0.1012 +/- 0.0048
MIL11	0.1090 +/- 0.0079
MIL12	0.1055 +/- 0.0047
Fomblin	0.1664 +/- 0.0047
Leybonol	0.1408 +/- 0.0048

In the literature, the first paper that produces Stribeck curves for ILs came in 2003.[88] In this paper the curves were acquired using a different method to those used in this work, whereby a steel ball on steel disk was used. This enabled the speed to be slowly increased where the slide to roll ratio was kept constant. This method is perhaps better due to a constant slide to roll ratio as opposed to a stop start reciprocating test used in this work. The curve produced uses speed as the x axis similar to this work, with the results also showing similar curves. In their curve the two control samples which are of the PAO type show much

higher initial COF values which then decrease and plateau to similar values as the ILs. The two ILs being tested were imidazolium-based cations with fluorinated NTf_2 and PF_6 anions. The overall shape of their curves matched that of the dysprosium-based MILs in this work. In their discussion of the Stribeck curves produced, with the little difference between their curve shapes, they show that there is no preferential boundary lubrication of the ionic liquid on the surfaces but with their structural differences under high pressures the ILs and the PAOs may produce differences on how they stack together.

In a literature search, this was the only paper to attempt to produce a Stribeck curve of an IL neat, the following discussion discusses the use of ILs as additives in other base oils.

Following on from the discussion on the previous paper, the next paper published with respect to ILs and Stribeck curves came in 2016.[36] In this paper, phosphonium type ILs were investigated as additives in varying mass percentages in a commercial base oil referred to as YUBASE. The additives were also compared with a traditional oil additive zinc dialkyldithiophosphate (ZDDP). The tests were completed using the reciprocating ball on plate test that was used in this work, with very similar test settings of 0.1-30 Hz under a constant load of 5N for a duration of 5 seconds with steps of 2 Hz.

In the Stribeck curves produced, the IL additives appear to effectively reduce the COF value at every percentage tested. Again, the curves produced are similar to those found in this work with a high onset of initial COF which decreases and then plateaus. There is no in-depth discussion found in this paper for reasoning of these results other than ‘all mixtures perform better than the base oil’ however they do discuss XPS data which will feature further in this report.

In a follow up paper published in 2019, the same two phosphonium based ILs are analysed as additives in a PAO type lubricant; though this paper utilized a 30N load value and a mini traction machine to produce Stribeck curves at 4 different temperatures.[89] In addition to this, as well as producing Stribeck curves utilizing the traction coefficient (a derivative of the COF which is produced from friction between the ball and rotating disk on the mini traction machine) they

also produced electrical contact resistance (ECR) plotted against entrainment speed. For all of the lubricant samples tested, in the hydrodynamic region of the curve, the traction coefficient reduced which was explained due to a reduction in the lubricant viscosity and subsequently in the lubricant film thickness. However in the mixed regime the inverse occurred with an increase in temperature resulting in a higher traction coefficient due to contact between the two lubricated surfaces; furthermore coupling this data with the ECR plots, as expected a decrease in ECR leads to a higher traction coefficient due to the increase in asperities contact from boundary and mixed lubrication regimes. Further papers published in this area utilizing ILs as additives have found similar results whereby in general the IL additive results in a lower COF or traction coefficient.[90-94]

Of the samples tested, it appears that MILs 8-12 show better Stribeck curves than the iron-based MILs 1-7. Whereby better means showing a more stereotypical curve, which can then be used to elucidate how the lubricant may perform, whereby comparing these experimental curves to curves produced by industry standard lubricants it would be hoped a close comparison would be suggestive of a greater success when in operation of a real pump; this can be backed up with comparison to the example curves given in figure 22, more specifically curves PAO-2 and PAO-10. Although with respect to boundary, mixed and hydrodynamic lubrication, all of the curves show the transition from mixed to hydrodynamic at the same speed as stated previously.

As is known, MILs 8-12 have a different structure to MILs 1-7 not only in elemental composition but also in general formula whereby the dysprosium samples have 3 cations per anion as opposed to the 1:1 ratio found in the iron-based samples. These 3 cations then suggest there could be 3 alkyl chains contributing to lowering the COF through physical adsorption on the surface or alternatively because of the different chemical compositions of the anions more beneficial tribochemical reactions could be happening at the surface interfaces resulting in a tribofilm which positively affects COF values.

3.1.4.2 XPS and IR analysis as a result of COF studies

One method of analysing chemical composition of ILs in general is using XPS. This has already been briefly mentioned in a previous chapter for bridged dicationic species of IL. What will now follow is an in-depth analysis comparing pre and post wear samples to gauge if there is any difference in chemical composition that is suggestive of physical or chemical changes in the MILs.

The same approach as the previous chapter is applied here, whereby accepted models have been applied to the C1s region of the MIL samples with the imidazolium based cations having a 4 component model and the pyridinium based cations utilizing a 3 component model.[27, 28, 30, 65]

XPS provides two methods of analysis with respect to lubrication studies, the surfaces being lubricated can be analysed themselves to deduce whether a tribofilm has been formed to prevent further wear. This would be accomplished by scanning the region which was subject to wear and determining what elements can be found at the surface and their chemical states to help give an informed decision on the composition of the protective tribofilm. A tribofilm being a protective layer that forms during wear testing as a result of tribologically stressed surfaces. Alternatively, and what is going to be applied in this work is pre wear spectra of the MIL samples compared with the post wear counterparts to determine any obvious or subtle changes in the spectra. This could be the presence of new elements or a change in state of an existing element.

For a change in state this would be most obvious in the carbon region whereby the model utilized in the pre wear sample no longer fits the same sample which has been subjected to wear testing. An example of an obvious source of change could be carbon debris from the tribological testing being present in the MIL sample as adventitious carbon, which would then alter the ratios of the model resulting in a change of spectrum.

To begin this work, first presented are the C1s spectra of the samples before wear testing, showing the models applied with each component representing a carbon environment present in the structure. For the imidazolium-based cations they have been charge corrected following work by Sauer, and the pyridinium cations have been charged corrected following work by Licence.[30, 95]

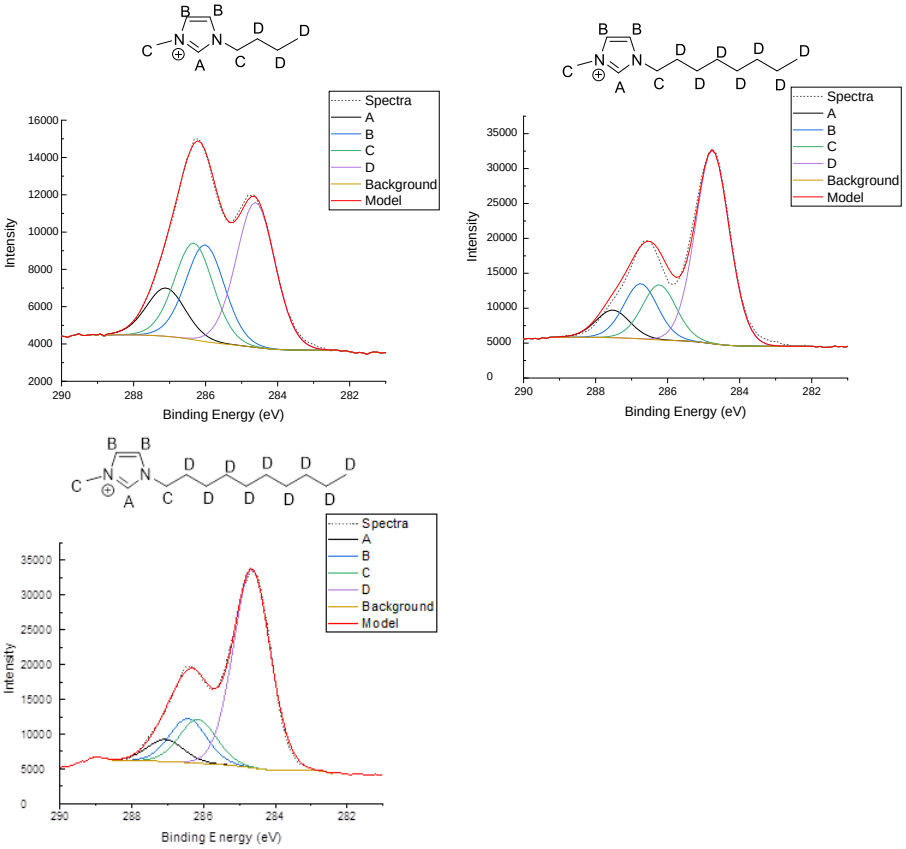

Figure 25 C1s model for MILs 1-3, showing overall model fit in red and the spectra in the dashed line

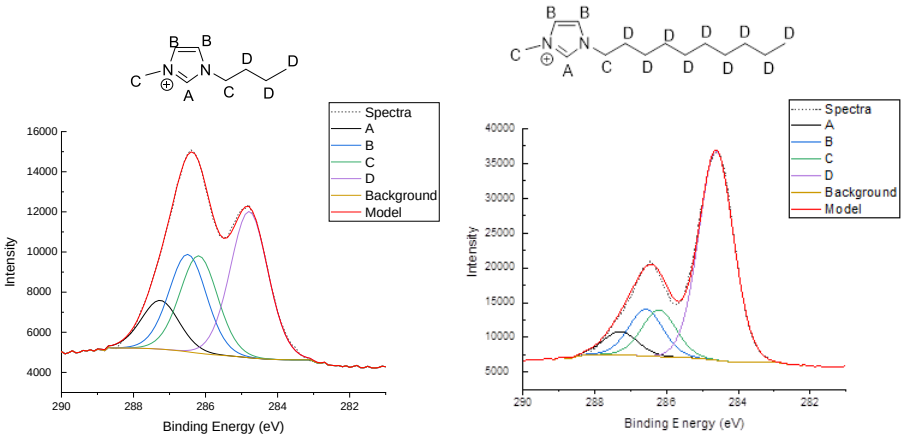

Figure 26 C1s models for MILs 4 and 5, showing overall model fit in red and the spectra in the dashed line

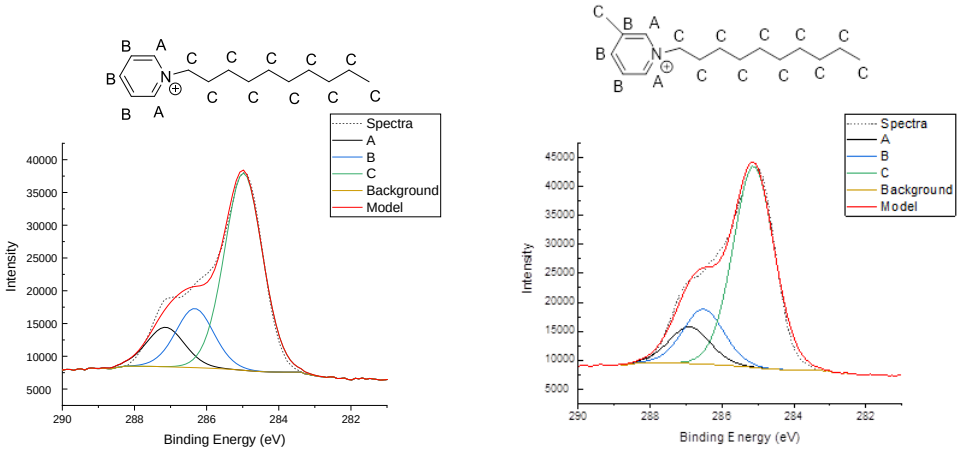

Figure 27 C1s models for MILs 6 and 7, showing overall model fit in red and the spectra in the dashed line

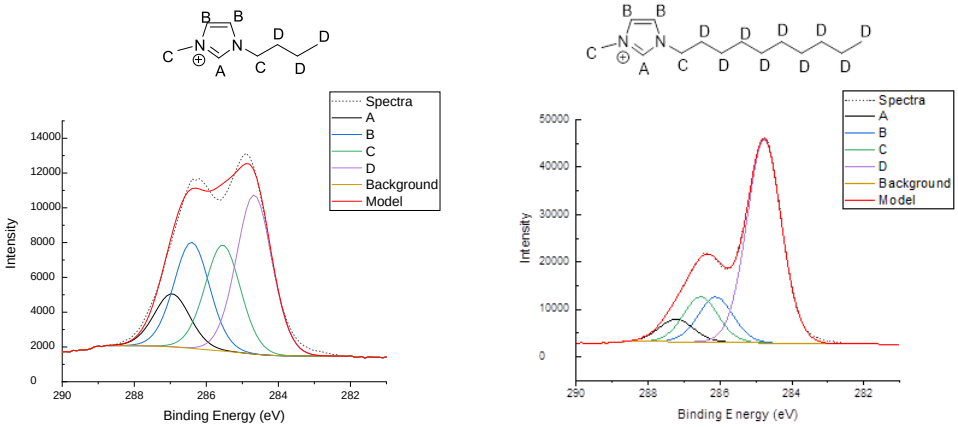

Figure 28 C1s model for MILs 8 and 9, showing overall model fit in red and the spectra in the dashed line

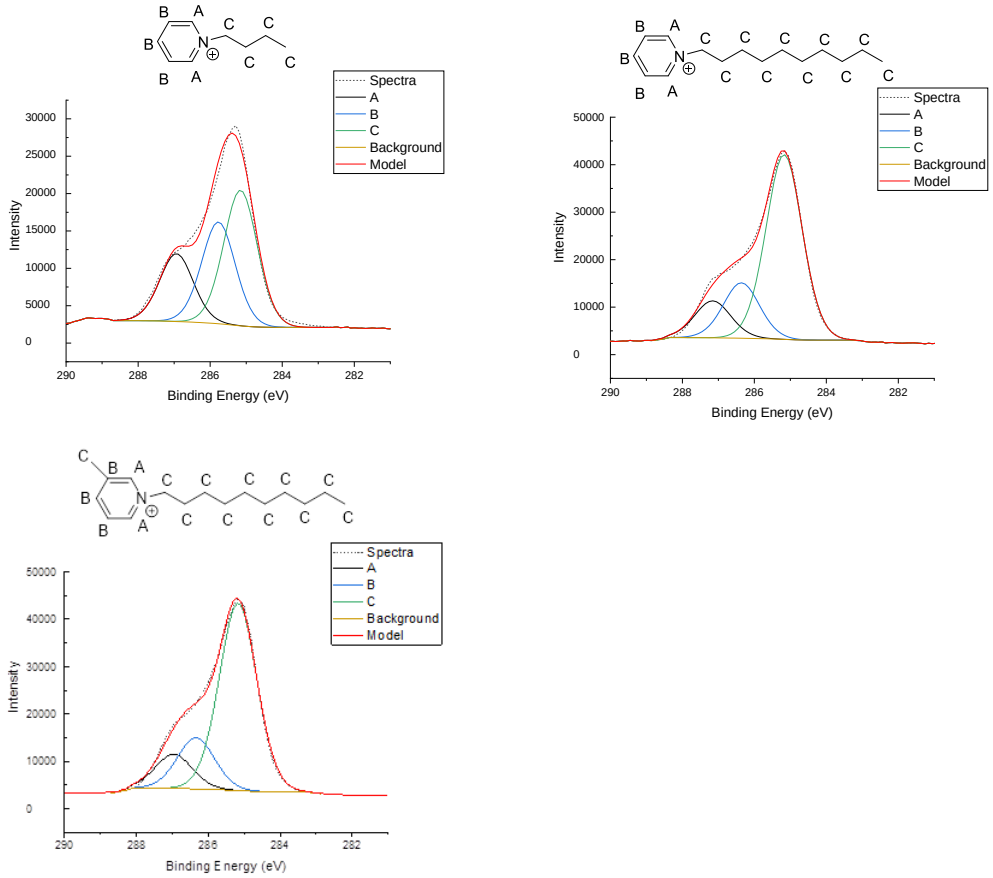

Figure 29 C1s model for MILs 10-12, showing overall model fit in red and the spectra in the dashed line

As can be seen in figures 25 to 29 the carbons in each sample have been labelled and assigned to different components in the XP spectra. For the imidazolium-based cations, proven rules have been applied whereby the carbon between two nitrogens within the imidazolium ring appears at the highest binding energy, followed by the two remaining carbons which are bonded to each other and a nitrogen. There are two sets of aliphatic components, the 2 aliphatic components bonded to the nitrogens on the ring and finally the aliphatic chain bonded to itself, and the carbon bonded to the nitrogen. This fitting procedure has been backed up extensively in the literature; however, for the pyridinium-based cations a different approach has been taken. This is to build on the previous chapter whereby a new fitting model was introduced to accommodate for bridged dicationic moieties. Therefore, there are only 3 components in this model as opposed to potentially 4 or 5 due to the nature of more components always resulting in a better fit whereas the aim is to have the most robust model.

For this model, the three components are aromatic carbons bonded to nitrogen, 2 in each sample and appearing at the highest binding energy. Followed by aromatic carbons within the pyridinium ring for a total of 3. This could have been split further to accommodate for carbons bonded to carbon versus carbons bonded to nitrogen but it was decided against. The final component is the aliphatic component which covers the carbon atoms in the alkyl chain which varies for each sample; again this could have been divided up further to accommodate for carbons bonded to the nitrogen in the pyridine ring, as well as for the methyl substituted samples where there is a carbon bonded to the aromatic carbons in the pyridine ring.

Overall, as can be seen by the figures the overall model fits closely to the spectra. With this in mind, the C1s post wear spectra will be presented as an overlay of the original spectra, this allows for comparison in the carbon region as a first port of call for potential tribochemical reactions.

Below in figures 30, the normalised C1s spectra of pre and post wear samples for MILs 1, 4 and 8 overlayed on each other are presented. Other spectra can be found in the appendix.

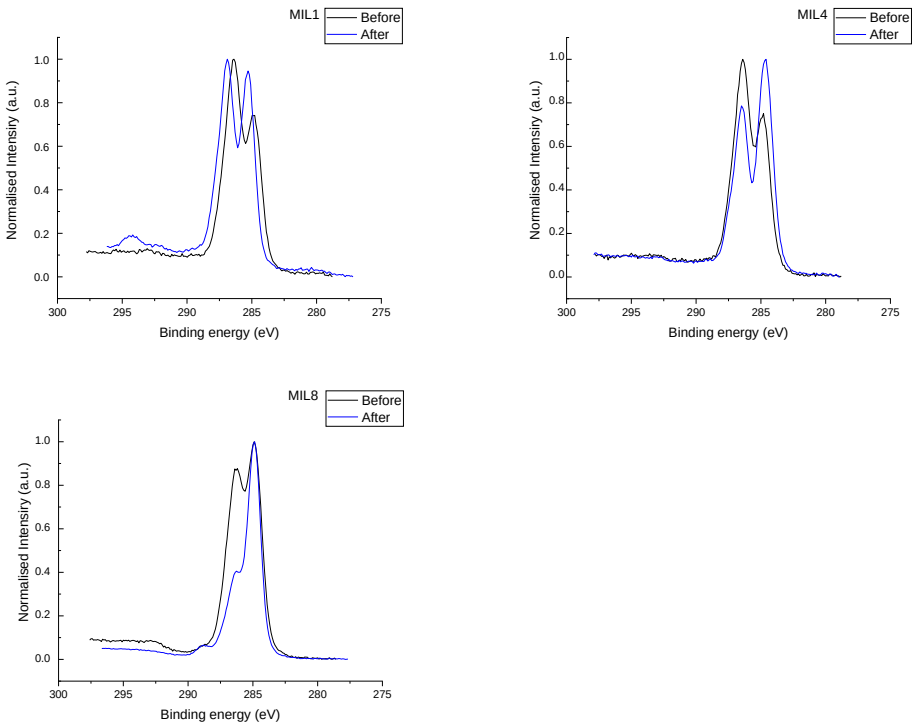

Figure 30 Normalised C1s spectra of before and after wear testing for MILs 1, 4 and 8 which showed the biggest differences in relation to the other samples which can be found in the appendix

As can be seen by the figure and spectra in the appendix, there are some subtle differences in the C1s normalized spectra, charge corrected to their respective N components. The most obvious differences in spectra occur in MILs 1, 4 and 8. These correspond to MILs with the same cation, C_4C_1Im with each of the different anions.

For MIL1, there has been an overall shift to a slightly higher binding energy as well as an increase in peak intensity for the lower binding energy peak which is typically attributed to an alkyl component. For MIL4, there is also a slight overall shift in the spectra though this time the shift is to lower binding energy though again there is an increase in peak intensity for the aliphatic component. For MIL8, there appears to be no shift in overall peak position but again the aliphatic component has increased dramatically in intensity.

Further analysis of the C1s spectra has been completed whereby the two obvious peaks for aromatic and aliphatic component have been converted to ratios using a 2 component model (1 component for each peak), this two component model has then been repeated for the post wear sample and the ratios of each can be seen in table 16.

Table 16 Table showing left vs right peak ratios before and after wear testing

MIL	Pre-wear			Post-wear		
	High BE %	Low BE %	Ratio H/L	High BE %	Low BE %	Ratio H/L
1	65	35	1.86	58	42	1.38
2	38	62	0.61	39	61	0.64
3	38	62	0.61	39	61	0.64
4	66	34	1.94	43	57	0.75
5	35	65	0.54	36	64	0.56
6	43	57	0.75	42	58	0.72
7	43	57	0.75	40	60	0.67
8	54	46	1.17	31	69	0.45
9	39	61	0.64	39	61	0.64
10	37	63	0.59	33	67	0.49
11	40	60	0.67	37	63	0.59
12	38	62	0.61	36	64	0.56

This data further indicates the greatest amount of change in spectra is occurring in MILs 1, 4 and 8.

In an attempt to characterize the changes, survey spectra data has also been compiled, what will follow is an overlay of survey spectra for pre and post wear samples. The purpose of this is to identify any changes that may arise from more intense peaks or new peaks caused from new elements being present.

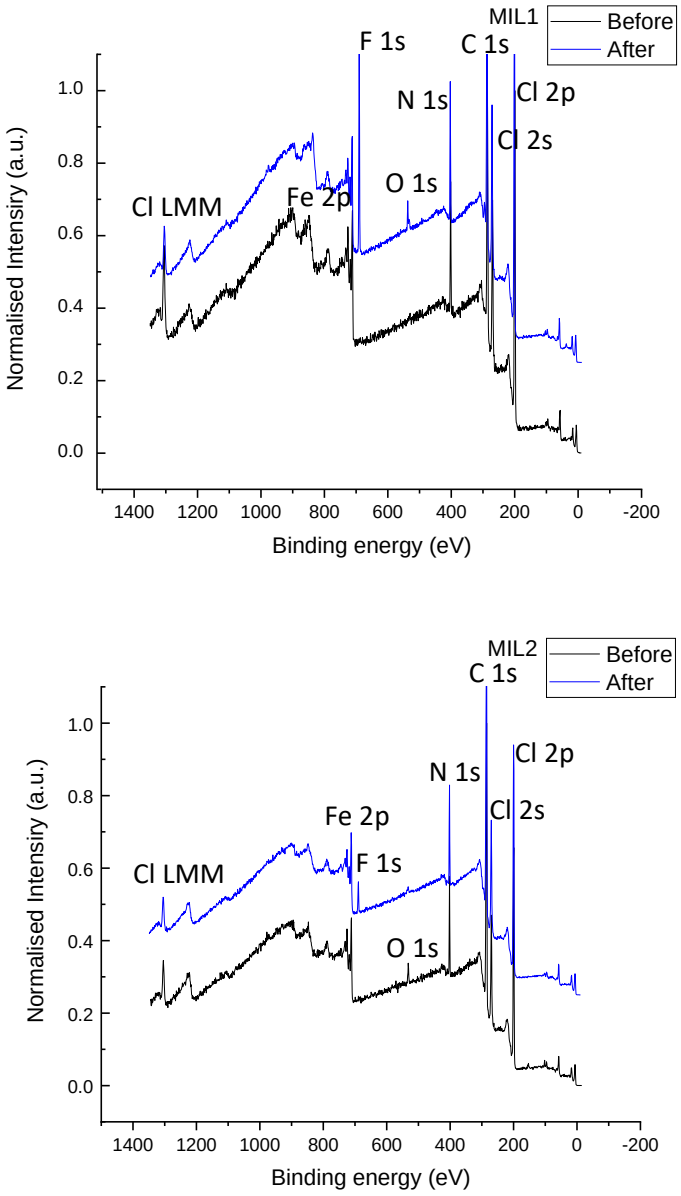

Figure 31 Normalised survey spectra for MILs 1 and 2 showing before and after wear testing, a new fluorine peak can be seen in the after spectra for both samples

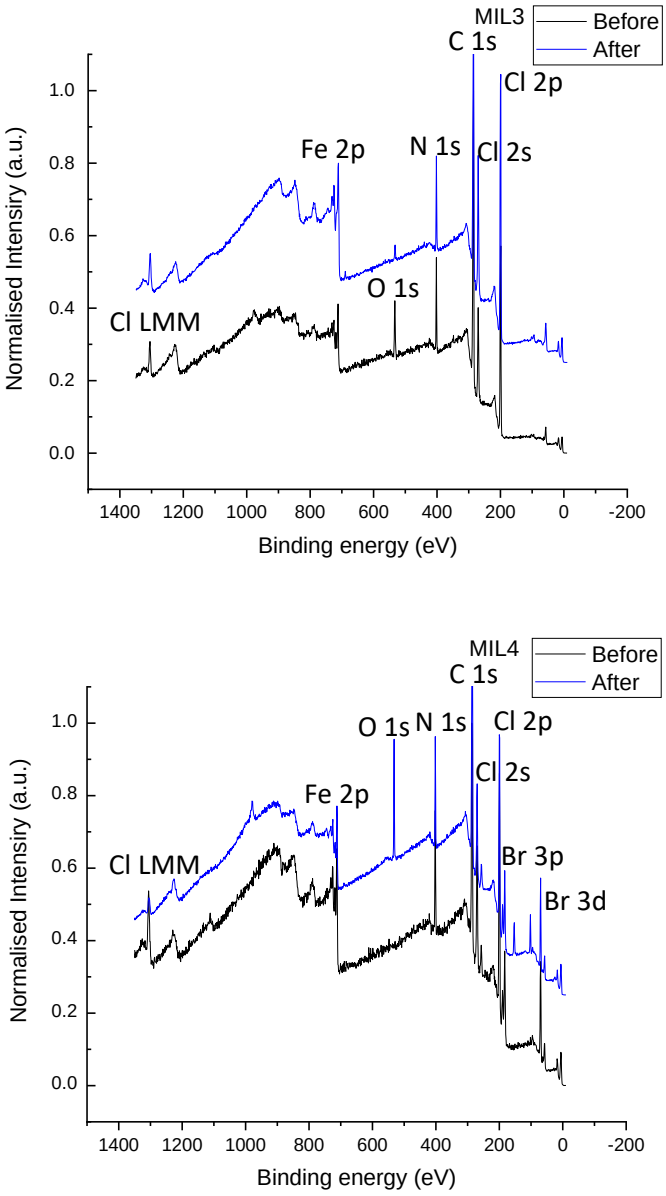

Figure 32 Normalised survey spectra for MILs 3 and 4 showing before and after wear testing, a new oxygen peak can be seen for the after spectra for MIL4

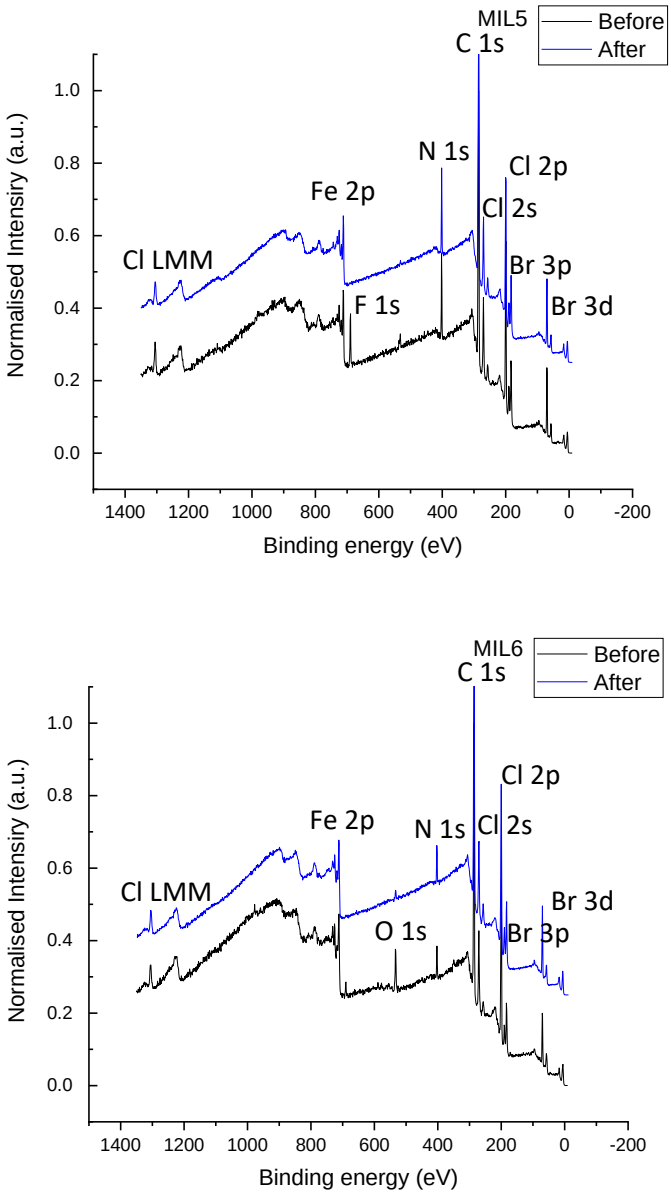

Figure 33 Normalised survey spectra for MILs 5 and 6 showing before and after wear testing, fluorine can be seen in the before specra of MIL5

The normalized survey spectra can be seen above in figures 31 to 33 and the appendix for further survey spectra. The most notable changes can be seen with new peaks present for oxygen in samples that previously contained none and fluorine peaks present in a mix of samples. This is primarily seen in the iron-based samples, with the dysprosium-based samples showing little difference in before and after wear testing.

An obvious O1s peak can be seen in the post-wear spectra of MILs 1 and 4 with minor O1s peaks in the pre-wear spectra of 2, 3, 5 and 6. Interestingly in the latter MILs the peak intensity decreases. Oxygen is inherently present for the

dysprosium-based samples that containing nitrate groups so the difference spectra will show little difference with respect to O, further analysis will continue with high res scans of this area to analyse full width half maximum (FWHM) values.

Furthermore, fluorine present in the post-wear spectra is presented as an F1s peak. This can be seen in the post-wear spectra of MIL 1, 2 and 3 in decreasing amounts respectively and a minor peak seen in MIL 8. Fluorine can also be seen in the pre-wear spectra of MILs 5 and 6. Seeing fluorine in the post wear samples could be due to inefficient cleaning between test samples. This is because the control lubricant Fomblin was used first which is a fluorine containing lubricant; as stated in the introduction this substance is difficult to handle and due to being used first this could be the cause of contamination. Between each test the coupon was washed with acetone, perhaps the reason for no contamination in the latter samples because the acetone washes were cleaning the coupon each time progressively removing the residual contamination from Fomblin from the first run.

Presence of fluorine in the pre wear samples is difficult to explain though the most likely answer is that it is contamination. Perhaps in glassware or other lab users working with fluorinated materials for example other ionic liquid users preparing fluorinated anions, since the synthesis process does not use any fluorine containing starting materials.

Based on this data, combined with the initial analysis of the C1s spectra also it can be deduced that MILs 1 and 4 are showing data suggestive of degradation or tribochemical reactions. High-res spectra for O are discussed later in this chapter for more in depth analysis as MIL 8 also showed potential degradation or tribochemical reaction though as the sample inherently contains O it is difficult to interpret.

If MIL4 and 8 had contained fluorine in their survey spectra, it may have been tentatively suggested that a carbon/fluorine component may have been formed as a result of wear testing though it is only MILs 1, 2 and 3 that show fluorine in the post-wear survey scans.

A high-res scan of the O1s region will now follow for the dysprosium-based anions, this is primarily to investigate the difference in MIL8 for pre and post wear. This is because it is the same cation as MIL1 and 4 which has already shown potential degradation/tribochemical reaction. If the oxygen region is noticeably different here, it too could back up a potential trend that is forming in that short chain imidazolium cations are potentially unstable with respect to friction and wear.

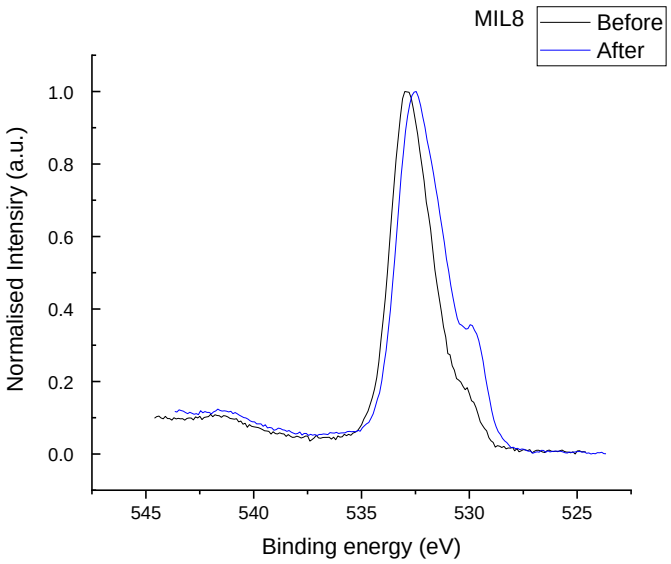

Figure 34 Normalised O1s spectra for MILs 8 showing before and after wear testing, a small shift to a lower binding energy can be seen along with a slight shoulder at lower binding energy

In figure 34, the normalised O1s spectra are shown for the dysprosium containing anion MIL8. The most obvious difference in spectra comes in MIL8, this was the sample that was anticipated to be affected from the wear testing. In the spectra it can be seen that there is an overall shift to a lower binding energy as well as a shoulder which looks to be an extra peak present at lower binding energy, which could be iron oxide. In relation to the other O1s spectra present, MILs 9-12 show very little difference for pre and post wear analysis.

With this data, it can be suggested that the short chain imidazolium cations are the least stable when compared with the others. The task is to now identify the species that could be present.

Another approach to help identify the new components/changes in the pre and post wear analysis is to complete infrared spectroscopy (IR) on the short chain

imidazolium samples MILs 1, 4 and 8. IR could be used to identify functional groups present, the most obvious peak is typically a carbonyl group, other oxygen peaks that could be diagnostic are alcohol and ether groups. In figure 35 below, the IR spectra are displayed.

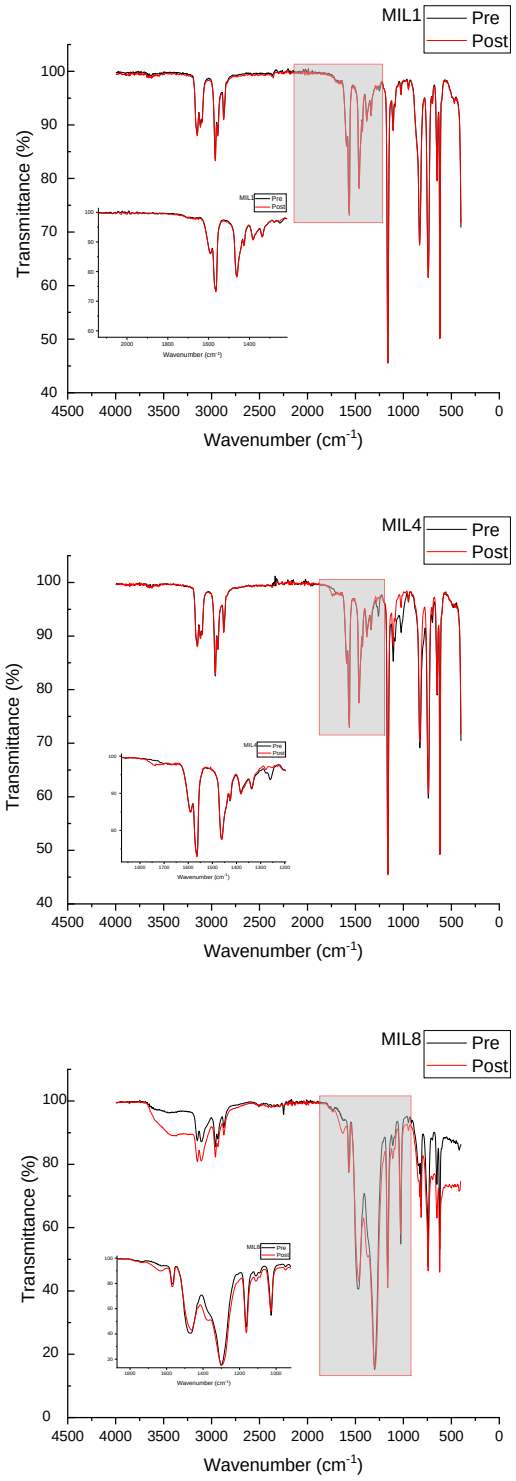

Figure 35 IR Spectra of MILs 1, 4 and 8 showing before and after wear testing, with key subtle differences highlighted in their spectra

IR spectroscopy gives complimentary information to Raman spectroscopy, where to be IR active there must be a change in dipole moment whereas Raman spectroscopy relies on a change in polarizability. To demonstrate the complimentary information, Raman was used to identify the tetrachloroferrate and trichlorobromoferrate anions, in their spectra there were no other peaks present to account for the cation. In the IR spectra presented, there are no peaks for these anions as the frequency is lower than the 'normal' 600-4000 cm^{-1} further to this, the bands that were Raman active are IR inactive due to each of the techniques usually giving complimentary data.

In the figure, it can be seen that the pre and post wear IR spectra are largely unchanged. The only difference is a broad peak in the post wear spectra of MIL8 which is likely to be an OH group from water which is characteristically broad and appears at around 3500 cm^{-1}.

MIL1 and MIL4, as anticipated, show very similar spectra; this is because the only difference is the anion which as previously mentioned is IR inactive resulting in effectively two spectra with the same cation. In the spectra, there are peaks between 2800 and 3150 cm^{-1}. These are likely to be caused by CH stretching of the imidazolium ring, the strong peak at around 1162 cm^{-1} is likely to be caused from CN stretching and the two peaks at 1560 and 1460 cm^{-1} likely to be caused by aliphatic CH bending.[96]

MIL8 has a largely similar spectrum to account for the same cation, however the nitrato groups that arise from the anion are also IR active. In the spectrum, the nitrato groups are likely to be attributed to the strong peaks at 1480 and 1300 cm^{-1} which arise from NO stretching of the single and double bond within the group.

With respect to the literature, generally the approach to the identification of tribochemical reactions occurs by XPS analysis of the wear scar. Due to the method of testing, the steel plates that have been used are too large to fit into the analysis chamber; hence analysis of pre and post wear MIL samples.

With this in mind, there are numerous papers discussing analysis of wear scars. This work has focused on analysis of the MIL, so far it has been seen that short alkyl chain samples are the most likely to undergo decomposition pathways.

With respect to carbon environment MIL1 has seen a shift to higher binding energy with an increase in aliphatic component or transversely a decrease in aliphatic component and an increase in higher binding energy component, as well as a new oxygen peak in the survey spectrum.

With the new oxygen peak, this could be the cause of the shift to a higher binding energy with a new CO bond perhaps being formed, however if this was the case, the same trend would have been seen for MIL4 and 8. With MIL4 and 8 there is no shift in binding energy for the C component but there is an increase in intensity for the lower binding energy aliphatic component. This is typically attributed to adventitious carbon but MIL4 also shows a large peak which is attributed to oxygen.

For MIL8 oxygen is already present in the sample, however upon further inspection of the O1s component for all of the dysprosium-based MIL samples MIL8 is the only sample that shows a difference in O peak. In the post wear sample, the is an overall shift to lower binding energy, with what appears to be a new smaller peak at lower binding energy. A lower binding energy peak could be caused from a new bond to carbon as opposed to nitrogen in the NO_3^- group bonded to dysprosium. Though if this was the case, there would be a shift in the carbon spectra to account for the new CO bond. Upon further inspection as well as the increase in aliphatic component there is a very small new peak which arises at a higher binding energy at roughly 289 eV, but this similar peak is not present for MILs 1 or 4.

In the literature, similar work has been completed on a dysprosium thiocyanate type sample. In this work, a C_1C_6Im cation is used which with respect to this work is a mid-length alkyl component.[97] In this paper, the worn surface is analysed as opposed to the sample itself but there is also no oxygen present in the sample unlike the oxygen containing nitrato groups found in this work. Despite this, in their analysis of the wear scar they have attributed components of the overall O1s peak to iron and dysprosium oxides as well as an iron sulphate and carbon ether type bonds.

To ascertain the new peak found at roughly 289 eV, IR spectroscopy was used to see if there was a characteristic peak present for carbonyls, esters or ethers.

MILs 1 and 4 are largely unchanged but MIL 8 shows a broad peak in the OH region but also a very minor new peak at around 1630 cm^{-1}. This region is very characteristic for a carbonyl but the peak is far too weak to confidently state the presence of one.

What can be deduced thus far in analysis is that the short chain samples are less stable than their longer chain counterparts, with XPS data showing clear differences.

3.1.5 Scale up and test pump trial

In order to carry the project forward, an evaluation of a sample in a live test pump should be completed to get a good indicator on progress being made. Due to time and equipment limitations only 1 sample can be assessed in a test pump.

To decide on which MIL to carry forward to this stage, an assessment of properties thus far shall take place. Viscosity, contact angle, thermal stability, magnetism and COF evaluations have been completed; with two control lubricants present for reference. The most likely sample to be scaled up is one that most closely resembles the control lubricants, in a belief that if similar performance criteria are met at this stage, then it should be a good candidate to carry forward.

Viscosities were the first properties to be assessed, the only sample to have a viscosity that was between the two control lubricants was MIL9, all the other MILs were either lower or higher than Fomblin and Leybonol. With this, viscosity indexes were also looked at, here there were two samples that fell within the accepted range (between the two control lubricants) these were MIL9 and MIL11 with values of 43 and 51 which fell between 7 and 57 for Leybonol and Fomblin respectively.

When looking at contact angles, all of the MILs assessed showed generally larger contact angles than the two control lubricants. Thermal stability also showed comparative results where all the MIL samples were stable up to 300 degrees, the same as the control lubricants.

Where magnetism was assessed, the latter MILs 8-12 containing the dysprosium anion showed more of a paramagnetic response than the iron containing anions of MILs 1-7. Although this property is not to the standard that is required to be able to also act as a sealant, it is still interesting from a lubricity perspective, and so the project will continue to assess their viability.

As a lubricant, COF studies showed that all of the MILs gave COF values that were lower than both of the control lubricants. This is one instance where a value lower and not within the parameters of the two control lubricants is desirable. These lower values were seen in both test parameters (first test with

excessive load force, and second test to produce Stribeck curves). When looking at the Stribeck curves, from a visual standpoint it can be seen that the dysprosium-based anion MILs showed more stereotypical curves where as the test progressed the COF value appeared more stable; all with lower COF values than the two control lubricants.

With lubricity tests came XPS analysis of the samples after being tested. Based on the data it can be seen that the short chain samples showed a lower stability than their longer chain counterparts.

Table 17 Summary of data accumulated thus far on core samples

Sample	Dynamic Viscosity /mPas (Viscosity Index)	Contact Angle /°			Thermal Stability /°C
		Steel	Alum	VFH	
MIL1	46 (138)	64 +/- 1	67 +/- 1	69 +/- 1	>300
MIL2	84 (151)	40 +/- 1	47 +/- 3	61 +/- 2	>300
MIL3	150 (80)	34 +/- 3	24 +/- 4	49 +/- 4	>300
MIL4	36 (138)	50 +/- 1	65 +/- 3	80 +/- 3	>300
MIL5	95 (84)	50 +/- 4	49 +/- 3	59 +/- 2	>300
MIL6	142 (127)	44 +/- 4	36 +/- 5	64 +/- 2	>300
MIL7	145 (79)	40 +/- 2	46 +/- 4	62 +/- 2	>300
MIL8	104 (157)	48 +/- 4	60 +/- 3	79 +/- 2	>250
MIL9	358 (43)	43 +/- 6	40 +/- 7	43 +/- 3	>250
MIL10	47 (191)	71 +/- 2	66 +/- 4	80 +/- 2	>250
MIL11	706 (51)	39 +/- 5	42 +/- 6	47 +/- 3	>250
MIL12	105 (134)	26 +/- 4	38 +/- 5	43 +/- 4	>250
Fomblin	463 (57)	24 +/- 5	29 +/- 6	29 +/- 5	>250
Leybonol	258 (7)	29 +/- 3	24 +/- 5	35 +/- 3	>250

Table 18 Summary of data collected thus far on core samples

Sample	Initial COF	COF at take-off	XPS Stability
MIL1	0.2879 +/- 0.031	0.1046 +/- 0.0064	No
MIL2	0.1666 +/- 0.005	0.1162 +/- 0.0054	Yes
MIL3	0.1428 +/- 0.003	0.1295 +/- 0.0095	Yes
MIL4	0.1489 +/- 0.003	0.1178 +/- 0.0071	No
MIL5	0.1743 +/- 0.011	0.1112 +/- 0.0052	Yes
MIL6	0.1537 +/- 0.003	0.1080 +/- 0.0112	Yes
MIL7	0.1532 +/- 0.007	0.1016 +/- 0.0068	Yes
MIL8	0.1550 +/- 0.003	0.1223 +/- 0.0073	No
MIL9	0.1516 +/- 0.006	0.1088 +/- 0.0054	Yes
MIL10	0.1444 +/- 0.005	0.1012 +/- 0.0048	Yes
MIL11	0.1507 +/- 0.006	0.1090 +/- 0.0079	Yes
MIL12	0.1527 +/- 0.005	0.1055 +/- 0.0047	Yes
Fomblin	0.1524 +/- 0.006	0.1664 +/- 0.0047	N/A
Leybonol	0.2196 +/- 0.010	0.1408 +/- 0.0048	N/A

With all of this data thus far, it can be deduced that a long chain MIL should be used, that showed good viscosity data and ideally a stronger magnetic response. This deemed MIL9 a good fit due to its promising viscosity data along with it utilizing a dysprosium-based anion for a stronger paramagnetic response and good lubricity data.

The initial challenge faced was to scale up the desired sample to the litre scale, where previously the sample scale produced less than 10 mL at 0.06 M. The first scale up preparation was completed on a 0.25 M scale, with this longer reaction times were noted for the first quaternisation step and upon the first anion exchange step replacing the bromide anion for nitrate, an exothermic reaction was observed for the first time. Care was taken in future steps to slowly add the silver nitrate to the reaction vessel to control this exothermic reaction.

Further syntheses were completed on the 0.3 M scale until roughly 800 mL of MIL9 had been prepared in total.

Figure 36 Scaled up sample of MIL9 ready to be added to the test pump, two containers combining multiple smaller scale preparations

3.1.5.1 Early Test stages

To begin the test, the test vacuum pump was taken apart, cleaned using an on-site industrial cleaning machine known as a turbex and then rebuilt. Then the sample lubricant was poured into the relevant parts of the pump, the motor end and non-motor end, where both parts have an oil gauge to ensure the correct amount has been added. With that completed the test pump had a computer plugged in to record vibrational frequencies as the pump was running. Finally, the vacuum pump containing the oil was switched on and became operational. At this point, the pump would be monitored for a month to assess compatibility but the ideal scenario would be that the pump runs without major issues for three months continuously.

Initial issues arose upon assembly of the test pump. Whilst pre-lubing the bearings before being fitted they were left overnight due to time constraints. When returning the next day to finish assembly it was found that the bearings

showed surface corrosion, an obvious red flag. Despite this corrosion, the bearing still functioned and spun freely and it was decided that the test should still go ahead as planned and that analysis on this issue could be completed in tandem to the long term scale up test.

Figure 37 Left showing dismantled pump, right showing pump back together with gears on top and throwers sitting below, outer casing yet to be attached on the side it is standing up on

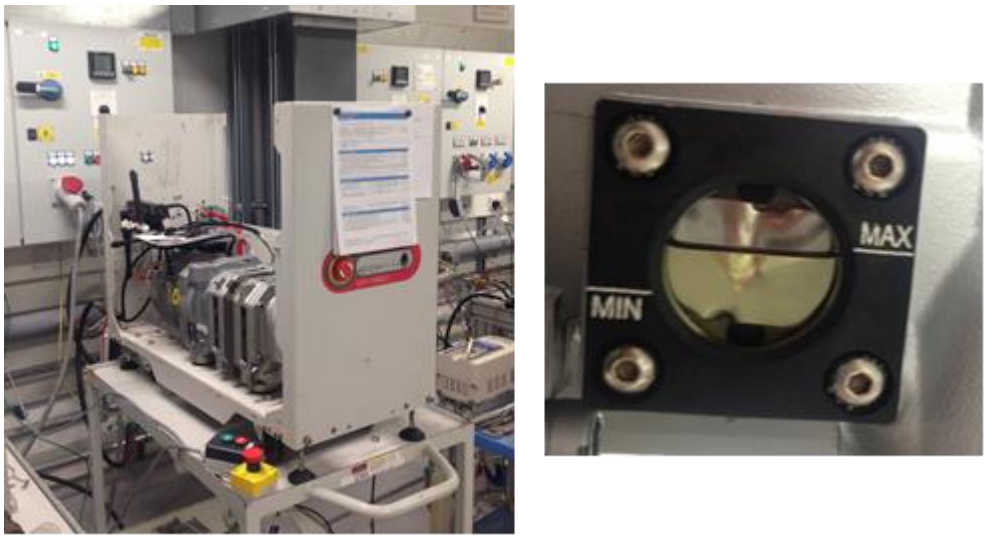

Figure 38 Pump ready to be started on left, right with indicator showing the correct amount of lubricant has been added

Figure 39 Early issue of corroded bearing (right) after being pre-lubed and left overnight

As can be seen in figure 39, on the left is a clean bearing and on the right is a corroded bearing that had been left overnight coated with the MIL sample. As stated in the beginning, all of the pump parts had been cleaned in an industrial turbex cleaning machine and left to dry, there should be no potential contaminants anywhere on the machine. To analyse this issue, first IR spectra were taken of the clean sample and three spots taken from the corrosion residue on the surface of the bearing.

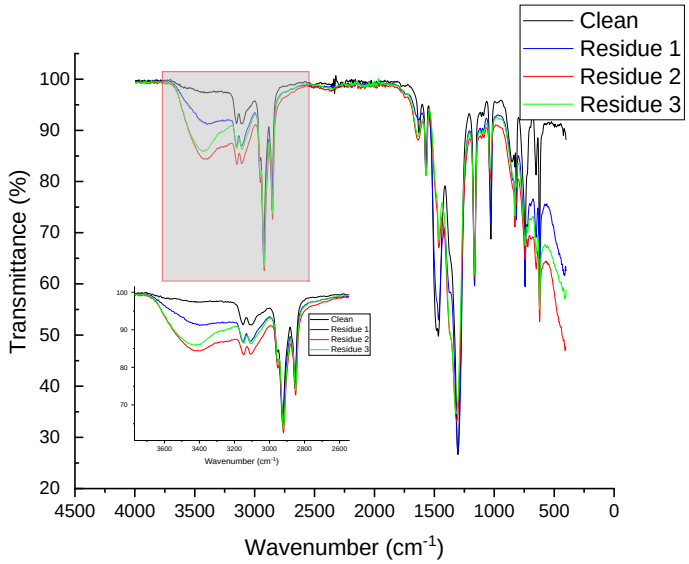

Figure 40 IR spectra of corrosion residues taken from the corroded bearing and the clean sample, key differences highlighted in the spectra

In figure 40, above the fingerprint region, there are no obvious new peaks in the IR spectrum but with the spectra of the residue spots there is a broader peak in the region of 3000 – 3500 cm^{-1} which is suggestive of an OH peak. This is not present in the clean sample which suggests that there could be water in the

residue being analysed, meaning that potentially the bearing was not completely dry when being lubricated ready for insertion into the vacuum pump.

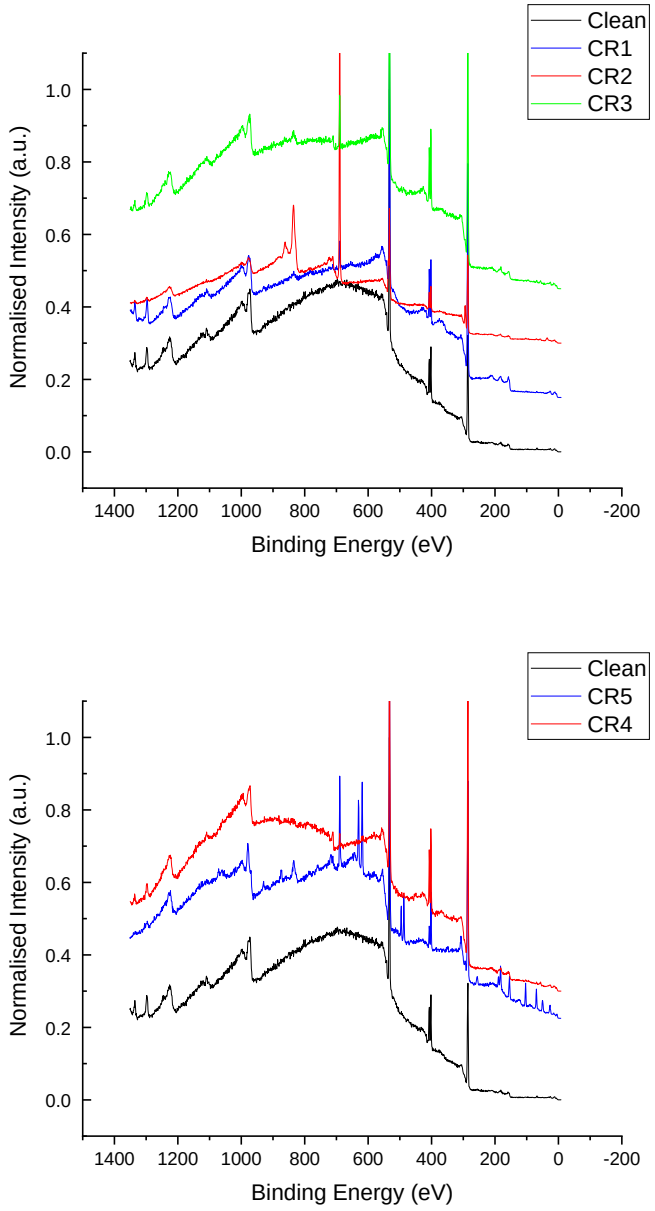

Figure 41 Survey Spectra of the clean sample and 5 residues taken from the corroded bearing, Fluorine present in the residue spectra at roughly 686 eV

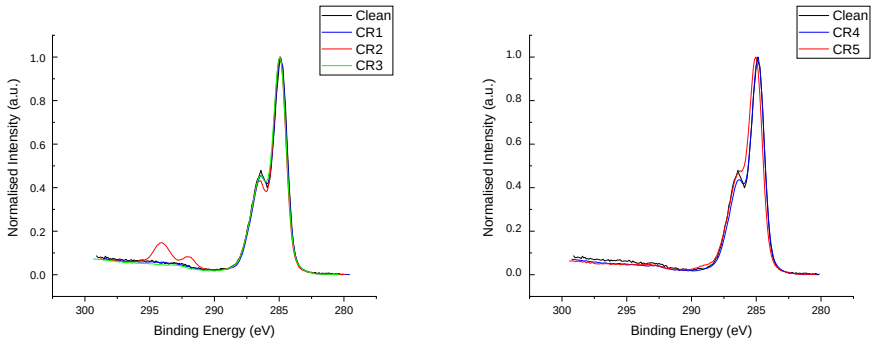

Figure 42 C1s spectra taken from the clean sample and 5 residues taken from the corroded bearing, possible fluorine contamination seen for residue 2

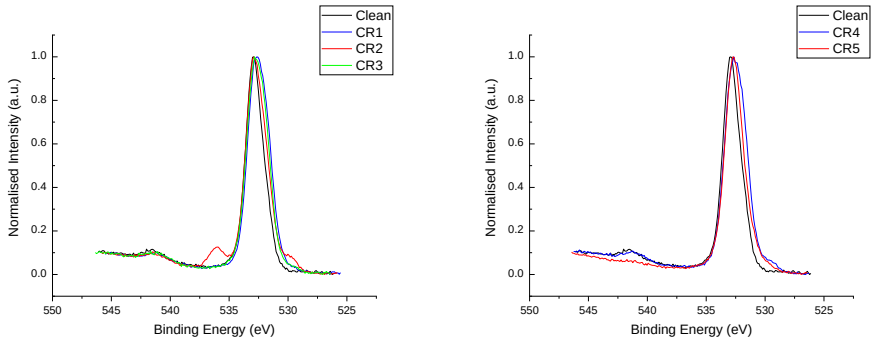

Figure 43 O1s spectra taken from the clean sample and 5 residues taken from the corroded bearing, shoulder peaks seen for residue 2

From the survey scans in figure 41 it can be seen that all of the corrosion residue spots show a peak for fluorine at 687 eV. Further to this, as well as all being charge corrected to nitrogen 1s at 401.8 eV, there are extra peaks also in the carbon region for corrosion residue spot 2 as seen in figure 42. These arise at 292 and 294 eV and are likely to be attributed to CF_2 and CF_3 groups most likely arising from contamination from the original fomblin lubricant which is a PFPE type lubricant. This can be backed up by data in the literature where the common NTf_2 anion which consists of bis(trifluoromethane)sulfonimide consisting of CF_3 groups, arise in the region of 292 to 294 eV.[98, 99] The main peak shape of the carbon environment looks unchanged for each of the spots. With respect to oxygen as seen in figure 43, it is again corrosion residue spot 2 which shows the biggest difference; here there are minor peaks either side of the main peak. The lower binding energy peak at 530 eV could be attributed to metal oxides such as iron oxygen bonds which could be backed up by the fact that this spot also shows peaks in the survey scan for iron. However, spots 2, 3

and 5 all show that iron is present but it is only spot 2 which shows differences in peak shape for oxygen.

As well as this, the higher binding energy minor peak at 536, although very high could be attributed to oxygen fluorine bonds also potentially caused by interactions with residue from the original fomblin lubricant which may not have been cleaned thoroughly.

Upon suspicion that there could still be water residue in the pump which could impair performance when mixed with the MIL; a small test was completed once the machine was running. It was found that when mixing the MIL with water, a gel-like substance formed which can be seen below in figure 44.

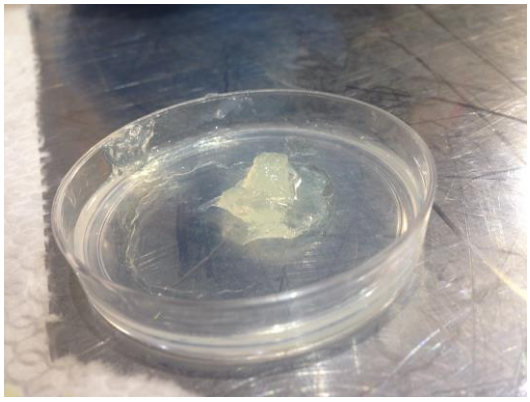

Figure 44 Gel formation upon addition of water to the sample

Upon heating, the gel returned to the original state but nevertheless this could be an early warning sign of potential degradation in the pump where other contaminants could also be present despite industrial cleaning at the beginning. To begin troubleshooting, the pH was tested with litmus paper to ascertain if the gel was acidic, this was in belief that the gel could be formed from nitric acid. However, as anticipated the ionic liquid showed no change with litmus paper due to the lack of presence of acidic protons; furthermore the gel also showed no response to litmus paper. The paper was also tested with hydrochloric acid to ensure it was functioning where it turned red, demonstrating it is a strong acid and the paper worked.

With this, more IR data was acquired, first with the clean sample then with the gel that formed upon the addition of water and then with the sample after it had been dried. Results can be seen below in figure 45.

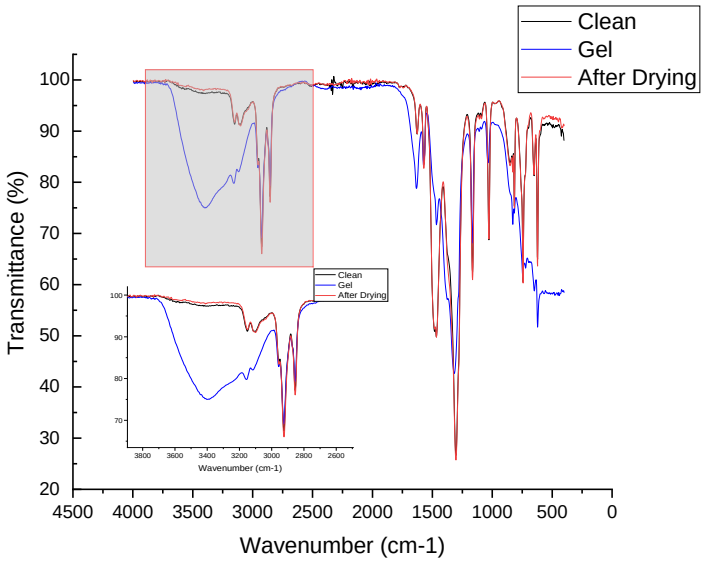

Figure 45 IR Spectra of the clean sample, the gel and the same gel sample after drying

As shown in figure 45, the spectrum for the gel shows a strong OH band typical of water, but the clean and post drying spectra are very similar suggesting that if a reaction is occurring on the addition of water then it could also be reversible. An obvious reaction that could be occurring may be an anion exchange, however if this was the case, as anticipated with the litmus paper it would be thought that a hydroxide ion may replace a nitrate anion and then the resulting nitrate anion could be balanced with the now free proton from the water. But this new species did not affect the litmus paper meaning a different type of reaction must be happening.

Further diagnostic tests were undertaken, two more samples were prepared. These were the same $C_{10}C_1Im$ cation with a single NO_3 anion and an even simpler Br anion. Both of these mixtures also formed a gel upon addition of water before returning to a homogenous liquid. This offers positive news that the magnetic dysprosium hexanitrato anion is not the root cause of the issue.

Further to this, after having the pump run for 24 hours the oil level display showed changes in the ionic liquid appearance. As can be seen in figure 53, compared with the original clear liquid the two displays now appear opaque with an orange tinge. As well as this, the pump leaked a very small amount of sample which was then being replaced back into the pump without stopping the test. This then allowed some of the leaked sample to be analysed to investigate

any differences in the starting sample compared to the leaked sample and its change in physical appearance.

Figure 46 Oil display showing discolouration of lubricant on both gauges of the test pump

As seen in figure 46, each oil display shows the ionic liquid's physical appearance. On the left is the non-motor end showing an opaque liquid and on the right shows an opaque liquid with a more vivid orange colour along with bubbles at the surface.

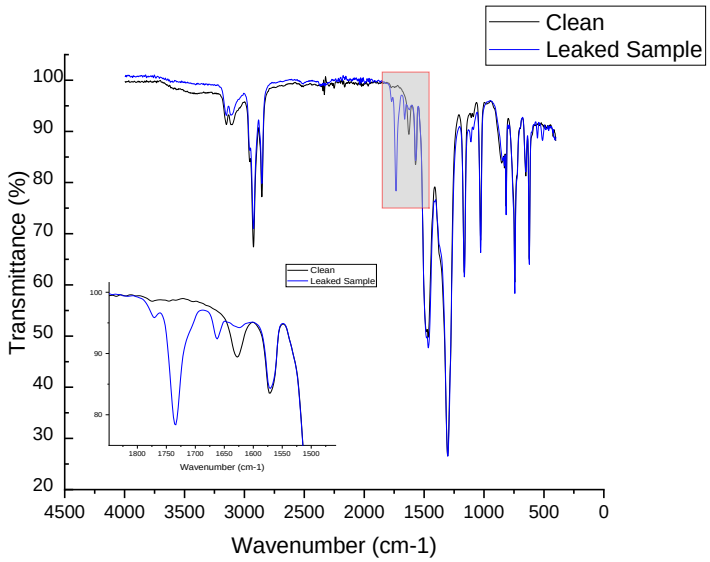

Figure 47 IR spectra of the clean sample and leaked sample, with a highlighted region showing the presence of a new peak for the leaked sample

The IR spectra can be seen in figure 47. The main difference in the spectra is that the leaked sample shows a peak at 1735 cm^{-1}. Typically, this is assigned to a carbonyl stretch however the intensity of the peak is low compared to what is normally a strong diagnostic peak. The reason for its low intensity could be that it is caused by only a small amount of impurity whereas the bulk sample remains unchanged. On the other hand, carbon carbon double bonds typically

arise at 1640 – 1680 cm^{-1}. This is not where the peak has occurred in this spectrum but the intensity of the peak does match a characteristic double bond.

As seen in figure 37, the test pump is shown both dismantled and put together. Typically, the pump will have two different operating temperatures for each end of the pump. The engine end with the gears and throwers which can be seen on the right of the figure, and two rotating shafts where one is pictured on the left of the figure. If this had been a fully operational pump, the engine end would operate at a slightly lower temperature than the other end; this is because the other end is where the compressed gas is being removed under a high amount of pressure which leads to an increase in temperature. For the purpose of this test, there was no vacuum being created, it was purely a lubrication test to ensure the MIL sample can operate as a lubricant. However even in this test, there was a difference in temperature, only this time the non-motor end had a slightly lower temperature because there were no any gases actually being compressed. However as seen can be seen in results presented later in this work, this slight temperature difference has still resulted in two very different outcomes for the lubricant.

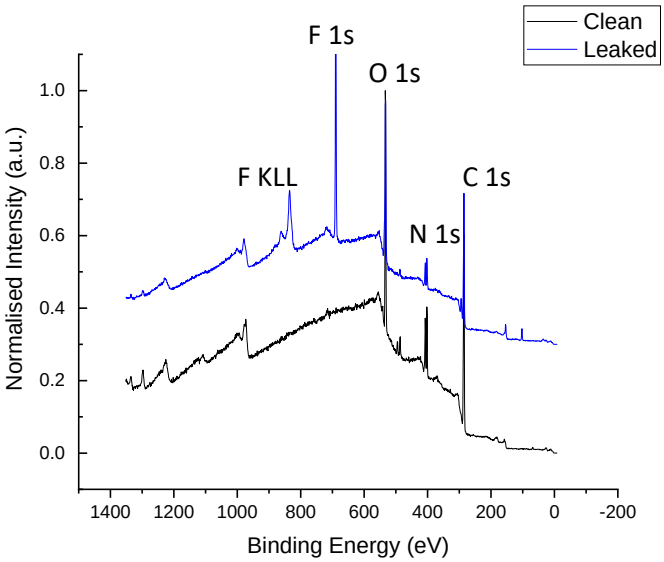

Figure 48 Survey spectra of the clean and leaked sample, the leaked sample showing a new Fluorine peak

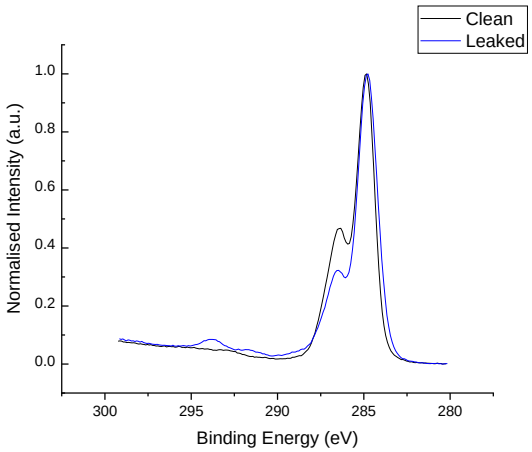

Figure 49 C1s spectra of the clean and leaked sample, the leaked sample showing a minor peak between 293 and 295 suggestive of fluorine

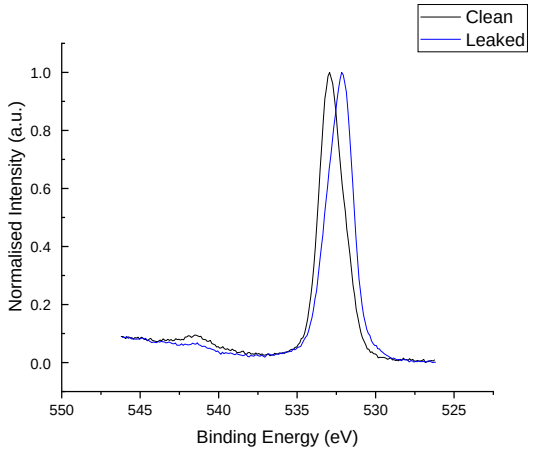

Figure 50 O1s spectra of the clean and leaked sample, leaked sample showing a shift to lower binding energy

Within the XP spectra from figures 48 to 50, it can be seen that in the survey scan there are new peaks at 688 and 834 eV which can be assigned to fluorine 1s and KLL auger peak respectively; this is the main difference between the clean and leaked sample.

Further to this, in the C1s spectra the stereotypical 2 component carbon spectra is seen. Though as seen earlier in this work there appears to be a decrease in the higher binding energy carbon for the leaked sample. As well as this, there are 2 very minor peaks which can be seen between 290 and 295 eV which could be assigned to organic fluorine such as CF_2 or CF_3 groups as stated previously. If this was the case, it could be that left over fomblin in the machine has mixed with the clean IL sample as there is no fluorine found in the IL sample at any stage of the synthesis process.

With respect to oxygen, in the spectra it can be seen that the leaked sample has been slightly shifted to an overall lower binding energy. A shift to a lower binding energy could be caused from a formation of a metal oxide bond, with a source of metal coming from degradation of the surfaces been lubricated or it could also be caused from a carbon oxygen bond.

Due to suspected corrosive properties of the MIL sample that arose from discolouration of the sample in the test pump, as well as analysis of the leaked sample the next stage in the project was to aim for intentional corrosion under controlled circumstances. This meant exposing the sample to various surfaces that would be possible to analyse after corrosion, if it occurred.

Initially, the MIL sample was exposed to metal foil from the laboratory but the sample had no effect. Following this, a piece of stainless steel (alloy unknown) was exposed to the MIL, this also had no effect. This test was repeated again but with piece of steel first washed with hydrochloric acid to clean the surface and remove any potential boundary film. Having completed this, there was still no obvious signs of corrosion caused by the MIL.

Following discussion, 3 further pieces of metal in various alloys were acquired from Edwards Vacuum. All three pieces of metal had iron as the base element in the alloy composition; material 1 and 2 showed corrosion after 48 hours of the IL being present on the surface. Material 3 showed no corrosion, the

difference here being the reduced percentage of iron present and the addition of chromium, nickel and silicon.

Due to size restrictions, only material 1 that showed corrosion could be analysed in XPS. In the analysis, a line scan was performed across the sample covering exposed and unexposed surfaces of the material. Below in figure 58, a diagram of the scans completed can be seen.

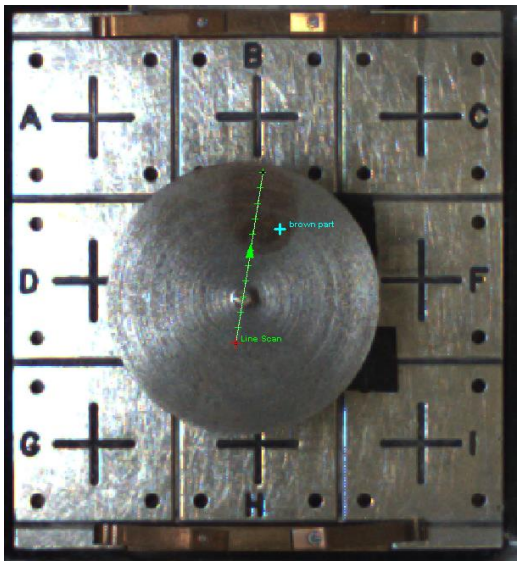

Figure 51 Line scan to be completed on a piece of corroded material, the raised centre point is difficult to see along with another point labelled 'brown part' where the IL was applied and then removed

From the figure it can be seen that 12 points across the surface have been scanned. Though due to the 2D nature of the image it cannot be seen but the centre of the circular piece has a raised point, this caused a weak signal in XPS and therefore meant there are only 4 points for the non-exposed surface compared with 6 for the exposed surface, as well as a singular scan named 'brown part' in the figure.

In the spectra, the first 2 and last 2 points of the line scan are presented showing clear differences. With the brown spot presented on its own against the clean surface. This experiment is an investigative analysis of the surface as opposed to the IL.

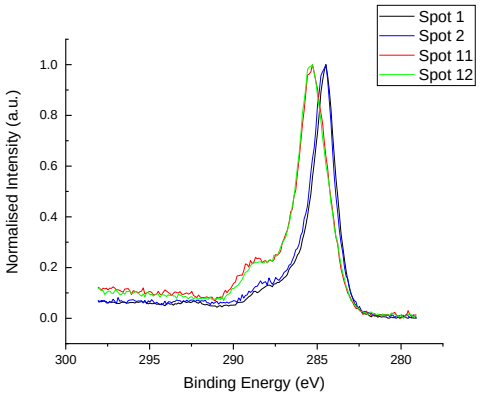

Figure 52 C1s spectra showing 4 spots from the line scan, spots 11 and 12 show a clear shift to a higher binding energy

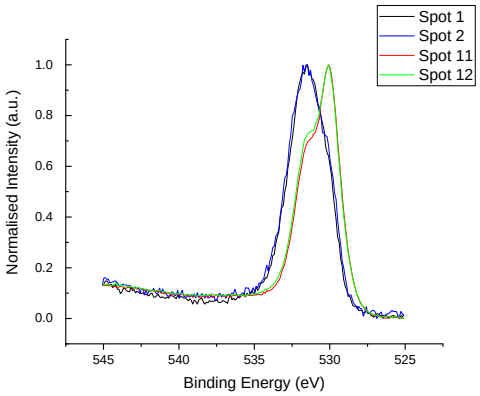

Figure 53 O1s spectra showing 4 spots from the line scan, spots 11 and 12 show a clear shift to a lower binding energy

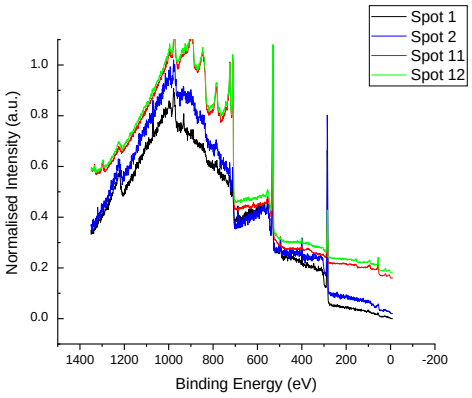

Figure 54 Survey spectra showing 4 spots from the line scan, the spectra from spots 11 and 12 appearing more resolved

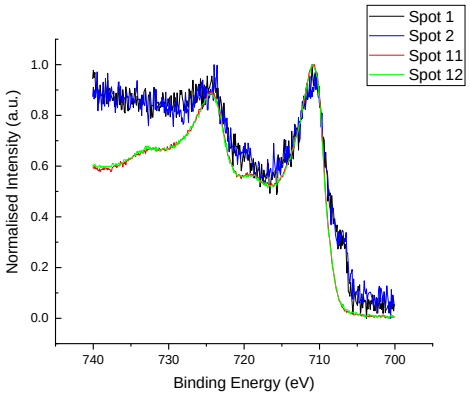

Figure 55 Fe2p spectra showing 4 spots from the line scan, with spots 11 and 12 appearing more resolved

In this experiment, the IL was applied to the surface of the metal over a 48 hour period, it was then wiped away with blue roll where the resulting clean and brown corroded part was analysed with XPS.

The spectra can be seen in figures 52 to 55. In the carbon spectra, the peak shape is largely similar with a 1 component peak but also with a minor peak at slightly higher binding energy. This could be attributed to a shake up feature or possibly the formation of a carbon oxygen bond. Shake-up features are caused by the probability that after photoionization an ion will be left in a specific excited energy state which is a few eV above the ground state due to the outgoing photoelectron. When this occurs, the kinetic energy of the emitted photoelectron is reduced resulting in a shake-up peak which is at a higher binding energy relative to the main peak. In addition to this, the overall peak shape has shifted to a higher binding energy for the latter spots that were left visually corroded.

With respect to oxygen, the opposite is true whereby there is an overall shift of the spectra to a lower binding energy. Though with this, the peak shape of the latter spots shows there could be a two-component model present made up of lower binding energy oxygen bonded to carbon. This would correlate with what has previously been seen in the carbon spectra whereby carbon bonded to oxygen would result in a higher binding energy shift for the carbon spectra but a lower binding energy shift for the oxygen spectra.

Further to this, the survey spectra shows no presence of fluorine unlike the previous spectra that were investigating the leaked sample. But on the other hand the survey spectra here show more prominent peaks for iron content, this

is further backed up when high resolution scans of the Fe 2p region were completed. Here it can be seen in the spectra that the latter points covering the brown part of the surface show more clearly defined and pronounced peaks compared with the surface that has not been in contact with the IL.

With this information, it can be seen that the IL is clearly affecting the surface chemistry of the steel. It could be ascribed that the IL is etching the surface, creating a more reactive surface underneath. This could be explained that the carbon present in the surface is being activated by the IL and exposing it to oxygen in the air. This would explain the complimentary spectra shifts of both the carbon and oxygen spectra, further to this the iron is also being exposed to the air; this offers another explanation for the lower binding energy shift of the oxygen peak in that it could be the formation of iron oxides.

However contrary to this, rather than an etching process, it could simply be that the IL is cleaning the surface, despite the spectra being normalized what is evident in the survey scan is that spots 1 and 2 show a much larger peak for carbon than spots 11 and 12 suggesting that the IL has simply cleaned the surface removing the excess adventitious carbon. This could also be the reason that the iron peaks are also much more prominent in spots 11 and 12 versus 1 and 2. However the cleaning process would not explain the complimentary shifts in the carbon and oxygen peaks.

Further work in this area was completed, whereby a single point in the brown part caused by the IL on the metal piece was compared with a clean part which had not been exposed to the IL.

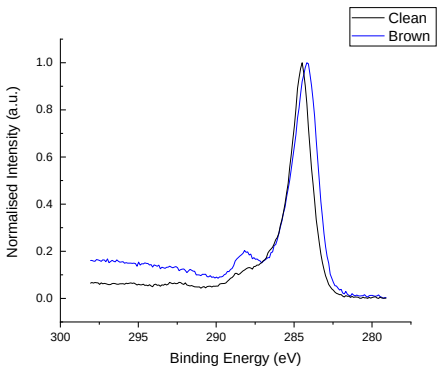

Figure 56 C1s spectra for the clean and brown part from the piece of material, the brown appearing to shift to lower binding energy slightly

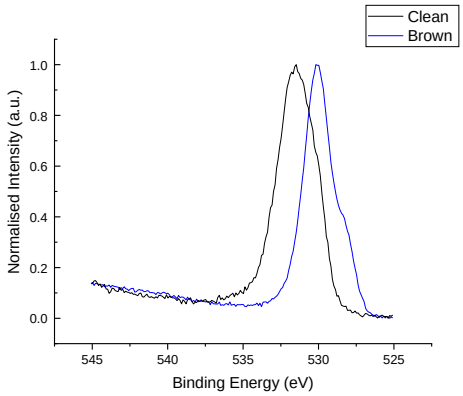

Figure 57 O1s spectra for the clean and brown part from the piece of material, the brown showing a clear shift to lower binding energy

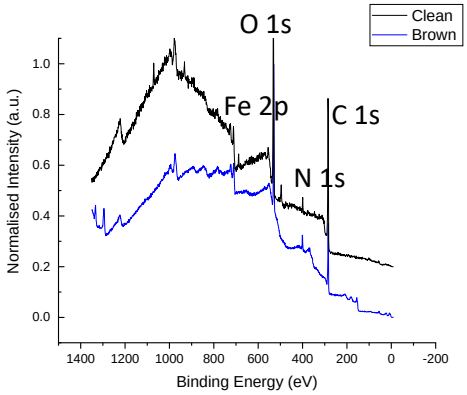

Figure 58 Survey spectra for the clean and brown part from the piece of material, spectra showing no obvious differences other than more resolved peaks

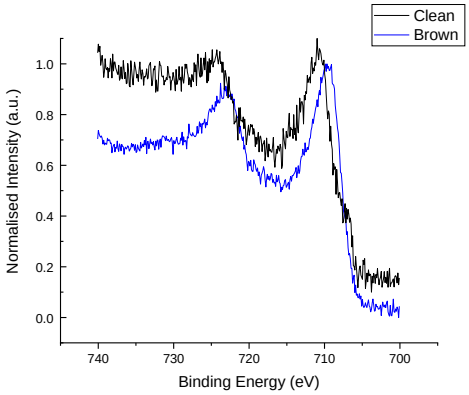

Figure 59 Fe2p spectra for the clean and brown part from the piece of material, spectra showing that the brown sample appears more resolved

As can be seen in the clean and brown spectra from figures 56 to 59, they are largely the same as the previous sets of data. Again, there is no fluorine present this time, likely because it has not been in the pump for testing yet and been exposed to a surface contaminated with the previous lubricant.

Contrary to the last data, the carbon and oxygen brown parts have both been shifted to lower binding energy this time as well as this, the carbon component in the survey scans are largely similar suggesting that there is no adventitious carbon present at the surface this time. The oxygen peak appears to have a minor shoulder peak at lower binding energy which appears to be more prominent in the brown scan versus the clean scan, this could be suggestive of metal oxygen bonds such as iron.

With respect to iron, the brown part again shows a more prominent peak shape with a slight shift to lower binding energy, suggesting the IL has etched or cleaned the surface exposing iron in the alloy.

3.1.5.2 Post Pump Analysis

The post pump analysis comes as a tale of two halves. The way the pump is built, as seen in figures 37 and 38, means it can be effectively divided in two. Each end has slightly different materials and also a slight temperature difference of roughly 10 – 15 °C with neither side having a temperature above 100 °C. As a result of this, the IL has been subject to two different environments. As can be seen in the figure 60 below, the hotter end has resulted in the physical appearance of the IL to turn into a black solid, whereas the other slightly cooler end has resulted in the IL turning orange with an obvious increase in viscosity.

Figure 60 Results from scaled up lubrication testing, on the left a solid black residue has stuck to the inner and on the right a viscous orange liquid has formed

Initial testing showed that the black solid melted at 45 °C meaning that when the pump was operational it was likely to have been a liquid. Due to equipment restrictions it was not possible to measure the viscosity of the orange sample though it was observed that there is an increase in viscosity compared to the starting sample.

To deduce the physical and likely chemical changes in the sample, further testing was required. A useful tool not utilized yet is Mass Spectrometry (MS), it was hoped the fragmentation patterns produced might correlate to show

potential degradation products dissolved in the sample or if the whole composition had changed. As can be seen below in figure 61, positive and negative mode MS spectra have been produced.

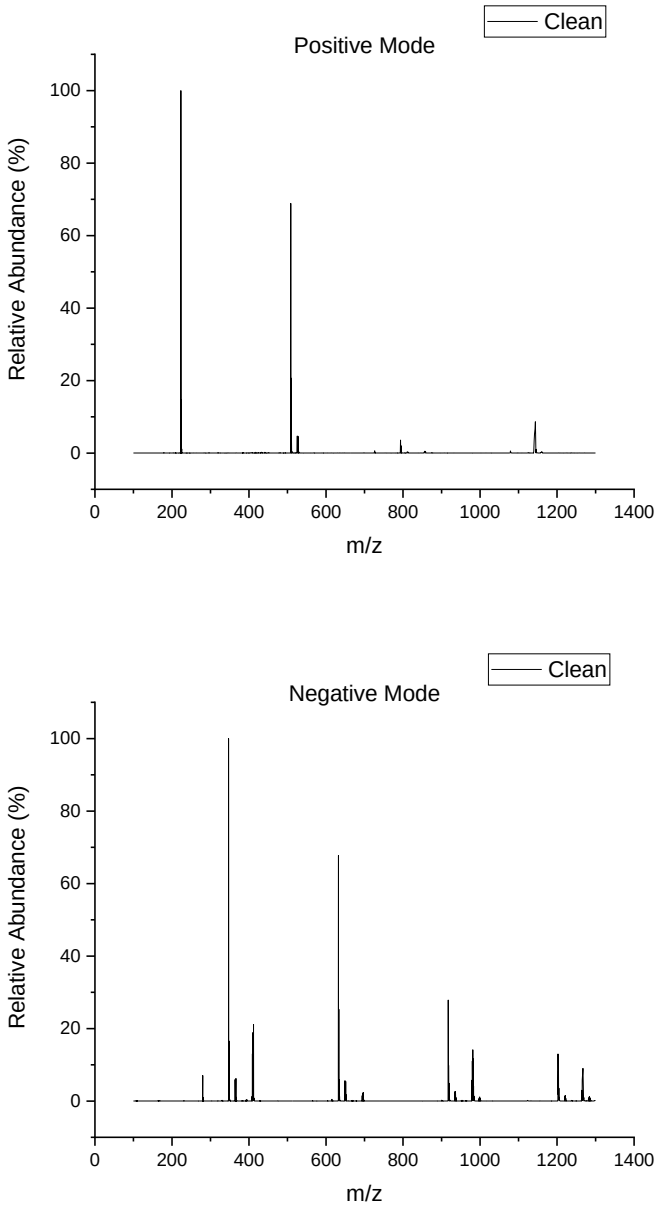

Figure 61 Mass spectrometry spectra for the clean sample in positive and negative mode

Table 19 Table showing positive mode m/z values and their associated fragmentation pattern

Clean sample, Positive mode	
m/z value	Fragment
223.23	$[Cation]^+$
508.46	$2[Cation]^+ [NO_3^-]$
793.67	$3[Cation]^+ 2[NO_3^-]$
1143.59	$3[Cation]^+ [Dy(NO_3)_5]^{2-}$

Table 20 Table showing negative mode m/z values and their associated fragmentation pattern

Clean sample, Negative mode	
m/z value	Fragment
347.12	$[Cation]^+ 2[NO_3^-]$
632.25	$2[Cation]^+ 3[NO_3^-]$
917.41	$3[Cation]^+ 4[NO_3^-]$
1202.58	$4[Cation]^+ 5[NO_3^-]$

In figure 61 and tables 19 and 20 mass spectrometry data for the clean sample are shown. For the positive mode MS, the most abundant ion also known as the base peak is shown at 223.23 m/z which corresponds to a singular cation. Further to this, the next peaks at 508.46 and 793.67 correspond to cation and nitrate combinations, with the former being 2 cations and 1 nitrate and the latter 3 cations and 2 nitrates. Finally the peak furthest to the right at 1143.59 m/z corresponds to 3 cations and a dysprosium penta nitrato anion, here with a 2^- charge.

For the negative mode MS, there are more peaks present but data can still be deduced. The base peak in this spectrum is a singular cation with 2 nitrates causing an overall 1^- charge. From this point the other peaks are derivations of this with 632.25 being 2 cations and 3 nitrates, 917.41 being 3 cations and 4 nitrates and 1202.58 being 4 cations and 5 nitrates; with an unidentified peak arising at 411.77 m/z.

What is interesting at this point is that all of the fragments that have been identified generally show that the IL is present as cation and nitrate combinations and not of the expected composition they were prepared as in the synthesis stages. Further to this, dysprosium is only deduced to be present in the positive mode MS in 1 peak. This could then suggest that the cause of corrosiveness of the IL that has been seen and has potentially been the cause of the discolouration of the pump sample could be from a more reactive nitrate ion as opposed to the full $[Dy(NO_3)_6]^{3-}$.

What follows next is the MS data for the orange and black samples overlayed on the original clean sample, in figure 62.

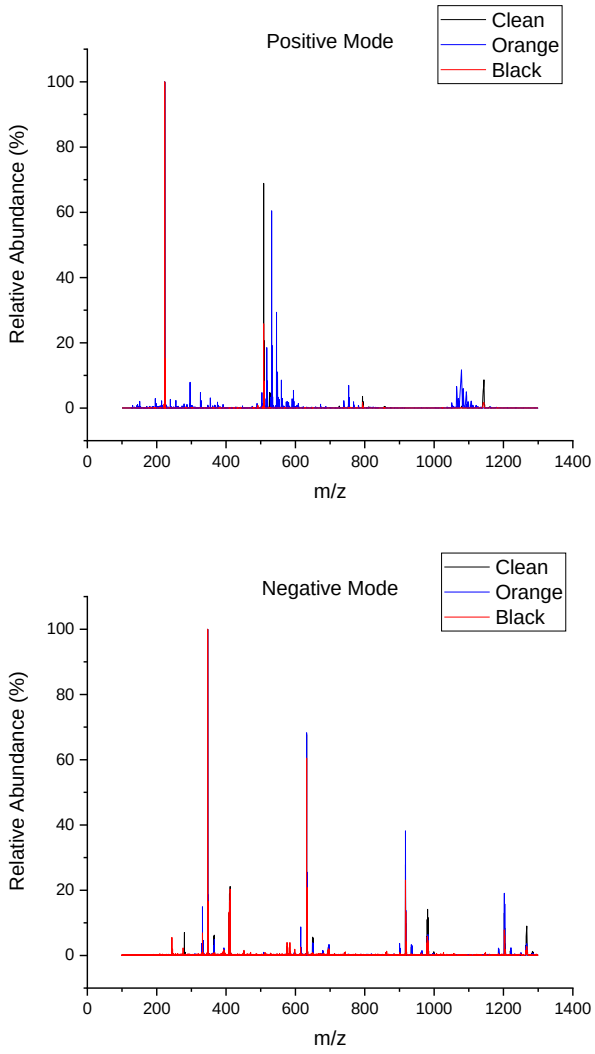

Figure 62 Positive and Negative mode MS spectra showing the clean sample and two used samples from the test pump, the two used samples showing minor impurities

In the positive mode MS, it can be seen that there are obvious clusters of new peaks seen for the orange sample along with smaller more noisy peaks for the black sample. The highest peaks for each of the clusters from the orange sample appear at 531.47 and 1078.98 m/z. According to data taken from Fisher Scientific, the former peak at 531.47 can be assigned to a common contaminant known by its brand name Irganox, with the peak being caused by an $[M+H]^+$ fragment.[100] Irganox is known as a brand name manufactured by BASF which covers antioxidants used in plastic manufacturing. These antioxidants ensure processing stability, namely colour and viscosity retention as well as long term thermal stability and durability of polymers. With this description it sounds like this may be a component found in the original Fomblin composition, further suggesting that the pump was not sufficiently cleaned before the IL was added. However, if that was the case, the IL should also not be reacting since ILs are renowned for their chemical inertness.

For the negative mode MS, the peak positions are largely unchanged just with different intensities and some more noisier peaks all below 10% abundance. Even the orange sample that showed large changes in positive mode looks relatively unchanged in comparison to the clean sample in negative mode.

TGA was completed to ascertain whether there were any changes in chemical stability after being tested for 2000 hours. As stated earlier in this section the black sample turned solid with a melting point temperature around 45 °C meaning it would be especially interesting to see how that sample faired in the test. Results can be seen below in figure 63 with the clean, orange and black sample all displayed in the same graph.

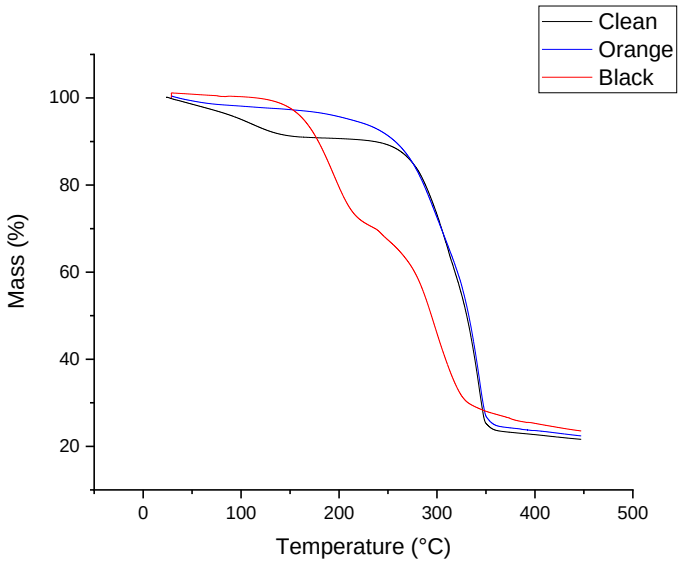

Figure 63 TGA data for the clean sample and two used samples from the test pump, the black sample represented by the red line appearing to decompose in two stages

As can be seen in the graph, the black sample shows a decomposition temperature much lower than the clean (standard) and orange sample. Further to this it can also be seen that it looks to decompose in two stages the first around 160 °C and then the second around 220 °C. The orange sample follows the clean sample indicating no change in thermal stability, with both the orange and black sample decomposing to the same mass percentage as set out by the clean control sample.

At this point mixed results have been attained. The MS results show that the biggest changes in composition are found in the orange sample with suspected contaminants coming from a brand of additives known as Irganox. However, in accordance with the TGA plot, it is the black solid sample that shows deviation from the expected result. What will follow next is XPS analysis of the orange and black samples.

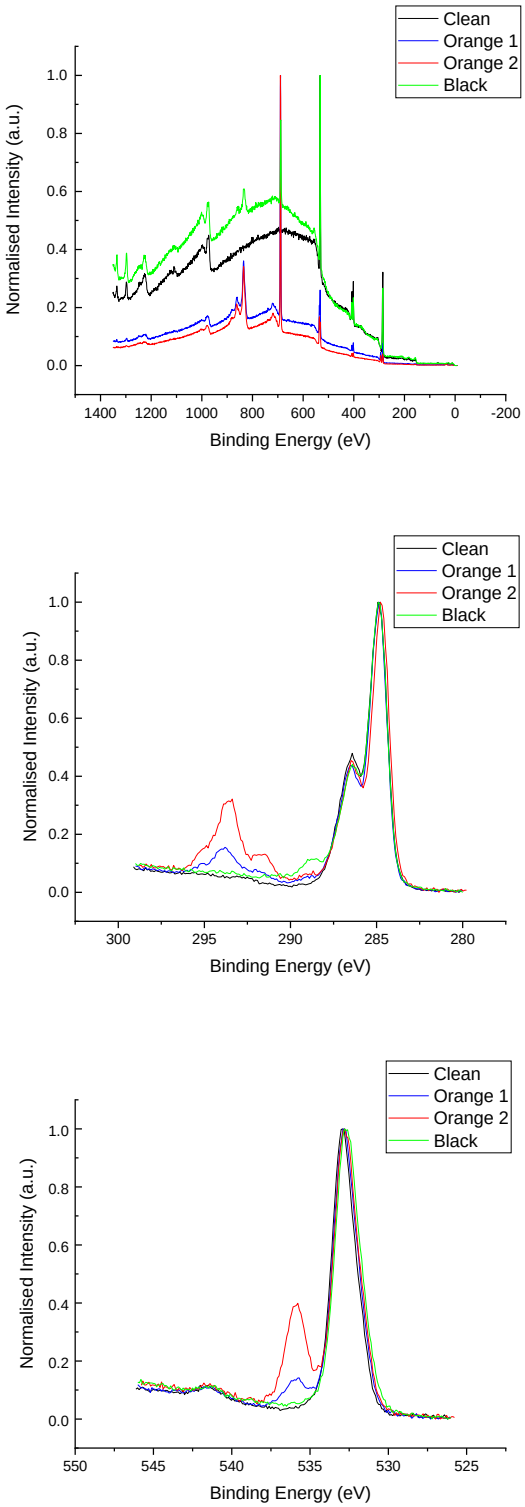

Figure 64 XPS data showing the survey, C1s and O1s data for the clean sample and used samples from the test pump, Fluorine appears to be present for both of the orange samples. As seen by two peaks in the C1s and 1 peak in the O1s

As can be seen from the XPS data in figure 64, there are 4 samples being analysed, the clean sample, the black sample and 2 orange samples. The reason for the 2 orange samples is that similar coloured samples were collected

from slightly different parts of the vacuum pump and it was decided both should be analysed for completeness and ensure no diagnostic data was accidentally missed out.

As can be seen by the survey scan, all of the pump samples now show peaks for fluorine in the survey scan; there is also an unidentified peak at 835 eV which is present for all of the samples that have been in the pump. Initially this was assigned to iron, but there is a distinct lack of peaks that should be present for iron at roughly 735 eV and even lower binding energy peaks at 97 and 59 eV suggesting that the new peak is not caused by iron.

For the Carbon 1s spectra, both of the orange samples show distinct peaks at higher binding energy which again are likely to be caused by CF_2 and CF_3 groups most likely from previous lubricant contamination. However, the interesting result is that this is not present for the black sample despite fluorine being present in the survey scan. There is a minor peak at 289 for the black sample but again this suggests despite obvious physical differences there are also chemical differences in the different post pump samples.

The oxygen spectra also show key differences, both of the orange samples show peaks at 535 – 536 eV but there are no extra peaks for the black sample. It is known that each end of the pump has slightly different operating temperatures, with the black sample coming from the part of the pump that has the higher operating temperature.

It is interesting that there are no diagnostic carbon fluorine bonds present for the black sample and no obvious changes in the oxygen spectra either despite it being very likely that it will have come into contact with left over residue from the original lubricant similar to the orange sample; clearly the slight temperature difference must be a significant factor in the potential degradation pathway. However, referring back to the MS data, it was the orange sample that showed more peaks potentially related to contaminants.

Infrared spectroscopy was also completed on the samples, as can be seen below in figure 65. In the figure it can be seen that the subtle differences are assigned to the 1700 cm^{-1} region. Typically this region is the most diagnostic often caused by carbonyls in the structure. The IL does not contain carbonyls but the nitrate group present shows typical strong peak at roughly 1300 and 1500 cm^{-1} caused by nitrogen oxygen bond stretching. The subtle differences in the spectra are seen at 1627 cm^{-1} for a peak in the clean sample, this peak then appears to shift to 1713 cm^{-1} for both of the orange samples; the black sample shows strong peaks at both of these wavenumbers. This perhaps suggests that the black sample is an intermediate structure whereby the clean sample either degrades or reacts with external contaminants to then form the final product which is the orange sample.

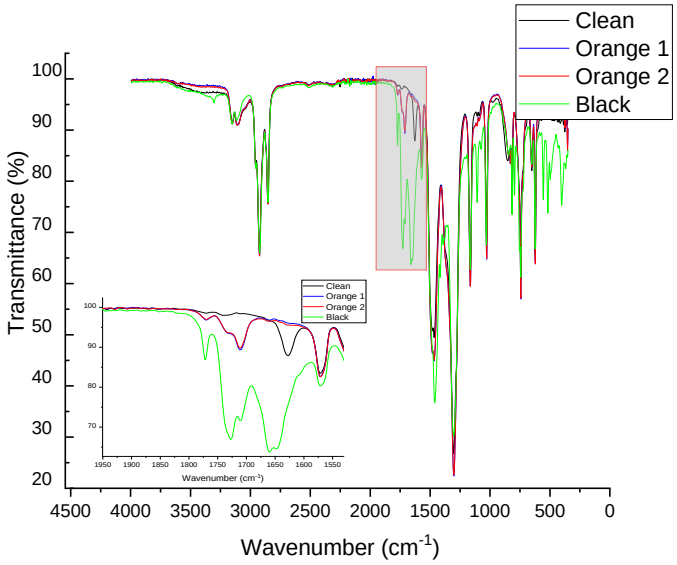

Figure 65 IR spectrum showing the clean sample and samples taken from the used test pump, seen is a highlighted region showing subtle differences between the samples

Traditionally a peak found in this area would be diagnostic of a carbonyl as previously stated though a carbonyl peak is very strong whereas these peaks are less than half the size expected. This could be due to the carbonyl perhaps being a minor impurity in the bulk material, or alternatively this peak could also be assigned to a double bond but the former is believed to be more likely.

In an attempt to recreate the black sample in the laboratory in a bid to further analyse the sample two approaches were taken. The first was to mix the IL sample with the control lubricant fomblin in roughly a 50:50 mix and to then heat

the resulting mixture at 90 °C for an extended period of time and analyse any differences.

The second approach was to use some of the o-ring that is used as a sealant between different parts of the pump and to heat that in the IL for an extended period of time and analyse the results. This latter approach was taken primarily to assess whether the o-ring could be the source of fluorine that has been seen in the XPS spectra as it is made from Viton, a fluorocarbon material.

As can be seen in figure 66, IR data is presented for the clean sample, the clean sample mixed with a piece of o-ring, the clean sample mixed with Fomblin and finally pure fomblin. The spectrum shows that for Fomblin, there is no change in IR spectra when it is mixed with the clean sample despite clear physical changes where the two components form a white liquid when mixed together. Conversely, when the clean sample is mixed with a piece of the o-ring there is no obvious change in physical appearance but a subtle change in spectra, the peak at 1568 cm^{-1} disappears from the clean spectra once it has been mixed with the o-ring.

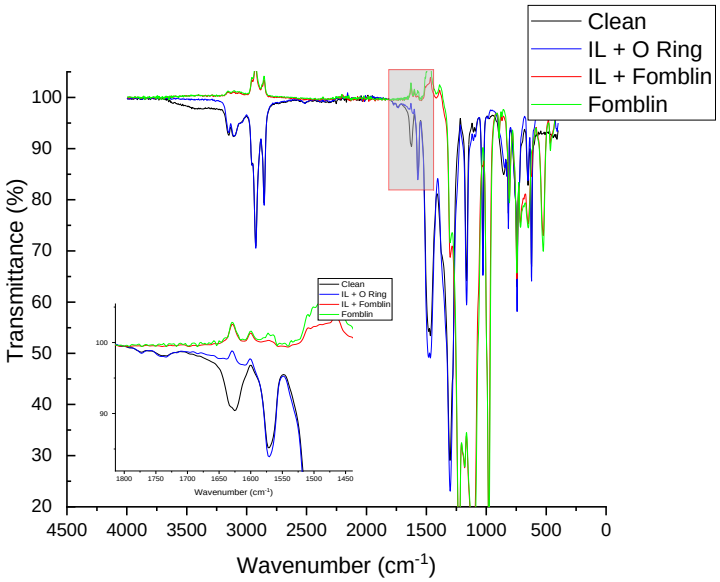

Figure 66 IR spectrum showing the clean sample and the clean sample mixed with Fomblin, an O ring and then pure Fomblin, highlighted is a region of interest where the subtle changes are observed

For further analysis, XPS was completed on the sample containing the IL and o-ring where the data can be seen below in figure 67.

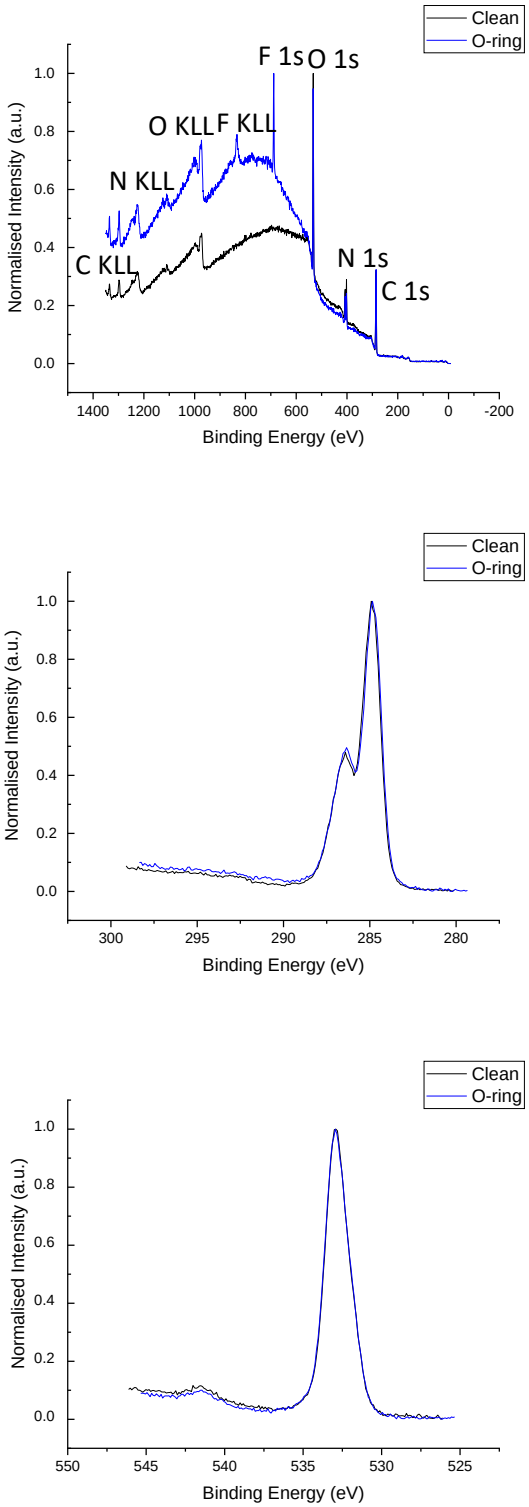

Figure 67 XPS data showing the survey, C1s and O1s data for the clean sample and the sample mixed with a piece of O-ring, the survey spectra shows the presence of a new fluorine peak, but no correlation is seen for this observation in the C1s or O1s spectra

In figure 67, the survey spectra shows clearly that fluorine is present within the sample with peaks present for the F1s and also auger F KLL. For the C1s data, interestingly there are no extra peaks which had previously been seen and

attributed to CF_2 and CF_3 groups caused by residual fomblin lubricant. Further to this, the samples that did show the peaks likely caused from CF_2 and CF_3 groups also showed extra peaks in the O1s peaks, in this data set there are no extra peaks in the O1s region.

This data shows that fluorine is still present in the sample when it has only been exposed to the o-ring; suggesting that the sample could possess leaching properties whereby reacting with the surface of the o-ring has resulted in fluorine being extracted. The physical appearance of the o-ring after these tests was a slightly pitted, where it has lost it's initial smooth finish. This could also further explain the corrosivity issues where earlier in this work it was suggested that the sample was etching or cleaning the surface when in actual fact it could be leaching or dissolving surface contaminants with the two different physical states owing to different levels of contamination.

3.1.6 Further Magnetism Studies

Thus far, the MIL samples have been studied and assessed; despite showing promising results for thermal stability, viscosity, contact angles and early lubrication results their magnetic properties have not reached the anticipated levels that would be required to act as a sealant.

At this point, Fe^{3+} and Dy^{3+} have been utilized in standard anion/cation ILs. To push this work further, other methods of boosting magnetism is deemed necessary. In the introduction to this work FFs were discussed as a competing pathway for the work but were classed as unsuitable due to the likeliness of the carrier solvent to evaporate whilst engaging with the vacuum pump system.

3.1.6.1 Nanoparticle Investigations

One method of working around this could be to disperse the magnetic nanoparticles found in the FF in an IL to form a hybrid system. The IL could be as simple or technical as required, the importance would be keeping the nanoparticles suspended in the IL. The use of an IL as the carrier solvent is vital due to their inherent properties already discussed (negligible volatility, wide liquid range, chemical inertness).

Exploring nanoparticles (NPs) with regards to ILs began at the turn of the 21st century, a review article published in 2017 describes the relationship between IL and NP hybrid mixtures.[101] The review covers the structure and interactions between the two, as well as describing applications they are found in; such as electrochemistry and separation techniques.

The paper states there are three known methods of incorporating NPs into an IL; simply dispersing nanoparticles in the carrier IL through physical adsorption, NPs grafted onto ILs through chemical bonding and localizing NPs into preformed structures based on ILs such as liquid crystalline structures, emulsions or films.

The first method, adsorbing NPs into the IL began around the 2007 mark, two examples being nickel and platinum with the former consisting of nickel and nickel oxide and the latter platinum, fluorine and oxygen.[102, 103] In both papers' work, imidazolium based ILs are used as the dispersion media. The paper dispersing nickel nanoparticles used a hydrophobic NTf_2 IL with increasing alkyl

chain on the cation. In this study it was found that the length of the alkyl chain influenced the size of the NP and the size distribution with increasing length of the alkyl chain. For the platinum-based NPs, a hydrophobic PF_6 anion and a hydrophilic BF_4 anion were both used with the same imidazolium cation. Here, a similar principle has been deduced relating to size of the NPs where the more coordinating anion PF_6 results in smaller nanoparticles compared with BF_4 containing anion. Though XPS was used and 'clearly demonstrated the formation of an ionic liquid protective layer surrounding the nanoparticle surface'.

This protective layer surrounding the nanoparticles is known as an ionic liquid double layer. This layer offers electrostatic interactions which serve the purpose of inhibiting aggregation between the NPs and is achieved through a balancing of this and van der Waals forces, as described by DLVO theory.

A paper published in 2011 describes attempts on suspending magnetic NPs in ionic liquids.[104] In this paper the IL C_2C_1Im $CH_3CH_2OSO_3$ was used, along with magnetite, Fe_3O_4, which was synthesized themselves following the co-precipitation method. They then explore several surfactants including citric acid, humic acid and oleic acid as well as a control experiment with no surfactant used. To determine stability tests several methods were employed such as magnetic sedimentation, centrifugation and redispersion as well as in-situ High Resolution Episcopic Microscopy (HREM) pictures.

In their conclusions they found that the oleic acid surfactant offered the best stabilization effects which gave rise to 'a true (stable) ferrofluid'. Citric acid offered short term stability, humic acid and the bare magnetite particles proved to be unstable in all tests. In their work they state that strong steric repulsion is needed to ensure long-term stability, though this is based on limited data. Furthermore, the stability tests lasted for a maximum duration of 30 minutes with the 'true (stable) ferrofluid' showing very slight sedimentation after 30 mins during the centrifugation and redispersion test. It could be argued that a true stability test should be completed over a longer period of time.

Following on from NPs being adsorbed onto the IL, the next approach to enhance stability can come from NPs chemically bonding to the IL. This is

known as supported ionic liquids (SILs) where the IL layers are immobilized onto the surface of the desired solid support, in this case the solid support being the NP. This research came about due to some limitations with the former method; those being poor dispersion of the metal NPs in ILs as well as agglomeration of the NP.

Advantages of NPs with surface functionalization include better dispersibility and thermostability. To demonstrate this, in a paper by Fukushima, the author explored carbon nanotubes chemically modified by ILs.[105] When the imidazolium-based IL utilized a halide anion, the material was dispersible in water yet with hexafluorophosphate (a hydrophobic anion) the hybrid material was dispersible in organic solvents. Furthermore, other papers explored how NPs can modify the physicochemical properties of the IL itself. In a paper by Liu *et al,* they demonstrated how ILs immobilized onto silica nanoparticles had a change in melting point, where the nanoparticles lowered the melting point compared with that of the bulk IL.[106] This phenomena is believed to be caused by van der Waals interactions between the nanoparticles and the formation of hydrogen bonds between the anions of the IL and the silanol groups at the surface of the silica NPs; which consequently decrease the mobility of the IL cations near the interface trapping them at a state of higher entropy leading to a decrease in melting point.

NPs that are surface modified by chemical bonding with ILs can combine properties of both the NPs and the ILs resulting in a superior hybrid material. A stable dispersion can increase the lifetime of the material, once experimental work has been completed to find a suitable hybrid. With this work, a stable dispersion of a functioning IL-based lubricant as the carrier, along with a NP dispersion to boost paramagnetism, a new material could be prepared to meet the requirements set out in the beginning of this report.

Initially, work was inspired by Shi *et al* who prepared an ionic liquid-based ferrofluid.[107] This was achieved by synthesizing magnetic Fe_3O_4 nanoparticles using a coprecipitation method, coating the bare nanoparticles with an IL-based surfactant 1-butyl-3-(9-carboxydecyl-1*H*-imidazol-3-ium bromide and then

dispersing in three imidazolium-based ILs, $C_2C_1Im\ BF_4$, $C_4C_1Im\ BF_4$ and $C_6C_1Im\ BF_4$.

Within this work, stability, magnetic and lubrication studies are completed. For stability, the three imidazolium-based tetrafluoroborate ILs have a 10% by weight amount of nanoparticles dispersed in the IL. After 6 hours the two shorter chain samples show sedimentation though the $C_6C_1Im\ BF_4$ shows short term stability. To demonstrate further long-term stability, the $C_6C_1Im\ BF_4$ then had the coated nanoparticles dispersed in 5, 10 and 20 % by weight with a figure in the paper showing stability after 30 days.

With regards to magnetism, hysteresis loops of the stable IL dispersions with different particle mass fractions are displayed. It can be seen that the larger percentage by weight of nanoparticles dispersed in the carrier, as anticipated, shows a stronger response to the magnetic field; whereby the curves of the samples also show no coercivity (resistance to change in magnetization) or remanence (magnetization left behind after the external magnetic field is removed).

Lubrication studies were completed with a steel ball and reciprocating steel plate, both made from nonmagnetic 304 stainless steel. The tests were completed with and without a magnetic field; when the magnetic field was present it was completed with a low and high strength field of 45 and 105 millitesla (mT). The load for the test was set to 0.5 N with a sliding velocity of 10 mm/s for 400 seconds at room temperature.

With these parameters, it was found that increasing the percentage of nanoparticles resulted in a decrease in the COF. Furthermore, when the nanoparticles were subjected to the magnetic field the COF decreased even further. The authors hypothesize that the magnetic field causes an increase in viscosity of the sample and therefore results in lubrication operating in the mixed film regime due to the decrease in direct contact of the surface asperities.

To begin, reproducing work from this paper was attempted with a view to then applying new concepts. This meant preparing and coating the nanoparticles as set out in the paper following the co-precipitation method, the structure was then confirmed using XRD which can be seen below in figure 68.

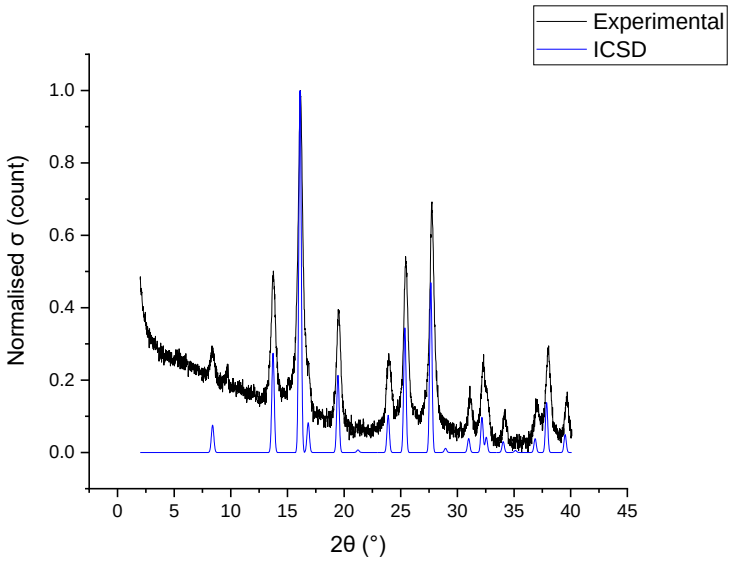

Figure 68 XRD data showing the experimentally prepared nanoparticles correlate with data taken from ICSD

With the nanoparticles successfully prepared, the next step was coating them with a surfactant that would stabilize them when in the IL solution. Characterizing the coated surfactant was completed with proton NMR to confirm synthesis of the carboxylic acid containing IL and IR spectroscopy to confirm successful coating of the surfactant on the surface of the bare magnetite nanoparticles.

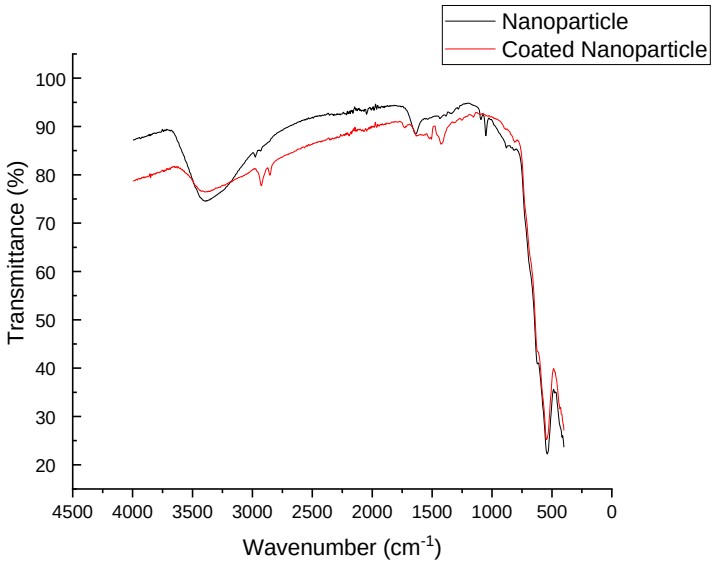

Figure 69 IR data for the coated and uncoated nanoparticles, the bare nanoparticles showing a large OH peak likely caused from improper drying

The above figure 69, shows the IR spectra of the bare nanoparticles and the coated nanoparticles. The bare nanoparticles show a larger OH peak than the

coated nanoparticles, this is because the coated nanoparticles are synthesized in NH_4OH and then washed with water, the resulting slurry is then dried at 50 °C for 1 hour. Evidently there is still water present when compared with the coated nanoparticles, the latter has a smaller OH peak because in the coating step excess surfactant is washed away with ethyl acetate and this resulting slurry is dried at 60 °C overnight in a vacuum oven.

Inspired from work in the afore mentioned paper, it was first elected to investigate viscosity changes with respect to nanoparticle concentration. With this work, the same IL was prepared $C_6C_1Im\ BF_4$. The results can be seen below in table 21.

Table 21 Table showing viscosity changes as percentage of nanoparticles is increased

% by weight nanoparticle	Viscosity /mPas	
	50 RPM	100 RPM
0	168	166
1	143	141
5	130	129

In the table it can be seen that increasing the concentration of nanoparticle results in a decrease in viscosity.

In the paper, their initial viscosities are 41, 98 and 300 mPas for C_2, C_4 and C_6C_1Im respectively, where it can be seen that in this work the C_6C_1Im based IL has a viscosity of almost half that recorded in the paper 168 versus 300 mPas, however moving forward, within the paper their lubrication studies described a decrease in the COF with respect to increasing the percentage of nanoparticle. This could be ascribed to forming a thick layer between the surfaces with a greater proportion owing to the percentage of nanoparticle as opposed to the pure IL it is formed in.

With this limited data it could be seen that adding nanoparticles could be a method of tailoring the viscosity further. However, both concentrations of nanoparticle fell out of solution causing sedimentation at the bottom of the vial within 24 hours. This was an unexpected result as data from the paper this work is based on described them as being stable for 30 days, however this could be caused from the lower viscosity of the sample prepared in the lab versus

reported in the paper. The paper describes nanoparticle stability being related to the length of the alkyl chain from an enthalpic point of view, with the longer alkyl chains forming a more densely packed structure and therefore producing greater steric repulsion between the nanoparticles. However, as from this work clearly the viscosity of the sample must also have an effect on nanoparticle stability.

To address the sedimentation issue, it was hypothesized that perhaps an MIL could help stabilize the magnetic nanoparticles. To investigate this work, the same nanoparticles coated with the decanoic acid surfactant was used along with MIL5, this was chosen as it was anticipated the 10-carbon alkyl chain would offer stabilization to the coated nanoparticles.

With this, the coated nanoparticles were dispersed in MIL5 by sonication. The nanoparticles were added at the 5 percent by weight amount; Sedimentation again occurred within 24 hours the same as with the standard IL prepared earlier in this work.

With the work so far, it was then hypothesized that perhaps the nanoparticles could be prepared in-situ, and if possible would this lead to an inherently stable nanoparticle/IL dispersion. The same method of nanoparticle preparation was followed (co-precipitation) though an IL was used as the reaction solvent. The method can be seen below in scheme 6.

$$Fe^{2+} + 2Fe^{3+} + 8OH^{-} \xrightarrow[90\ ^{o}C]{IL} Fe_3O_4 + 4H_2O$$

Scheme 6 Nanoparticle co-precipitation synthetic method

To begin this work, a simple ionic liquid C_1C_{10}Im Br was used to determine feasibility. Following the scheme, on the addition of $FeCl_2$ there was a yellow colour change to the reaction mixture, upon addition of $FeCl_3$ exothermic gassing was observed as NH_4OH was added more exothermic gassing was observed though this was considered excessive and the addition of NH_4OH was stopped. Once the mixture cooled, the reaction flask contained a sticky brown solid.

Initially thoughts were that this solid could contain the $FeCl_3Br$ anion or its derivatives but upon Raman spectroscopic analysis this proved inconclusive. Further notes were that this brown solid did not show the strong response to a magnet that the magnetite nanoparticles display.

Furthermore, perhaps the IL itself was the cause of the problem; because the IL used was in its most simple form, upon addition of the iron species, demonstrated by the colour change and gassing this could translate to an anion exchange step. To work around this, another IL was used as reaction media. The IL used was the same cation only with a PF_6 anion, this was chosen for its hydrophobic character that could make the final reaction media easier to handle because the hydrophobic nature of the IL and nanoparticles dispersed therein would be separate from the water produced in the synthesis step.

The same process was repeated, the colour change, gassing and exotherm was observed again and the reaction flask was left with a burnt yellow solid and black sediment with no liquid phase. Neither of these solids showed an obvious paramagnetic response to a magnet. The black sediment was able to be collected and dried, using Raman 1 strong peak was observed at 263 cm^{-1} which is tentatively suggested to be caused from an Fe Cl bond.

The same process was again repeated though due to the exothermic reactions that were occurring, the reaction temperature was reduced to room temperature. With this, the final mixture contained the IL as the bottom layer along with a brown aqueous mixture as the top layer. Upon filtering and drying the brown aqueous layer and subjecting the resultant solid to Raman spectroscopy no peaks were observed. This led the investigation to conclude that neither the formation of a new $FeCl_3Br$ or $FeCl_4$ anion was being synthesized due to a lack of Raman peaks and with the evident lack of paramagnetic response the magnetite nanoparticles were also not being synthesized.

Further to this, a different cation was also investigated with the same PF_6 anion. This was a 3-methyl substituted pyridinium ring with varying lengths of alkyl chain. These included 6, 8 and 10 carbon chain to see if this had any effect on the reaction. With all three of the ILs when completing the reaction at room

temperature, a brown water soluble solid was left with the IL again with no peaks shown in the Raman spectra.

To help deduce which reactants are causing the brown solid, multiple steps were taken. For the same ILs, there was no obvious reaction when Fe^{2+}/Fe^{3+} were added on their own, there was also no gassing when only the IL and the source of OH^- was added. Gassing was only observed when all three reactants were in the reaction vessel with the IL.

The final approach for the in-situ method of preparing nanoparticles was to attempt the reaction using a hydrophilic IL. The hydrophilic ILs used in these experiments were the methyl substituted pyridinium cation with alkyl chains of 6 and 10 carbons long with the BF_4 anion.

The same reaction scheme was followed as set out in scheme 6. With this, magnetic nanoparticles were successfully prepared showing an obvious paramagnetic response to the magnet; this can be seen in figure 70, however despite showing promising results the in-situ prepared nanoparticles were still causing sedimentation (but staying in solution longer than their ex-situ counterparts).

Figure 70 Nanoparticles synthesised in-situ showing a clear paramagnetic response to the white magnet seen in the figure

Following this success, the next phase was to explore other hydrophilic ILs to explore their ability to disperse nanoparticles. As the aim of this work is to explore magnetic ionic liquids, it was decided to next use a dysprosium-based MIL. An iron-based was decided against due to its colour making it difficult to

see nanoparticles dispersed but also because there had already been negative results when attempting to disperse ex-situ prepared nanoparticles.

With the dysprosium based ionic liquids, a 3-methyl pyridinium-based IL was chosen with a 6-carbon alkyl component. However, the IL did not facilitate in-situ nanoparticle synthesis. Instead a brown sediment was formed that showed no obvious paramagnetic response to a magnet. The brown sediment was Raman inactive, though the IR showed 3 peaks related to oxygen peaks, furthermore it is tentatively believed that Fe_2O_3 had been prepared though XRD would not be able to distinguish between Fe_2O_3 and Fe_3O_4.

The final exploration regarding nanoparticles and MILs came back to coating ex-situ prepared nanoparticles with a compatible surfactant. This was a 3-methyl substituted pyridinium ring combined with 1-bromodecanoic acid to give a 10 carbon alkyl component and a bromide counter anion.

This surfactant was then used to coat ex-situ prepared nanoparticles and then dispersed in two different MILs. The first was a very similar MIL, a 3-methyl substituted pyridinium ring with a decanoic acid alkyl chain only with an $FeCl_3Br$ anion as opposed to bromide. With this MIL, a 1% by weight nanoparticle dispersion was added to the MIL with sonication and use of a vortex. The other sample was MIL12 from the bulk samples of this work; chosen because the 10-carbon chain could display positive interactions with the coated nanoparticles. The latter dispersion showed an obvious colour change when dispersed (due to the nanoparticles), there was stability for 24 hours but after 72 hours the nanoparticles had caused sedimentation in the vial. For the iron-based IL, the dispersion showed similar results, but as stated previously due to the dark colour of the dispersant it was difficult to see and interpret the solution.

With this work, it has been demonstrated that nanoparticles could be synthesized in an IL. To explore this further, dynamic light scattering (DLS) was used to determine if there was differences in nanoparticle size due to different reaction conditions.

Table 22 DLS data showing difference in Z value for different preparation methods

Method	Nanoparticle	Temperature / °C	Z-Average diameter /nm
Standard Ex-situ preparation	1	24.9	1466
	2	24.9	1335
	3	25.1	910
	4	25.0	1005
In-situ method using C_6C_1Py BF_4	1	25.1	478
	2	25.1	391
	3	24.9	333
	4	25.0	348
In-situ method using $C_{10}C_1Py$ BF_4	1	24.9	171
	2	25.1	205
	3	24.9	187
	4	25.0	198

Results from DLS were mixed, to prepare a sample suitable for DLS the nanoparticles must be dissolved fully, this was not possible for the nanoparticles in this work. However, relative to each other, there were differences in Z values. The Z value is a size parameter, and amongst the 3 NP's analysed there were subtle differences as can be seen in table 20. The NP's analysed were the regular ex-situ method and 2 in-situ methods from a 6 carbon IL and a 10 carbon IL. It was found that the in-situ NP's had smaller values than the NP's synthesized ex-situ. However, with this data it must be clearly stated that the data is rough and although the 3 NP's had different Z values, this does not necessarily mean differences in size it could also mean that the surfaces themselves were different which would also result in a different z value. This could be attributed to nanoparticles which aren't actually on the nanometer scale or agglomeration of nanoparticles resulting in a larger bulk particle; because of this, the larger particles are causing sedimentation because they are too bulky or heavy to stay in solution. Further work in this area is to be completed, possibly with transition electron microscopy (TEM) to determine the size difference.

3.1.6.2 Polymer-based Investigations

The motivation for this research stemmed from a patent dated March 2020, which talked about a magnetic poly(ionic liquid) (PIL). The structure can be seen in the figure 71. As can be seen from the figure the magnetic PIL is based on a quaternary ammonium cation, with magnetic properties coming from the already known tetrachloroferrate anion.

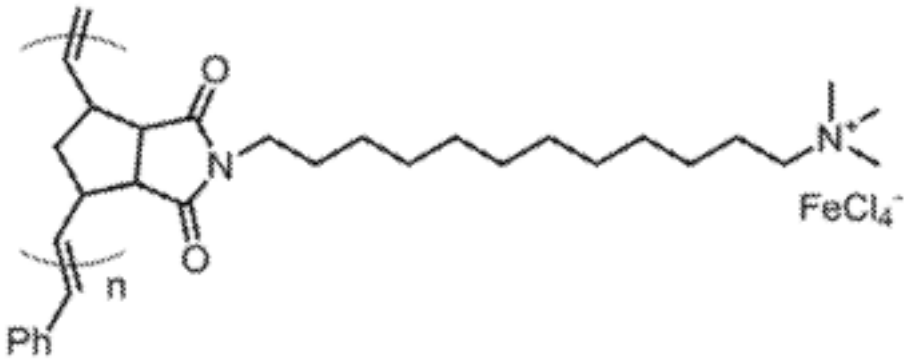

Figure 71 A magnetic poly(ionic liquid) as presented in a patent document

In the patent, it is stated that the repeating unit can range from n = 50 to n = 500, though ideally it is controlled to be in the region of 100 – 300. Furthermore, when in aqueous media the magnetic PIL can self-assemble (a process in which a disordered system of pre-existing components forms an organized structure or pattern as a consequence of specific, local interactions among the components themselves without external direction) into a product that boosts its paramagnetic properties to display super paramagnetism; though within the patent it states that the magnetic PIL is a brown *solid.*

A similar article was published in 2018, which reported the same magnetic PIL which can be seen in figure 72.[108] The paper details the method of preparation as well as explaining in more detail the magnetic properties, going on to say that long alkyl chains allow the full arrangement of the $FeCl_4$ anion so that magnetic units can align in a more stable and ordered system. This leads to the promotion of magnetism to ferromagnetic spin coupling, though again the product is described as a brown solid as opposed to a liquid.

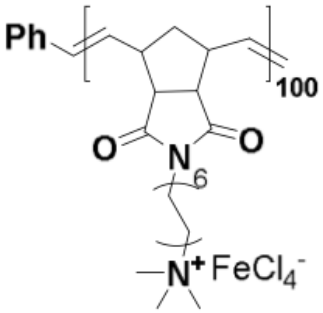

Figure 72 The same magnetic poly(ionic liquid) as presented in the patent but reported in the literature

Further work published in this area in 2019 by Yu described a soft 'super paramagnetic ionic liquid'.[109] The unique point of this paper is that it introduced bi-phenyl groups in the repeating unit which promoted π-π stacking interactions between the bi-phenyl groups of each repeating unit, in effect allowing them to pack more closely when compared with a magnetic PIL without bi-phenyl groups which shortens the Fe-Fe distance. The paper utilizes a helpful diagram demonstrating this phenomenon which can be seen in figure 73, though again the magnetic PIL described is a brown solid and not a liquid.

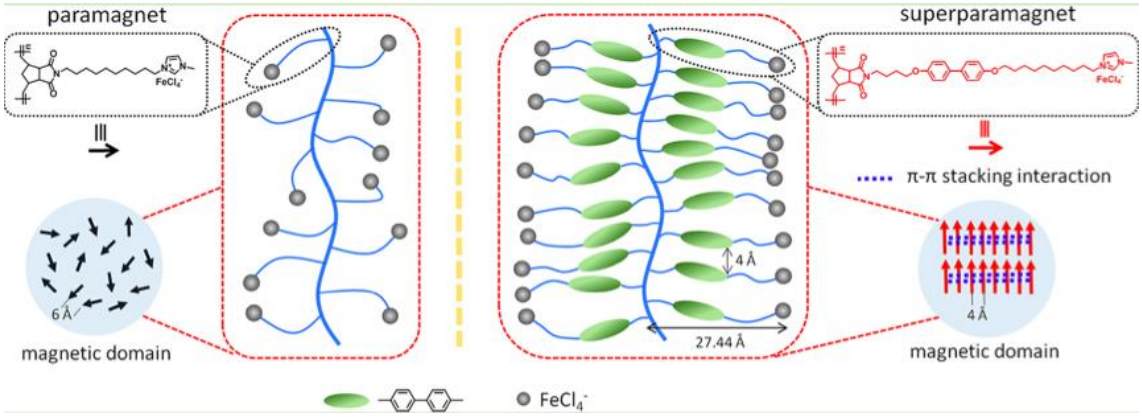

Figure 73 Paper showing the effectiveness of π-π stacking interactions[109]

PILs can be traced back to the 1970s where the polymerization of quaternary cationic polyelectrolytes were first published by Hoover followed by numerous papers by Salamone *et al* describing the free radical polymerization of vinylpyridinium and imidazolium salts .[110-113] As is well known, ILs have tunable properties and this is the same for PILs where glass transition temperature and solubility can also be tweaked by modifying the polymer backbone or counter anion. Further to this, the major advantages of a PIL over an IL is the enhanced

mechanical stability and durability as well as improved processability and special controllability.

Methods of preparing PILs can be split into two categories, either direct polymerization of IL monomers or chemical modification of existing polymers.[114] An IL monomer is an IL which contains one (or more) polymerizable units for example a vinyl, styrenic or (meth)acryloyl component which could be present either on the cation or on the anion; though the polymerizable cation is the more dominant species.

Methods of polymerizing IL monomers include free radical polymerization using a common initiator such as 2,2'-azo-*bis*-isobutyronitrile (AIBN) in a thermal polymerization step, which 'opens up' the double bond component to create a polymer backbone. This would result in a homopolymer whereby all repeating units are the same, though conversely some IL monomers could have two polymerizable groups. These could then be used as crosslinkers to prepare more complex PIL networks which are likely to be more stable.

In recent works, there has been an emphasis on controlled/living radical polymerization. This approach offers the opportunity to design and control the macromolecular structure of the IL species, these methods include atom transfer radical polymerization (ATRP) and reversible addition-fragmentation chain transfer (RAFT).[115, 116]

In the latter method of preparing PILs, the chemical modification of existing polymers, this entails using an existing polymer and its predefined architecture to then generate the PIL through, as the name suggests, chemical modification. An example of this would be reacting a halo-alkane with a polymer that already contains an imidazole thus resulting in a polymer that contains the typical IL intermediate before performing the anion exchange step to achieve the complete IL species in a preformed polymer network. A recent example of this can be seen in the work of Glinska *et al* who started with poly(vinyl alcohol) which was then modified by grafting on a fluorinated protic IL.[117]

Due to their versatile nature, PILs have found applications in many fields of work; these include solid state electrolytes and fuel cells due to their ionic conductivity.[118, 119] Further to their inherent thermal stability and solvation

capability this had lead to PILs also being used as catalysts.[120, 121] Another important application that PILs have found use is as membranes for gas separation, capture, storage and transport. Numerous papers have been published recently that utilize PILs as membranes for carbon capture, an important cause in the modern world.[122-125]

Despite these steps forward in research, relatively little data has been published on the application of PILs as lubricants. Perhaps this is because, as stated previous, PILs are usually solids or highly viscous liquids.

Two recent papers that describe PILs as *additives* in lubricants were published in 2017 and 2018 respectively.[126, 127] In the former, a poly(isobutylene)-based ionic liquid was synthesized and dispersed in commercially available group I-IV hydrocarbon base oils. Their test methods included comparing this novel PIL additive with a well known zinc dialkyldithiophosphate (ZDDP) type anti-wear additive, both being dispersed in the same base oil at 1% level, and a hybrid with 0.5% of each additive.

From their work it can be seen not only is the PIL more thermally stable than the commercially available additive but in their friction and wear testing the PIL additive has a lower COF value when evaluated on a four-ball tester. It was also hypothesized that as an additive, the lubricating mechanism of the PIL played an important role against wear at an early stage in the test whereas the ZDDP took slightly longer to decompose to form the protective tribofilm.

In the latter paper, oil soluble random and diblock copolymers of dodecyl methacrylate and IL methacrylates are presented; with the IL monomers made of quaternary ammonium cations with NTf_2 and dicyanamide counter ions.

Initially, their solubility in PAO type oils was evaluated, with all of the PILs showing solubility at 5 weight% concentration. Within the PILs, there were 6 random copolymers prepared using the RAFT method and 6 block copolymers prepared following the same method but in two sequential steps. The tribological properties were assessed using a ball on reciprocating plate test with the 5 weight % solutions. Within these solutions with regard to friction and wear behaviour there was no obvious correlation between polymer molecular weight and COF value. However within the solutions, for the PILs that had

similar molecular weights the block copolymers performed better than their random polymer counter parts.

In a paper published in 2019, a PIL is presented as a high performance lubricating grease, not directly as an additive.[128] The paper describes how a PIL made up of an imidazolium cation with NTf_2 as an anion is used as the building block for a high performance grease, with a further IL namely a bis-butyl imidazolium dication with a 5 carbon chain bridge which is abbreviated to BIm_5-$(NTf_2)_2$. The grease being tested is made up of 96% PIL and 4% of the dicationic species.

The mixture shows good thermal properties, in line with most ILs and PILs but with a large viscosity, effectively making it a solid at room temperature however with increased shear rate the viscosity does reduce due to sheer thinning. Because of this viscosity, tribological properties are assessed under high pressures of 3 and 3.5 GPas and also temperatures of 200 °C. With these parameters there is no control but the 96% mixture shows a lower COF than each of the individual components.

Building on this work presented, the aim is to prepare a magnetic PIL which is anticipated to be a solid but to then use another functioning IL to create a hybrid mixture that acts as a lubricant but also offers an enhanced magnetic moment ideally super-paramagnetic like the paper presented at the beginning of the introduction to this chapter.

This type of work has previously been published in 2021 whereby a PIL/IL solution was investigated for rheology, structuration and ionic transport properties.[129] The PIL is made from an imidazolium acrylate-based IL and polymerized following a RAFT method. The PIL and carrier IL (C_4C_1Im Cl) can be seen below in figure 74 whereby the mixture is made up of a 10 weight% of PIL to IL.

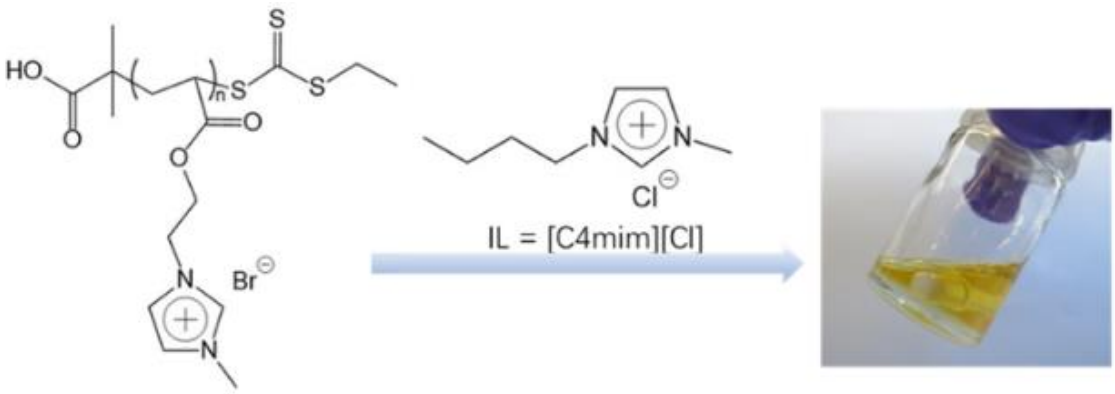

Figure 74 Stable dispersions of poly(ionic liquid)s and ionic liquids as presented in the literature

Within the paper by Zhang *et al* rheological studies are completed along with thermal, structural and ionic conductivity properties. For the rheological studies, steady shear viscosities are explored as well as analysis of the viscoelastic properties of the PIL/IL solutions.

The PILs themselves are split into 3 categories relating to theoretical molar mass, those being 10, 25 and 100 kg mol^{-1}, which are then dissolved in various concentrations in C_4C_1Im Cl. The PIL with a theoretical molar mass of 10 kg mol^{-1} was able to be dissolved up to 50 weight%, the 25 up to 30 weight% and the high molecular 100 up to 20 weight%. As anticipated, as the concentration of PIL dissolved in IL increases as does the viscosity of the solution where shear thinning at higher concentrations becomes more pronounced as the PIL molar mass increases. Shear thinning being a phenomenon characteristic of non-Newtonian fluids where the viscosity decreases with increasing shear stress.

Owing from this paper, it can be deduced that a new magnetic PIL could be stably dissolved in a carrier IL which could or could not also be magnetic.

To begin this work, two stable ILs were prepared and one PIL. The stable ILs were prepared as mentioned previously with quaternisation of methyl imidazole with the corresponding alkyl halide; in this case bromo-hexane followed by anion exchange. One IL was exchanged with potassium tetrafluoroborate and the other with iron (III) chloride hexahydrate leading to C_6C_1Im BF_4 and C_6C_1Im $FeCl_3Br$.

These ILs were then to have the PIL dispersed within them. The PIL was prepared by quaternisation of vinyl imidazole with bromo hexane to prepare the simplest vinyl containing IL C_6C_2Im Br. The polymer was prepared following a radical polymerization with AIBN in chloroform following the same procedure as set out in the previous section of this work.

As can be seen in figure 75, there are no signs of separation or sedimentation seen in the dispersions. With this, the next step is to prepare a novel magnetic PIL to then disperse to make a new hybrid mixture.

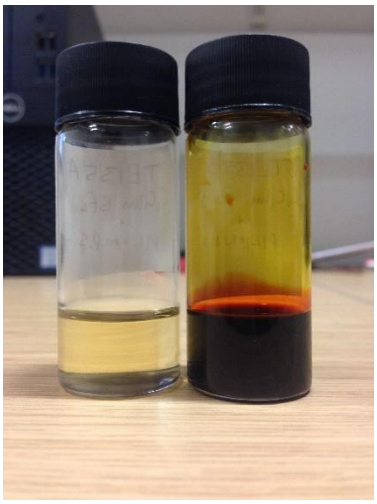

Figure 75 Stable dispersions of poly(ionic liquids) and ionic liquids

To boost paramagnetic behaviour a dysprosium based PIL was attempted to be prepared. This was completed in a similar vein to the PIL prepared previously using AIBN as the initiator. The general reaction scheme can be seen below in scheme 7.

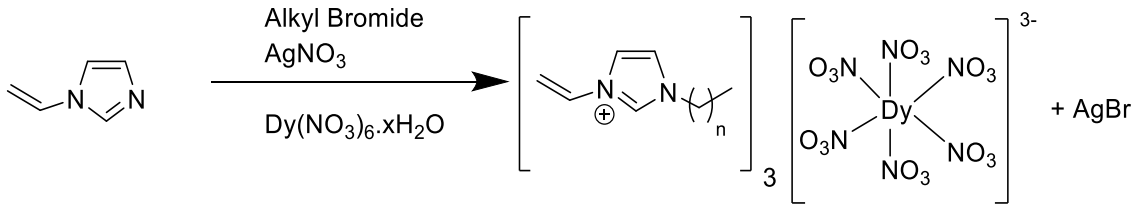

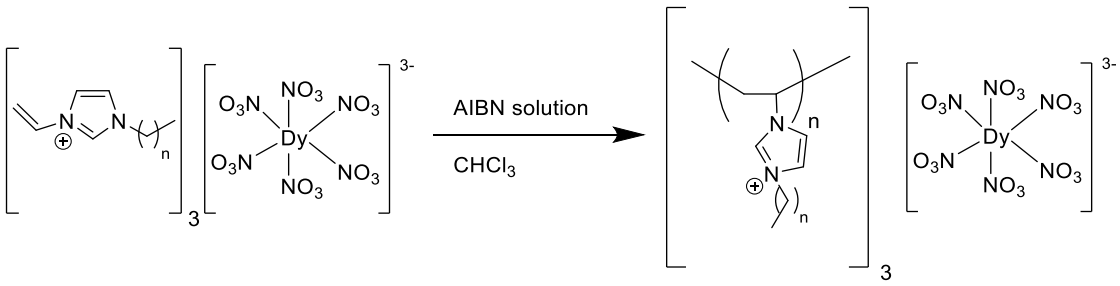

Scheme 7 Method of preparing the novel magnetic poly(ionic liquid)

The radical polymerization was carried out in chloroform for 2 hours at 60 °C, followed by an increase to 75 °C to slowly remove chloroform solvent; there was a final increase to 110 °C to remove the toluene present in the AIBN solution.

Polymerization was deemed to be successful owing to an obvious change in physical properties with the PIL sample showing a large increase in viscosity as well as being a different colour. A challenge presented by this work was the characterization of the monomer and polymer prepared due to the inherent paramagnetic behaviour; because of this proton NMR could not be carried out due incompatibility. However, if this was to be completed, it would be anticipated protons associated with the vinyl component in the monomer would show a different splitting pattern due to the opening of the double bond. Further to this, IR spectroscopy was also completed which offered inconclusive results also.

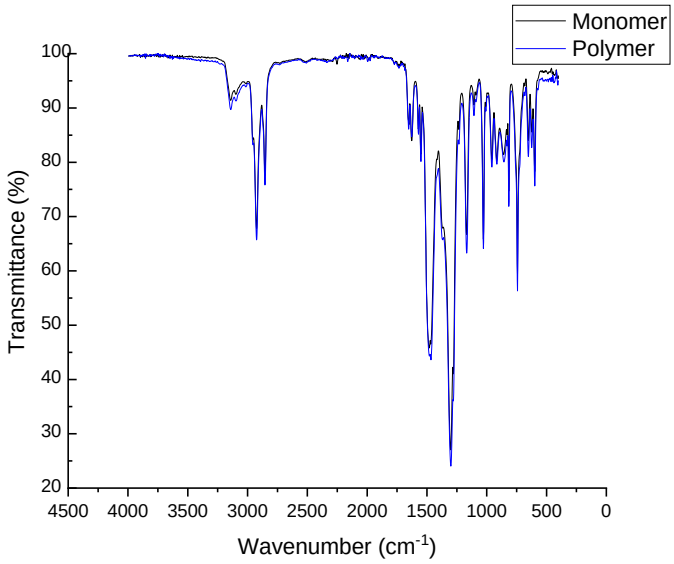

Figure 76 IR data for the monomer and polymer, appearing to show no difference in spectra

This being that the monomer and polymer showed very little difference in spectra, as can be seen in figure 77. It would be expected that there would also be subtle changes here owing to the disappearance of a carbon-carbon double bond stretch.

Due to the nature of polymers, they are likely to have much higher thermal decomposition temperatures than their monomer counterparts. With this in mind, TGA measurements were taken for the monomer and polymer whereby differences could possibly be seen here to deduce successful polymerization.

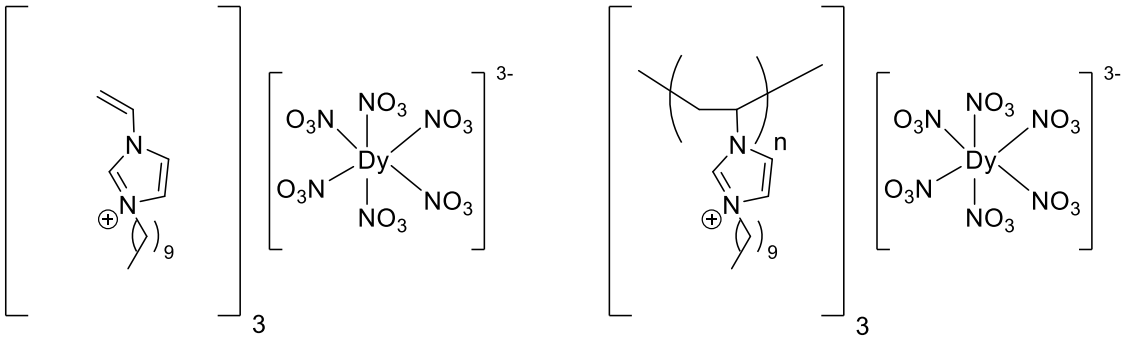

Figure 77 Vinyl Monomer (left) and polymer (right)

The first TGA measurements took place on the monomer and polymer shown in figure 78; 3[$C_{10}C_2Im$] [$Dy(NO_3)_6$], with the TGA curves of the monomer and polymer visible in figure 77.

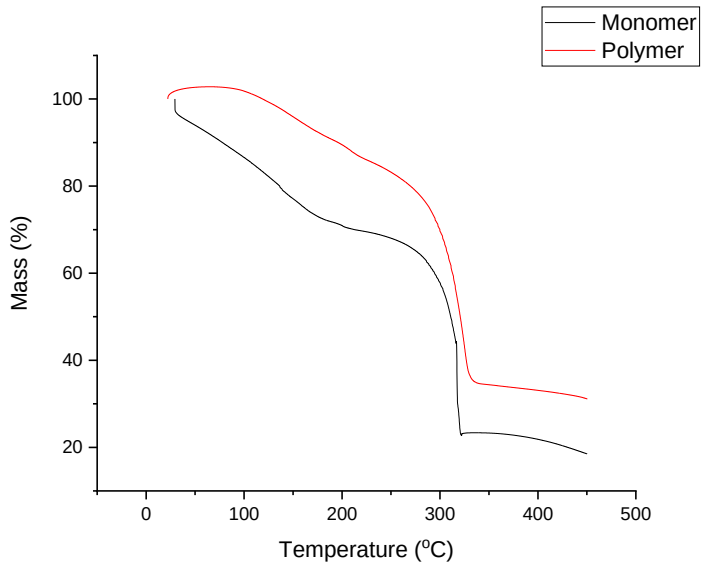

Figure 78 TGA curve for monomer and polymer, the monomer appearing to decompose before the polymer, as anticipated due to fewer bonds than the polymer

From this graph, it can be seen that the line for the polymer shows a slightly higher decomposition temperature as well as a higher mass percentage for the final mass. With this, and visual observations in the laboratory in which an obvious increase in viscosity can be seen, it is tentatively confirmed that the polymerization process has been completed.

Progressing this work, with the magnetic polymer there is still no obvious paramagnetic response when a magnet is held against the sample. With this, further work was completed whereby the resulting polymer was dispersed in a carrier liquid, the monomer. TGA was again completed for the monomer and polymer, but also for the stable dispersion. The stable dispersion was prepared with a 2:1 mixture by mass of monomer to polymer and dispersed with sonication and the use of a vortex. The resulting TGA curve for the 3 components can be seen below in figure 79.

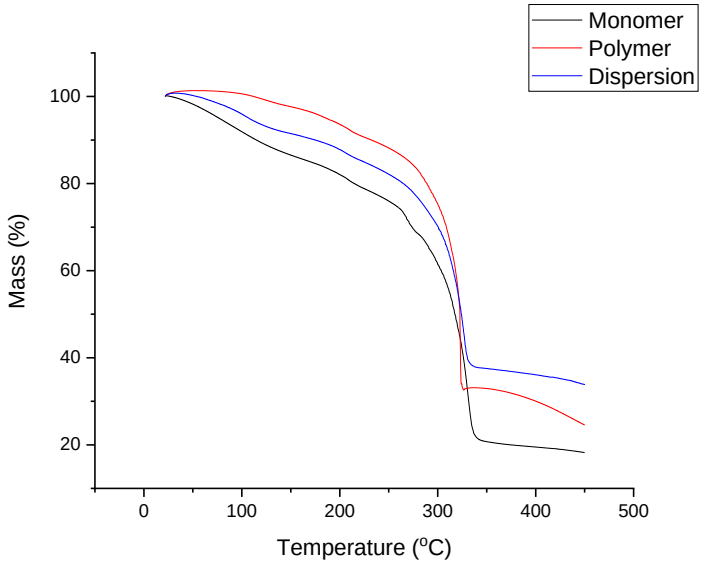

Figure 79 TGA curve showing monomer, polymer and the hybrid dispersion, the dispersion showing the highest final mass due to combination of monomer and polymer

With this graph, it can be seen that the polymer again shows an increased thermal stability, decomposing to a higher final mass than the monomer. The dispersion can be seen initially as a mid-point between the monomer and polymer whereby the onset of decomposition almost follows exactly between the monomer and polymer; this is until the final decomposition mass is reached.

Here, the dispersion shows the highest decomposition mass, believed to be a combination of each component in the dispersion.

Having confirmed stability of the dispersion, the next task was to assess magnetic moment of the components and final dispersion. This was completed in the same vein as work presented earlier in this report with final results shown below in table 23.

Table 23 Measured magnetic moment and conversion to Bohr Magneton

Sample	Magnetic Moment /erg G^{-1}	Bohr Magneton /emu g^{-1}
Monomer	8.8121	40.46
Polymer	7.8367	35.98
Dispersion	12.6730	29.09

These results show that the dispersion has a higher magnetic moment than each of the components individually. The dispersion shows the highest value for magnetic moment, but the lowest value when converted to Bohr magnetons which doesn't take into account the relative molecular mass. The results may be misleading but the dispersion is assumed to be a 50:50 by mass mixture, with this it then means the RMM is assumed to be double to account for each component in the mixture.

Further to this, the aim was to produce a hybrid that could be visibly manipulated with a magnet, this aim has still not been achieved despite an increase in magnetic moment. The MILs presented earlier in this report also all show higher values for magnetic moment than the monomer and polymer work seen in the table above.

Despite not attaining super-paramagnetic behaviour, this work has demonstrated the compatibility of monomer/poly(ionic liquid) dispersions. To further this work, stability studies were completed on an imidazolium dysprosium ionic liquid (MIL9) and its corresponding vinyl polymer.

Table 24 Measured viscosities where possible of MIL9, its corresponding polymer and the dispersion

Sample	Mix ratio	Viscosity /mPas
MIL9	-	41
Polymer	-	viscous gel
Dispersion	1:1	174

As can be seen in table 24, the viscosity of the 1:1 dispersion has significantly increased. Further to this, the dispersion is classed as stable following no sedimentation or immiscibility issues since preparation. The polymer is deemed a viscous gel, but the dispersion is a liquid. The viscosity of MIL9 has greatly increased since dispersing the polymer, offering a new method for tailoring properties of an IL.

Chapter 4

4.1 Conclusions

A new XPS fitting model for the C1s region in positively charged cations as part of an IL has been devised and applied to bridged dicationic moieties. This work was based on modelling methods that had previously been devised for predominantly imidazolium and pyridinium-based cations; the aim of this work was to adapt and assess current models for monocationic and then apply them for the use of DcILs.

Six DcILs were prepared in the lab based on simple pyridinium cations with bromide anions to ensure there is no contribution from the anion component. In the literature there is a known 3-component model which had already been utilised for pyridinium-based ILs, in addition to this, typical imidazolium modelling data was also investigated which incorporates a 4-component model. Taking the proven 4-component model and applying it to a new set of DcILs gave mixed results where two of the components in the model appeared at almost identical BE's. Being aware that a model with more components will always fit better and in a bid to keep the model as simple as possible the decision was made to combine the two components appearing at similar BE's to create a novel 3-component model.

This novel 3-component model, with components for aromatic carbons bonded to nitrogen, aromatic carbons bonded to themselves and aliphatic carbons consisting of the bridged carbons as well as the methyl bonded component that is present in three of the DcILs. With this model it has been proven that a simplified 3-component model can be applied for the fitting of the C1s region of pyridinium-based DcILs.

With this work, it provides a foundation to be built on for further complicated mono and di-cationic ILs. An immediate next step for this work could be the introduction of carbon containing anions such as the well studied bis(trifluoromethylsulfonyl)imide or dicyanamide and thiocyanate.

The bulk of the work in this thesis is aimed at developing a novel magnetic lubricant and sealant to be used in a vacuum pump. To achieve this, 12 core

samples of varying compositions were prepared and subject to key property evaluations, utilising two existing lubricants as controls in the evaluations.

Tests utilised in the core sample property evaluations included viscosity investigations, contact angles on vary substrates, thermal stability and magnetic properties. Viscosity investigations included initial viscosities at room temperature as well as measuring up to 80 °C and applying some data extrapolation in order to measure viscosity indexes of the samples. Key findings were the influence of the alkyl chain tail component on viscosity offering the option of tailoring viscosity, as well as the introduction of a methyl group in position three of pyridinium-based ILs offering further options of viscosity tailoring which is not as widely reported in the literature. All of the samples, excluding MIL11 which was higher, had a viscosity lower than Fomblin, the main lubricant in use and all but one of the samples, MIL9, had a viscosity lower than Leybonol, the other control lubricant. When calculating viscosity indexes, Fomblin had a value of 57 and Leybonol 7, there were only 2 of the core samples that had values within this range, again MIL9 at 43 and MIL11 at 51. With this work, promising samples were characterised as samples with values that closely followed the two lubricants, at this point MIL9 was the most promising showing a viscosity and viscosity index most closely correlating with the two control lubricants.

Contact angles were measured on aluminium, steel and vinylidene fluoride hexafluoropropylene, where values reported are timed averages using the dynamic measurement method. Fomblin and Leybonol both measured consistently low values of contact angle for each substrate; whereas all the MIL samples showed values higher with the exception of MIL12 which showed a value of 26 degrees for aluminium which was similar to Fomblin and Leybonol which were 24 and 29 respectively. Trends were seen that an increase in viscosity through elongation of the alkyl chain component resulted in smaller contact angles. The highest contact angles were seen for Viton throughout, with aluminium and steel showing mixed results for each sample.

Thermal stability is a key property, as the pump the new lubricant is to be used in will operate at roughly 85 °C. The test operated at RT up to 450 °C where all samples and the controls generally showed thermal stability up to 300 °C.

It was necessary in this work to evaluate the effectiveness of the 12 core samples' ability to act as a lubricant. This was initially completed by measuring COF values for each lubricant followed by more work to produce Stribeck curves which take into account COF at varying speeds. The core samples all gave values for average COF that were lower than the controls; further to this, when producing Stribeck curves the dysprosium containing MILs 8-12 showed curves that gave the most significant resemblance to a stereotypical curve.

One drawback on this method of evaluating the COF was that the test was completed in a reciprocating test, despite showing promising results it may have been better to perform the tests using a ball on rotating disc. This would better suit these samples because of the way the lubricant will act in the real pump lubricating rotating gears and screw-type vacuum pumps.

After these tests had been completed (also described as wear testing), post-test analysis was completed on the sample. This was completed by using predominantly XPS and IR where necessary to compare the before and after, this work found that the core samples with short alkyl chain components showed the biggest difference in C1s spectra. This was made easier by using modelling techniques set out in the first chapter of this work. The difference was down to an increase in intensity for the peak in the C1s spectra that was attributed to the aliphatic component ascribed to lower binding energy. As well as this, survey scans were completed where new oxygen peaks were found in some of the short alkyl chain samples as well as fluorine, both of which were not present pre test.

At this point in the work there were two avenues to explore, to address the magnetism issues but also to scale up a sample to gain an understanding of how an IL might perform in a test pump. Both avenues were addressed in tandem.

The aim of this work was to prepare a magnetic lubricant and sealant, in this work it has been demonstrated that all of the 12 core samples display a paramagnetic response to magnet as shown by the Evans balance data. However, the magnetic response shown to an external magnetic field was deemed not strong enough to enable the lubricant to be held in place to form a seal to then reduce pressure in the vacuum; this lead to further work being explored in a bid to rectify this issue.

Nanoparticles were explored in an approach to prepare a novel hybrid mixture taking inspiration from ferrofluids. This work explored the synthesis of magnetite nanoparticles using ionic liquids as a reaction medium, synthesis was successful but stability issues were encountered with the nanoparticles falling out of solution usually within 24 hours. This work was based on recent literature where it was believed a significant contribution could be made to the field, however stability of the nanoparticles proved a troublesome point and restricted work.

Another approach was to explore magnetic poly(ionic liquids), this approach was initially inspired by work in the literature that described polymers that displayed a super paramagnetic response an external magnetic field. The difficulty in this work was that these polymers were solids which meant they were unsuitable for this project. This lead again to hybrid mixtures combining magnetic polymers based on a dysprosium anion and dispersing them in a standard non-polymeric ionic liquid. Unfortunately, despite the hybrid mixtures showing good compatibility there was still no obvious increase in paramagnetic response. The premise of this work was exciting, offering a new type of magnetic polymer based on dysprosium however it too proved difficult in characterisation steps, and subsequent lack of paramagnetic response.

In order to scale up a sample, it must first be decided which is the most promising candidate; where it was decided MIL9 would be taken forward owing to it’s physical properties which most closely related to the control samples. Initial minor issues were encountered on scaling up from 10 mL to 1 L but once complete the sample was taken to Edwards Vacuum premises and poured into a test pump. The pump successfully ran for over 2000 hours where it was

initially expected to run for 1000 hours, but the overall results were mixed. As far as lubricating performance, the test was a success where it was agreed by personnel that MIL9 outperformed Fomblin and Leybonol on a strictly lubrication basis. However as detailed in the chapter, there was also a list of problems encountered.

Despite the problems, this work is highly relevant to the field in that typically lubricants are subjected to controlled experiments using clean equipment to predict how samples *might* perform in a pump based on COF values. This work has proved that the sample *can* be used in a vacuum pump, as proven by the length of time the pump operated. However, as detailed problems were encountered but these problems would likely never be encountered in a bench top experiment in the lab.

The most obvious problem was the change in physical appearance of the sample, the sample outputted from the pump gave a viscous orange sample notably more viscous than when it was inputted without the need for a viscometer; in addition to this, the other end of the pump resulted in a black solid residue that coated the inside of the test pump. Initial analysis found that the black residue melted at around 45 °C indicating that it must have been a liquid whilst the test pump was running. Causes for the change in physical appearance were attempted to be explained utilizing a range of diagnostic testing using the leftover clean sample as a control.

The main tools used to characterize the two materials that were outputted from the test pump were XPS and IR spectroscopy, as well as utilizing TGA and MS. TGA found that the black residue appeared to decompose in two steps whereas the orange sample appeared unchanged when compared with the clean sample. MS found that the main differences were in positive mode for the orange sample where a common contaminant known by the brand name Irganox, this is hypothesized to be an additive found in Fomblin’s composition. An interesting point that was found in the MS spectra was that the fragments are largely attributed to different ratios of cation and nitrate with dysprosium rarely being accounted for in the m/z peaks.

With regards to XPS, in the survey scan both the orange and black samples contained peaks for fluorine. When further analysing the C1s spectra, it appeared that the orange samples had extra peaks here caused by CF_2 and CF_3 groups, this was hypothesized to be from residual fomblin present in the pump. However, the black sample did not show these peaks, to ascertain where the fluorine came from for the black sample, the clean sample was mixed with an o-ring separately. The o-ring is made from Viton which is used in the seals for the test pump. When this mixture was analysed with XPS it showed the fluorine peak and as expected there was no CF_2 and CF_3 groups in the carbon region. This lead to a hypothesis that the IL is capable of leaching, whereby the IL is extracting fluorine from the o-ring whilst it is in contact.

Furthermore, in this work corrosivity tests were explored with the IL sample, it is now hypothesized that perhaps the IL is not inherently corrosive, it is simply cleaning the surfaces it comes into contact with resulting in a new nascent surface. This hypothesis can be backed up by the work in this thesis where a piece of metal was cleaned, then a spot of the IL was dropped onto the surface and left for 3 days. The drop was then removed to leave a brown corroded part of the metal. This piece of metal then had a line scan completed on XPS making sure to include the non-corroded part of the piece of metal also. The result was that the corroded surface had much cleaner peaks for the Fe2p region compared with the unexposed surface, suggesting a much cleaner surface.

Going back to analysis of the orange and black samples, to further try and recreate these two materials the clean sample was mixed with Fomblin. This gave a white gel like substance, unable to complete XPS due to Fomblin's likely volatility IR spectroscopy was used. This Fomblin mixture was scanned along with the mixture that contained the o-ring as well as the orange, black and clean sample and pure Fomblin to give a total of 6 spectra. There was only one very subtle difference with the disappearance of a peak at 1568 cm^{-1} for the clean sample when mixed with the o-ring. In addition the only changes for all of the spectra appeared with minor peak shifts in this region; where at this point it is hypothesized that perhaps the orange and black materials are related in a way that one of these is an intermediate product and the other is a final product,

more work is to be completed in this area. However again, if only benchtop experiments were completed with regards to lubrication these problems would never be encountered. Further, this is also demonstrated whereby it was attempted to recreate the problems on the benchtop that occurred in the vacuum pump, where even recreating the problems was difficult. This too shows that the novel work completed by utilizing an MIL as a real lubricant brings a high amount of insight to the field of ionic liquids and tribology.

Chapter 5

5.1 Future Work

There are three key areas of work to be addressed which include magnetism, poly(ionic liquid) characterization and further analysis work with regards to the scaled up sample.

With respect to magnetism, nanoparticles were explored as well as polymers in a bid to achieve an improved paramagnetic response to an external magnetic field. As nanoparticle research continued with frequent negative results relating to nanoparticle stability, work led by Zheng *et al* offered a new method of stabilizing nanoparticles.[130] This work effectively found a middle ground between a polymer and a nanoparticle dispersion, whereby nanoparticles were prepared and then adsorbed onto silica dioxide which were then immobilized onto vinyltriethoxysilane. This vinyl monomer was then copolymerized with 1-vinyl-3-hexyl imidazolium bromide to produce a block copolymer consisting of an ionic liquid and magnetic nanoparticles. However, again this copolymer is a solid but perhaps this technique could be explored with a magnetic poly(ionic liquid) to further boost magnetism as well as the resulting copolymers mixed with carrier ILs similar to the hybrids presented in this work. This would be interesting because the paper describes the copolymer displaying a paramagnetic response, however the anion here is a simple bromide. To specifically build on this work, a paramagnetic anion could be used such as Fe^{3+} or Dy^{3+}. This would boost the paramagnetic response further, and the increase in size of the paramagnetic anions could potentially result in a highly viscous ionic liquid as opposed to the solid which is presented in this work. Further to this, different ratios of monomers could be explored to produce different copolymers offering further tailoring to result in a liquid.

With respect to the novel magnetic poly(ionic liquids) presented in this work, further characterization is key to the understanding. As there are 3 cations per anion it would be very interesting to explore the physical relationship for example once polymerized is there only one polymer backbone entangling around the singular anion or perhaps is there a triple helix type structure with

three polymer back bones surrounding a singular anion. This further structure exploration could then feed into the next steps presented in the previous chapter with regards to copolymer characterization.

With this in mind, the first steps towards future work would be to characterize the magnetic polymer presented in the latter stages of this thesis; if successful, the work would then move on to explore the copolymer method which brings together polymers and nanoparticles with effective characterization of the resulting copolymer. With further novelty arising from the incorporation of magnetic anions in the polymer chain.

Here, further work could continue to try and reduce the viscosity of the resulting copolymer (assuming it is very high, or a solid), this could be in the form of dilution with a low viscosity IL to create a hybrid material similar to what was achieved in this thesis. The ultimate aim of this work is to produce a new material suitable for the vacuum pump to act as a lubricant and sealant.

Finally, further work needs to be completed with regards to the scaled up pump sample. What was not possible in the time frame due to constraints on size was XPS analysis on clean and corroded parts from the actual pump the lubricant was working in. During the dismantling process clean and corroded screws were kept safe however due to their large size and inability to be cut into smaller pieces due to time constraints this work was not completed. In a similar vein, scanning electron microscopy (SEM) could also not be completed due to size constraints of the screw.

But perhaps the most important issue yet to be completed is the characterization and subsequent confirmation of chemical composition for the orange and black samples which came from the pump after the lubrication test. Successful characterization of these samples would help inform other future work at the synthesis stage to avoid this happening again.

The overall work process would then begin with characterizing the magnetic poly(ionic liquid) from this work, whilst also characterizing the samples that have came from the test pump. This would then provide strong foundations to carry on the other future work. Being able to characterize the poly(ionic liquid) could offer insight into potentially better methods of synthesis for example.

Characterizing the sample from the pump would give valuable information also on potential degradation pathways which in itself would provide useful information for the synthesis stage to avoid degradation happening again.

This information could then be used to explore the poly(ionic liquid)/nanoparticle copolymers, which as part of this work may also explore the use of low viscosity ionic liquids to reduce overall viscosity of the copolymer and improve its effectiveness as a lubricant.

Chapter 6

6.1 References

1. Brief history of lubricants, https://iselinc.com/brief-history-lubrication/, (accessed 03/02/2022).
2. The History of Synthetic Oil, https://blog.amsoil.com/the-history-of-synthetic-oil-and-amsoil/, (accessed 03/02/2022).
3. P. Jost, *Lubrication (Tribology) - A report on the present position and industry's needs*, Department of Education and Science, 1966.
4. Fomblin PFPE lubricant, https://www.solvay.com/en/brands/fomblin-pfpe-lubricants, (accessed 29/10/2020, 2020).
5. M. Freemantle, *An Introduction to Ionic Liquids*, 2009.
6. H. M. Mobarak, E. N. Mohamad, H. H. Masjuki, M. A. Kalam, K. A. H. Al Mahmud, M. Habibullah and A. M. Ashraful, *Renewable & Sustainable Energy Reviews*, 2014, **33**, 34-43.
7. Lubricant Additives - A Practical Guide, https://www.machinerylubrication.com/Read/31107/oil-lubricant-additives, (accessed 14/02/2022).
8. C. J. M. Friedel C., *Comptes rendus de l'academie des Sciences*, 1877, **84**, 1392 and 1450.
9. N. Nambu, N. Hiraoka, K. Shigemura, S. Hamanaka and M. Ogawa, *Bulletin of the Chemical Society of Japan*, 1976, **49**, 3637-3640.
10. G. S., *Ber.*, 1888, **21**, 2669.
11. P. Walden, *Bulletin de l'Académie Impériale des Sciences de Saint-Pétersbourg*, 1914, **8**, 405.
12. C. Nanjundiah, K. Shimizu and R. A. Osteryoung, *Journal of the Electrochemical Society*, 1982, **129**, 2474-2480.
13. J. S. Wilkes, J. A. Levisky, R. A. Wilson and C. L. Hussey, *Inorganic Chemistry*, 1982, **21**, 1263-1264.
14. J. S. Wilkes and M. J. Zaworotko, *Journal of the Chemical Society-Chemical Communications*, 1992, 965-967.
15. H. L. Chum, V. R. Koch, L. L. Miller and R. A. Osteryoung, *Journal of the American Chemical Society*, 1975, **97**, 3264-3265.
16. N. V. Plechkova and K. R. Seddon, *Chemical Society Reviews*, 2008, **37**, 123-150.
17. R. F. de Souza, V. Rech and J. Dupont, *Advanced Synthesis & Catalysis*, 2002, **344**, 153-155.
18. R. S. Varma and V. V. Namboodiri, *Chemical Communications*, 2001, 643-644.
19. B. Clare, A. Sirwardana and D. R. MacFarlane, in *Ionic Liquids*, ed. B. Kirchner, Springer-Verlag Berlin, Berlin, 2009, vol. 290, pp. 1-40.
20. S. Hayashi and H. O. Hamaguchi, *Chemistry Letters*, 2004, **33**, 1590-1591.
21. S. Hayashi, S. Saha and H. O. Hamaguchi, *Ieee Transactions on Magnetics*, 2006, **42**, 12-14.
22. R. E. Del Sesto, T. M. McCleskey, A. K. Burrell, G. A. Baker, J. D. Thompson, B. L. Scott, J. S. Wilkes and P. Williams, *Chemical Communications*, 2008, 447-449.

23. B. Mallick, B. Balke, C. Felser and A. V. Mudring, *Angewandte Chemie-International Edition*, 2008, **47**, 7635-7638.
24. K. L. Cheng, W. L. Yuan, L. He, N. Tang, H. M. Jian, Y. Zhao, S. Qin and G. H. Tao, *Inorganic Chemistry*, 2018, **57**, 6376-6390.
25. K. R. J. Lovelock, I. J. Villar-Garcia, F. Maier, H. P. Steinruck and P. Licence, *Chemical Reviews*, 2010, **110**, 5158-5190.
26. W. M. Liu, C. F. Ye, Q. Y. Gong, H. Z. Wang and P. Wang, *Tribology Letters*, 2002, **13**, 81-85.
27. S. Men, K. R. J. Lovelock and P. Licence, *Physical Chemistry Chemical Physics*, 2011, **13**, 15244-15255.
28. I. J. Villar-Garcia, E. F. Smith, A. W. Taylor, F. L. Qiu, K. R. J. Lovelock, R. G. Jones and P. Licence, *Physical Chemistry Chemical Physics*, 2011, **13**, 2797-2808.
29. R. K. Blundell and P. Licence, *Physical Chemistry Chemical Physics*, 2014, **16**, 15278-15288.
30. S. Men, D. S. Mitchell, K. R. J. Lovelock and P. Licence, *Chemphyschem*, 2015, **16**, 2211-2218.
31. S. Men, J. Jiang and P. Licence, *Chemical Physics Letters*, 2017, **674**, 86-89.
32. B. S. Phillips and J. S. Zabinski, *Tribology Letters*, 2004, **17**, 533-541.
33. H. Kamimura, T. Kubo, I. Minami and S. Mori, *Tribology International*, 2007, **40**, 620-625.
34. V. Totolin, M. Conte, E. Berriozabal, F. Pagano, I. Minami, N. Dorr, J. Brenner and A. Igartua, *Lubrication Science*, 2014, **26**, 514-524.
35. A. H. Battez, M. Bartolome, D. Blanco, J. L. Viesca, A. Fernandez-Gonzalez and R. Gonzalez, *Tribology International*, 2016, **95**, 118-131.
36. R. Gonzalez, M. Bartolome, D. Blanco, J. L. Viesca, A. Fernandez-Gonzalez and A. H. Battez, *Tribology International*, 2016, **98**, 82-93.
37. V. Totolin, L. Pisarova, N. Dorr and I. Minami, *Rsc Advances*, 2017, **7**, 48766-48776.
38. N. Rivera, D. Blanco, J. L. Viesca, A. Fernandez-Gonzalez, R. Gonzalez and A. H. Battez, *Journal of Molecular Liquids*, 2019, **296**, 12.
39. C. F. Ye, W. M. Liu, Y. X. Chen and L. G. Yu, *Chemical Communications*, 2001, 2244-2245.
40. J. Qu, P. J. Blau, S. Dai, H. M. Luo, H. M. Meyer and J. J. Truhan, *Wear*, 2009, **267**, 1226-1231.
41. I. Minami, *Molecules*, 2009, **14**, 2286-2305.
42. F. P. Bowden and D. Tabor, *The Friction and Lubrication of Solids*, Oxford University Press, 2001.
43. Y. Kondo, S. Yagi, T. Koyama, R. Tsuboi and S. Sasaki, *Proceedings of the Institution of Mechanical Engineers Part J-Journal of Engineering Tribology*, 2012, **226**, 991-1006.
44. I. Minami, T. Inada and Y. Okada, *Proceedings of the Institution of Mechanical Engineers Part J-Journal of Engineering Tribology*, 2012, **226**, 891-902.
45. Z. H. Song, Y. M. Liang, M. J. Fan, F. Zhou and W. M. Liu, *Rsc Advances*, 2014, **4**, 19396-19402.
46. G. Q. Chen, F. Z. Li, C. Y. Zhang, X. X. Guo, Z. Z. Yang, Q. L. Yu, B. Yu, M. R. Cai and D. P. Tian, *Journal of Molecular Liquids*, 2021, **343**.

47. J. Qu, D. G. Bansal, B. Yu, J. Y. Howe, H. M. Luo, S. Dai, H. Q. Li, P. J. Blau, B. G. Bunting, G. Mordukhovich and D. J. Smolenski, *Acs Applied Materials & Interfaces*, 2012, **4**, 997-1002.
48. Q. L. Yu, C. Y. Zhang, R. Dong, Y. J. Shi, Y. R. Wang, Y. Y. Bai, J. Y. Zhang, M. R. Cai and F. Zhou, *Tribology International*, 2019, **132**, 118-129.
49. R. Gusain, A. Khan and O. P. Khatri, *Journal of Molecular Liquids*, 2020, **301**, 9.
50. M. Bartolome, D. Goncalves, A. G. Tuero, R. Gonzalez, A. H. Battez and J. H. O. Seabra, *Tribology International*, 2021, **156**, 10.
51. J. J. Jia, G. B. Yang, C. L. Zhang, S. M. Zhang, Y. J. Zhang and P. Y. Zhang, *Friction*, 14.
52. B. P. Payne, M. C. Biesinger and N. S. McIntyre, *Journal of Electron Spectroscopy and Related Phenomena*, 2012, **185**, 159-166.
53. J. H. Liu, S. Van den Berghe and M. J. Konstantinovic, *Journal of Solid State Chemistry*, 2009, **182**, 1105-1108.
54. A. P. Pijpers and R. J. Meier, *Chemical Society Reviews*, 1999, **28**, 233-238.
55. C. Kolbeck, T. Cremer, K. R. J. Lovelock, N. Paape, P. S. Schulz, P. Wasserscheid, F. Maier and H. P. Steinruck, *Journal of Physical Chemistry B*, 2009, **113**, 8682-8688.
56. V. Lockett, R. Sedev, C. Bassell and J. Ralston, *Physical Chemistry Chemical Physics*, 2008, **10**, 1330-1335.
57. A. R. Santos, R. K. Blundell and P. Licence, *Physical Chemistry Chemical Physics*, 2015, **17**, 11839-11847.
58. C. J. Clarke, S. Maxwell-Hogg, E. F. Smith, R. R. Hawker, J. B. Harper and P. Licence, *Physical Chemistry Chemical Physics*, 2019, **21**, 114-123.
59. N. E. A. Cousens, L. J. T. Kearney, M. T. Clough, K. R. J. Lovelock, R. G. Palgrave and S. Perkin, *Dalton Transactions*, 2014, **43**, 10910-10919.
60. A. W. Taylor and P. Licence, *Chemphyschem*, 2012, **13**, 1917-1926.
61. A. Zafar, T. Evans, R. G. Palgrave and T. A. Din, *Journal of Chemical Research*, 2022, **46**, 11.
62. C. Cadena, Q. Zhao, R. Q. Snurr and E. J. Maginn, *Journal of Physical Chemistry B*, 2006, **110**, 2821-2832.
63. B. Bittner, R. J. Wrobel and E. Milchert, *Journal of Chemical Thermodynamics*, 2012, **55**, 159-165.
64. M. Mahrova, F. Pagano, V. Pejakovic, A. Valea, M. Kalin, A. Igartua and E. Tojo, *Tribology International*, 2015, **82**, 245-254.
65. T. Hammer, M. Reichelt and H. Morgner, *Physical Chemistry Chemical Physics*, 2010, **12**, 11070-11080.
66. J. L. Wang, H. W. Yao, Y. Nie, X. P. Zhang and J. W. Li, *Journal of Molecular Liquids*, 2012, **169**, 152-155.
67. H. Abe, S. Maruyama, Y. Hata, S. Shimono and H. Kishimura, *Chemical Physics Letters*, 2020, **748**, 5.
68. X. Z. Dai, J. H. Li, Y. Z. Ma, X. Q. Lan and H. Song, *Journal of Molecular Liquids*, 2018, **254**, 226-230.
69. X. Z. Dai, X. L. Qiang, J. H. Li, T. Yao, Z. X. Wang and H. Song, *Journal of Molecular Liquids*, 2019, **277**, 170-174.

70. E. Toolbox, *Viscosity - Absolute (Dynamic) and Kinematic* . [online], https://www.engineeringtoolbox.com/dynamic-absolute-kinematic-viscosity-d_412.html, (accessed 13/01/2022).
71. J. G. Huddleston, A. E. Visser, W. M. Reichert, H. D. Willauer, G. A. Broker and R. D. Rogers, *Green Chemistry*, 2001, **3**, 156-164.
72. H. Tokuda, K. Hayamizu, K. Ishii, M. Abu Bin Hasan Susan and M. Watanabe, *Journal of Physical Chemistry B*, 2004, **108**, 16593-16600.
73. K. T. Greeson, N. G. Hall, N. D. Redeker, J. C. Marcischak, L. V. Gilmore, J. A. Boatz, T. C. Le, J. R. Alston, A. J. Guenthner and K. B. Ghiassi, *Journal of Molecular Liquids*, 2018, **265**, 701-710.
74. S. A. Pierson, O. Nacham, K. D. Clark, H. Nan, Y. Mudryk and J. L. Anderson, *New Journal of Chemistry*, 2017, **41**, 5498-5505.
75. Viscosity Index Calculator, www.tribonet.org/calculators/viscosity-index-calculator/, (accessed 06/06/2022).
76. Fomblin FAQs, https://www.solvay.com/en/brands/fomblin-pfpe-lubricants/faq#:~:text=Fomblin®%20PFPE%20lubricants%20cover,a%20wider%20operating%20temperature%20range., (accessed 31/10/2022, 2022).
77. L. Matczak, C. Johanning, E. Gil, H. Guo, T. W. Smith, M. Schertzer and P. Iglesias, *Tribology International*, 2018, **124**, 23-33.
78. S. Bhattacharjee and S. Khan, *Fluid Phase Equilibria*, 2019, **501**, 10.
79. H. L. Ngo, K. LeCompte, L. Hargens and A. B. McEwen, *Thermochimica Acta*, 2000, **357**, 97-102.
80. C. Maton, N. De Vos and C. V. Stevens, *Chemical Society Reviews*, 2013, **42**, 5963-5977.
81. C. J. Reeves, A. K. Kasar and P. L. Menezes, *Journal of Cleaner Production*, 2021, **279**, 14.
82. D. F. Evans, *Journal of Physics E-Scientific Instruments*, 1974, **7**, 247-249.
83. G. A. Bain and J. F. Berry, *Journal of Chemical Education*, 2008, **85**, 532-536.
84. Paramagnetism in Lanthanides, www.radiochemistry.org/periodictable/la_series/L8.html, (accessed 07/07/2022).
85. C. Iacovita, A. Florea, R. Dudric, E. Pall, A. I. Moldovan, R. Tetean, R. Stiufiuc and C. M. Lucaciu, *Molecules*, 2016, **21**, 21.
86. Coefficient of friction, https://www.sciencedirect.com/topics/engineering/coefficient-of-friction, (accessed 11/11/2020).
87. S. Shaffer, Stribeck Curve in reciprocating test, www.bruker.com/en/products-and-solutions/test-and-measurement/tribometers-and-mechanical-testers/stribeck-curves-in-reciprocating-test.html, (accessed 18/11/2021).
88. R. A. Reich, P. A. Stewart, J. Bohaychick and J. A. Urbanski, *Lubrication Engineering*, 2003, **59**, 16-21.
89. R. Gonzalez, J. L. Viesca, A. H. Battez, M. Hadfield, A. Fernandez-Gonzalez and M. Bartolome, *Journal of Molecular Liquids*, 2019, **293**, 10.
90. M. B. Saez, A. E. H. Battez, J. E. Casado, J. L. V. Rodriguez, A. Fernandez-Gonzalez and R. G. Rodriguez, *Industrial Lubrication and Tribology*, 2021, **73**, 137-144.

91. Y. R. Wang, P. Yang, B. Guo, N. Jiang, J. Y. Chi, J. J. Liu, Y. J. Liang, Q. L. Yu, S. Y. Yang, F. Guo, M. R. Cai and F. Zhou, *Tribology International*, 2021, **164**, 11.
92. M. J. G. Guimarey, D. E. P. Goncalves, J. M. L. del Rio, M. J. P. Comunas, J. Fernandez and J. H. O. Seabra, *Journal of Molecular Liquids*, 2021, **335**, 13.
93. J. Faes, R. Gonzalez, D. Blanco, A. Fernandez-Gonzalez, A. Hernandez-Battez, P. Iglesias and J. L. Viesca, *Lubricants*, 2022, **10**, 15.
94. C. T. Lee, M. B. Lee, S. H. Hamdan, W. W. F. Chong, C. T. Chong, H. Zhang and A. W. L. Chen, *Engineering Science and Technology-an International Journal-Jestech*, 2022, **35**, 10.
95. A. Foelske-Schmitz and M. Sauer, *Journal of Electron Spectroscopy and Related Phenomena*, 2018, **224**, 51-58.
96. IR Spectrum Table, www.sigmaaldrich.com/GB/en/technical-documents/technical-article/analytical-chemistry/photometry-and-reflectometry/ir-spectrum-table, (accessed 22/09/2022).
97. J. J. Jia, G. B. Yang, C. L. Zhang, S. M. Zhang, Y. J. Zhang and P. Y. Zhang, *Friction*, 2019, 14.
98. D. A. Beattie, S. L. Harmer-Bassell, T. T. M. Ho, M. Krasowska, J. Ralston, P. M. F. Sellapperumage and P. Wasik, *Physical Chemistry Chemical Physics*, 2015, **17**, 4199-4209.
99. B. P. Reed, J. Radnik and A. G. Shard, *Surface Science Spectra*, 2022, **29**, 8.
100. F. Scientific, Common background contaminants in Mass Spectrometry, https://beta-static.fishersci.ca/content/dam/fishersci/en_US/documents/programs/scientific/brochures-and-catalogs/posters/fisher-chemical-poster.pdf, (accessed 29/11/2022).
101. Z. Q. He and P. Alexandridis, *Advances in Colloid and Interface Science*, 2017, **244**, 54-70.
102. P. Migowski, G. Machado, S. R. Texeira, M. C. M. Alves, J. Morais, A. Traverse and J. Dupont, *Physical Chemistry Chemical Physics*, 2007, **9**, 4814-4821.
103. C. W. Scheeren, G. Machado, S. R. Teixeira, J. Morais, J. B. Domingos and J. Dupont, *Journal of Physical Chemistry B*, 2006, **110**, 13011-13020.
104. L. Rodriguez-Arco, M. T. Lopez-Lopez, J. D. G. Duran, A. Zubarev and D. Chirikov, *Journal of Physics-Condensed Matter*, 2011, **23**, 15.
105. T. Fukushima and T. Aida, *Chemistry-a European Journal*, 2007, **13**, 5048-5058.
106. Y. S. Liu, G. Z. Wu, H. Y. Fu, Z. Jiang, S. M. Chen and M. L. Sha, *Dalton Transactions*, 2010, **39**, 3190-3194.
107. X. Shi, W. Huang and X. L. Wang, *Lubrication Science*, 2018, **30**, 73-82.
108. X. L. Yu, X. Y. Yuan, Z. Y. Xia and L. X. Ren, *Polymer Chemistry*, 2018, **9**, 5116-5122.
109. X. L. Yu, X. Y. Yuan, Y. H. Zhao and L. X. Ren, *Acs Macro Letters*, 2019, **8**, 1504-1510.
110. M. F. Hoover, *Journal of Macromolecular Science-Chemistry*, 1970, **A 4**, 1327-&.

111. J. C. Salamone, E. J. Ellis and Bardoliw.Df, *Journal of Polymer Science Part C-Polymer Symposium*, 1974, 51-64.
112. J. C. Salamone, S. C. Israel, P. Taylor and B. Snider, *Journal of Polymer Science Part C-Polymer Symposium*, 1974, 65-73.
113. J. C. Salamone, P. Taylor, B. Snider and S. C. Israel, *Abstracts of Papers of the American Chemical Society*, 1974, 63-63.
114. J. Y. Yuan and M. Antonietti, *Polymer*, 2011, **52**, 1469-1482.
115. H. D. Tang, J. B. Tang, S. J. Ding, M. Radosz and Y. Q. Shen, *Journal of Polymer Science Part a-Polymer Chemistry*, 2005, **43**, 1432-1443.
116. K. Vijayakrishna, S. K. Jewrajka, A. Ruiz, R. Marcilla, J. A. Pomposo, D. Mecerreyes, D. Taton and Y. Gnanou, *Macromolecules*, 2008, **41**, 6299-6308.
117. P. Glinska, A. Wolan, W. Kujawski, E. Rynkowska and J. Kujawa, *Molecules*, 2021, **26**, 16.
118. J. Zhao, X. J. Shen, F. Yan, L. H. Qiu, S. T. Lee and B. Q. Sun, *Journal of Materials Chemistry*, 2011, **21**, 7326-7330.
119. W. Li, J. Fang, M. Lv, C. X. Chen, X. J. Chi, Y. X. Yang and Y. M. Zhang, *Journal of Materials Chemistry*, 2011, **21**, 11340-11346.
120. Y. Xie, Z. F. Zhang, T. Jiang, J. L. He, B. X. Han, T. B. Wu and K. L. Ding, *Angewandte Chemie-International Edition*, 2007, **46**, 7255-7258.
121. Q. Zhao, P. F. Zhang, M. Antonietti and J. Y. Yuan, *Journal of the American Chemical Society*, 2012, **134**, 11852-11855.
122. A. S. L. Gouveia, V. Oliveira, A. M. Ferraria, A. M. B. Do Rego, M. J. Ferreira, L. C. Tome, A. Almeida and I. M. Marrucho, *Journal of Membrane Science*, 2022, **642**, 13.
123. R. V. Barrulas, M. Zanatta, T. Casimiro and M. C. Corvo, *Chemical Engineering Journal*, 2021, **411**, 15.
124. Z. Y. Wang, Y. Y. Wang, J. H. Chen, M. Arnould, I. Popovs, S. M. Mahurin, H. Chen, T. Wang and S. Dai, *Langmuir*, 2021, **37**, 10875-10881.
125. S. Supasitmongkol and P. Styring, *Energy & Environmental Science*, 2010, **3**, 1961-1972.
126. Y. X. Zhang, T. Cai, W. J. Shang, L. W. Sun, D. Liu, D. Y. Tong and S. G. Liu, *Tribology International*, 2017, **115**, 297-306.
127. A. P. Bapat, R. Erck, B. T. Seymour, B. Zhao and L. Cosimbescu, *Reactive & Functional Polymers*, 2018, **131**, 150-155.
128. J. Wu, L. W. Mu, X. Feng, X. H. Lu, R. Larsson and Y. J. Shi, *Advanced Materials Interfaces*, 2019, **6**, 8.
129. B. A. Zhang, G. Sudre, G. Quintard, A. Serghei, J. Bernard, E. Fleury and A. Charlot, *Polymer*, 2021, **237**, 8.
130. X. Y. Zheng, L. J. He, Y. J. Duan, X. M. Jiang, G. Q. Xiang, W. J. Zhao and S. S. Zhang, *Journal of Chromatography A*, 2014, **1358**, 39-45.

6.2 Appendix

General remarks

^{1}H NMR and ^{13}C NMR were recorded at 500/400 MHz, 125/100 MHz and 470/376 MHz on Bruker Avance 500/400 spectrometers. All spectra are referenced to $(CD_3)_2SO$ residual solvent peaks (^{1}H NMR δ = 2.50 ppm; ^{13}C NMR δ = 39.52 ppm). All chemical shifts are quoted in parts per million (ppm), measured from the centre of the signal except in the case of multiplets which are quoted as a range. Coupling constants are quoted to the nearest 0.1 Hz. Splitting patterns are abbreviated as follows: broad singlet (br. s), singlet (s), doublet (d), triplet (t), quartet (q), quintet (quin), sextet (sext), multiplet (m) and combinations thereof. Raman spectra were acquired using a Renishaw inVia Raman microscope with a 50 x objective in a back scattering configuration. The excitation wavelength was 785 nm (130 mW, 10 %) and the acquisition time 20s. The laser spot size was around 1 μm^2.

Infrared (IR) spectra were recorded on a spectrometer as neat using a Bruker Alpha spectrometer.
All reagents and solvents were used as obtained from commercial source, unless otherwise stated.

6.2.1 Synthesis of MILs

Synthesis of 1-methyl, 3-butyl 1H imidazolium tetrachloroferrate, MIL1

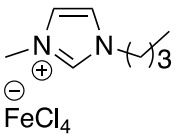

To a 100 mL round bottom flask, 1-methyl Imidazole (4.105 g, 0.05 mol, 1 eq.) was added, Chloro-butane (4.629 g, 0.05 mol, 1 eq.) was then added and the resulting mixture was stirred and heated under reflux conditions at 90 °C for 7 days. The reaction was monitored by ^{1}H NMR. Once complete the reaction was allowed to cool to room temperature where Iron (III) chloride hexahydrate (13.515 g, 0.05 mol, 1 eq.) was then added under stirring. An endothermic reaction took place, once complete the resulting mixture was then washed with ether (40 mL) and distilled water (40 mL). The final mixture was dried under

high vacuum for 5 hours at 65 °C. This yielded the title product as a brown liquid. (6.1581 g, 0.02 mol, 36 %)

^{1}H NMR (400 MHz, $(CD_3)_2SO$, ppm): **δ** 9.08 (s, 1 H), 7.74 (t, *J* = 1.67 Hz, 1 H), 7.67 (t, *J* = 1.88 Hz, 1 H), 4.15 (t *J* = 7.32 Hz, 2 H), 3.84 (s, 3 H), 1.81 – 1.73 (m, 2 H), 1.32 – 1.22 (m, 2 H), 0.90 (t, *J* = 9.53 Hz, 3 H); ^{13}C NMR (100 MHz, $(CD_3)_2SO$, ppm): **δ** 136.5, 123.6, 122.3, 48.5, 35.7, 31.4, 18.8, 12.2

Synthesis of 1-methyl, 3-octyl 1H imidazolium tetrachloroferrate, MIL2

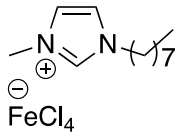

To a 100 mL round bottom flask, 1-methyl Imidazole (4.105 g, 0.05 mol, 1 eq.) was added, Chloro-octane (7.434 g, 0.05 mol, 1 eq.) was then added and the resulting mixture was stirred and heated under reflux conditions at 90 °C for 7 days. The reaction was monitored by ^{1}H NMR. Once complete the reaction was allowed to cool to room temperature where Iron (III) chloride hexahydrate (13.515 g, 0.05 mol, 1 eq.) was then added under stirring. An endothermic reaction took place, once complete the resulting mixture was then washed with ether (40 mL) and distilled water (40 mL). The final mixture was dried under high vacuum for 5 hours at 65 °C. This yielded the title product as a brown liquid. (12.463 g, 0.03 mol, 63 %)

^{1}H NMR (400 MHz, $(CD_3)_2SO$, ppm): **δ** 9.35 (s, 1 H), 7.82 (t, *J* = 1.67 Hz, 1 H), 7.75 (t, *J* = 1.88 Hz, 1 H), 4.17 (t *J* = 7.32 Hz, 2 H), 3.86 (s, 3 H), 1.81 – 1.73 (m, 2 H), 1.24 (br. s, 10 H), 0.85 (t, *J* = 6.9 Hz, 3 H); ^{13}C NMR (100 MHz, $(CD_3)_2SO$, ppm): **δ** 136.7, 123.6, 122.3, 48.8, 35.8, 31.2, 29.4, 28.5, 28.4, 25.5, 22.1, 13.9

Synthesis of 1-methyl, 3-decyl 1H imidazolium tetrachloroferrate, MIL3

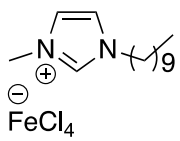

To a 100 mL round bottom flask, 1-methyl Imidazole (4.105 g, 0.05 mol, 1 eq.) was added, Chloro-decane (8.837 g, 0.05 mol, 1 eq.) was then added and the

resulting mixture was stirred and heated under reflux conditions at 90 °C for 7 days. The reaction was monitored by ^{1}H NMR. Once complete the reaction was allowed to cool to room temperature where Iron (III) chloride hexahydrate (13.515 g, 0.05 mol, 1 eq.) was then added under stirring. An endothermic reaction took place, once complete the resulting mixture was then washed with ether (40 mL) and distilled water (40 mL). The final mixture was dried under high vacuum for 5 hours at 65 °C. This yielded the title product as a brown liquid. (7.876 g, 0.02 mol, 37 %)

^{1}H NMR (400 MHz, $(CD_3)_2SO$, ppm): **δ** 9.18 (s, 1 H), 7.78 (t, *J* = 1.67 Hz, 1 H), 7.71 (t, *J* = 1.78 Hz, 1 H), 4.15 (t *J* = 7.24 Hz, 2 H), 3.85 (s, 3 H), 1.81 – 1.71 (m, 2 H), 1.24 (br. s, 14 H), 0.85 (t, *J* = 6.54 Hz, 3 H); ^{13}C NMR (100 MHz, $(CD_3)_2SO$, ppm): **δ** 137.9, 123.6, 122.3, 48.8, 35.8, 31.3, 29.4, 28.9, 28.8, 28.7, 28.4, 25.5, 22.1, 14.0

Synthesis of 1-methyl, 3-butyl 1H imidazolium bromo-trichloroferrate, MIL4

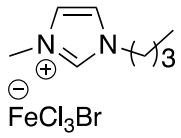

To a 100 mL round bottom flask, 1-methyl Imidazole (4.105 g, 0.05 mol, 1 eq.) was added, Bromo-butane (6.851 g, 0.05 mol, 1 eq.) was then added and the resulting mixture was stirred and heated under reflux conditions at 90 °C for 4 hours. The reaction was monitored by ^{1}H NMR. Once complete the reaction was allowed to cool to room temperature where Iron (III) chloride hexahydrate (13.515 g, 0.05 mol, 1 eq.) was then added under stirring. An endothermic reaction took place, once complete the resulting mixture was then washed with ether (40 mL) and distilled water (40 mL). The final mixture was dried under high vacuum for 5 hours at 65 °C. This yielded the title product as a brown liquid. (15.498 g, 0.04 mol, 81 %)

^{1}H NMR (400 MHz, $(CD_3)_2SO$, ppm): **δ** 9.10 (s, 1 H), 7.74 (t, *J* = 1.67 Hz, 1 H), 7.67 (t, *J* = 1.88 Hz, 1 H), 4.16 (t *J* = 7.32 Hz, 2 H), 3.85 (s, 3 H), 1.81 – 1.73 (m, 2 H), 1.32 – 1.22 (m, 2 H), 0.90 (t, *J* = 7.53 Hz, 3 H); ^{13}C NMR (100 MHz, $(CD_3)_2SO$, ppm): **δ** 136.5, 123.6, 122.3, 48.5, 35.7, 31.4, 18.8, 13.2

Synthesis of 1-methyl, 3-decyl 1H imidazolium bromo-trichloroferrate, MIL5

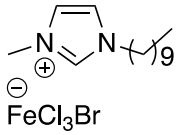

To a 100 mL round bottom flask, 1-methyl Imidazole (4.105 g, 0.05 mol, 1 eq.) was added, Bromo-decane (12.4615 g, 0.05 mol, 1 eq.) was then added and the resulting mixture was stirred and heated under reflux conditions at 90 °C for 3 days. The reaction was monitored by ^{1}H NMR. Once complete the reaction was allowed to cool to room temperature where Iron (III) chloride hexahydrate (13.515 g, 0.05 mol, 1 eq.) was then added under stirring. An endothermic reaction took place, once complete the resulting mixture was then washed with ether (40 mL) and distilled water (40 mL). The final mixture was dried under high vacuum for 5 hours at 65 °C. This yielded the title product as a brown liquid. (19.218 g, 0.04 mol, 83 %)

^{1}H NMR (400 MHz, $(CD_3)_2SO$, ppm): **δ** 9.15 (s, 1 H), 7.78 (t, *J* = 1.76 Hz, 1 H), 7.71 (t, *J* = 1.67 Hz, 1 H), 4.15 (t *J* = 7.35 Hz, 2 H), 3.85 (s, 3 H), 1.81 – 1.72 (m, 2 H), 1.24 (br. s, 14 H), 0.85 (t, *J* = 6.70 Hz, 3 H); ^{13}C NMR (100 MHz, $(CD_3)_2SO$, ppm): **δ** 136.5, 123.6, 122.3, 48.8, 35.8, 31.3, 29.4, 28.9, 28.8, 28.7, 28.4, 25.5, 22.1, 14.0

Synthesis of 1-Decyl Pyridin-1-ium bromo-trichloroferrate, MIL6

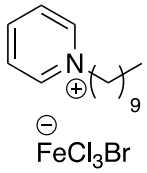

To a 100 mL round bottom flask, Pyridine (3.955 g, 0.05 mol, 1 eq.) was added, bromo-decane (12.462 g, 0.05 mol, 1 eq.) was then added and the resulting mixture was stirred and heated under reflux conditions at 90 °C for 3 days. The reaction was monitored by ^{1}H NMR. Once complete the reaction was allowed to cool to room temperature where Iron (III) chloride hexahydrate (13.515 g, 0.05 mol, 1 eq.) was then added under stirring. An endothermic reaction took place, once complete the resulting mixture was then washed with ether (40 mL) and distilled water (40 mL). The final mixture was dried under high vacuum for 5

hours at 65 °C. This yielded the title product as a brown liquid. (16.517 g, 0.04 mol, 71 %)

^{1}H NMR (400 MHz, $(CD_3)_2SO$, ppm): **δ** 9.14 (d, *J* = 5.66 Hz, 2 H), 8.64 – 8.59 (m, 1 H), 8.17 (t, *J* = 7.08 Hz, 2 H), 4.62 (t, *J* = 7.08 Hz, 2 H), 1.9 (quin. 2 H), 1.22 (br. S, 14 H), 0.84 (t, *J* = 6.37 Hz, 3 H); ^{13}C NMR (100 MHz, $(CD_3)_2SO$, ppm): **δ** 145.5, 144.8, 128.1, 60.7, 31.3, 30.7, 28.9, 28.8, 28.7, 28.4, 25.4, 22.1, 14.0

Synthesis of 1-Decyl, 3-Methylpyridin-1-ium bromotrichloroferrate, MIL7

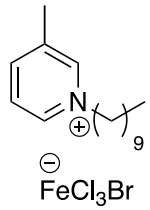

To a 100 mL round bottom flask, 3-methyl pyridine (4.657 g, 0.05 mol, 1 eq.) was added, bromo-decane (12.462 g, 0.05 mol, 1 eq.) was then added and the resulting mixture was stirred and heated under reflux conditions at 90 °C for 3 days. The reaction was monitored by ^{1}H NMR. Once complete the reaction was allowed to cool to room temperature where Iron (III) chloride hexahydrate (13.515 g, 0.05 mol, 1 eq.) was then added under stirring. An endothermic reaction took place, once complete the resulting mixture was then washed with ether (40 mL) and distilled water (40 mL). The final mixture was dried under high vacuum for 5 hours at 65 °C. This yielded the title product as a brown liquid. (15.856 g, 0.03 mol, 67 %)

^{1}H NMR (400 MHz, $(CD_3)_2SO$, ppm): **δ** 9.05 (s, 1 H), 8.94 (d, *J* = 6.07 Hz, 1 H), 8.44 (d, *J* = 8.35 Hz, 1 H), 8.05 (m, 1 H), 4.55 (t, *J* = 7.59 Hz, 2 H), 3.33 (s, 4 H), 2.49 (br. S, 3 H), 1.23 (br. s, 12 H), 0.85 (t, *J* = 6.83 Hz, 3 H); ^{13}C NMR (100 MHz, $(CD_3)_2SO$, ppm): **δ** 145.8, 144.3, 142.0, 138.8, 127.4, 60.6, 31.3, 30.7, 28.9, 28.8, 28.7, 28.4, 25.4, 22.1, 17.9, 14.0

Synthesis of Tri(1-Butyl-3-methyl Imidazolium) Hexanitratodysprosate, MIL8

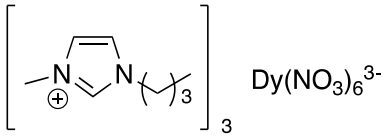

To a 100 mL round bottom flask, 1-methyl imidazole (4.105 g, 0.05 mol, 1 eq.) was added. Bromo-butane (6.861 g, 0.05 mol, 1 eq.) was then added and the resulting mixture was stirred and heated under reflux conditions at 90 °C for 3 hours. The reaction mixture was monitored by ^{1}H NMR, once complete the resulting mixture was allowed to cool to room temperature where silver nitrate (5.493 g, 0.05 mol, 1 eq.) was then added in acetonitrile where a yellow precipitate then formed. The precipitate was filtered and removed, and the solvent was removed under vacuum. The mixture was then re-dissolved in acetonitrile (30 mL) and filtered twice where acetonitrile was then removed again under vacuum. Dysprosium nitrate (5.809 g, 0.016 mol, 0.33 eq.) was then added and the resulting mixture was dried under high vacuum at 80 °C for 4 hours. This yielded the title compound as a pale grey/yellow liquid. (8.407 g, 0.008 mol, 55 %)

^{1}H NMR (400 MHz, $(CD_3)_2SO$, ppm): **δ** 9.10 (s, 1 H), 7.74 (t, *J* = 1.67 Hz, 1 H), 7.67 (t, *J* = 1.88 Hz, 1 H), 4.16 (t, *J* = 7.32 Hz, 2 H), 3.85 (s, 3 H), 1.81 – 1.73 (m, 2 H), 132 – 1.22 (m, 2 H), 0.9 (t, *J* = 7.53 Hz, 3 H); ^{13}C NMR (100 MHz, $(CD_3)_2SO$, ppm): **δ** 136.5, 123.6, 122.3, 48.5, 35.7, 31.4, 18.8, 13.2; IR ν_{max} (neat) /cm^{-1}: 3152, 3110, 2962, 2875, 1570, 1467, 1298, 1163, 1112, 1027, 949, 830, 815, 742, 652, 621

Synthesis of Tri(1-Decyl-3-methyl Imidazolium) Hexanitratodysprosate, MIL9

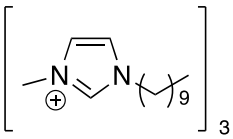

$Dy(NO_3)_6^{3-}$

To a 100 mL round bottom flask, 1-methyl imidazole (4.105 g, 0.05 mol, 1 eq.) was added. Bromo-decane (12.462 g, 0.05 mol, 1 eq.) was then added and the resulting mixture was stirred and heated under reflux conditions at 90 °C for 24 hours. The reaction mixture was monitored by ^{1}H NMR, once complete the resulting mixture was allowed to cool to room temperature where silver nitrate (5.493 g, 0.05 mol, 1 eq.) was then added in acetonitrile where a yellow precipitate then formed. The precipitate was filtered and removed, and the solvent was removed under vacuum. The mixture was then re-dissolved in acetonitrile (30 mL) and filtered twice where acetonitrile was then removed

again under vacuum. Dysprosium nitrate (5.809 g, 0.016 mol, 0.33 eq.) was then added and the resulting mixture was dried under high vacuum at 80 °C for 4 hours. This yielded the title compound as a pale yellow liquid. (10.759 g, 0.008 mol, 55 %)

^{1}H NMR (400 MHz, $(CD_3)_2SO$, ppm): **δ** 9.15 (s, 1 H), 7.78 (t, *J* = 1.76 Hz, 1 H), 7.71 (t, *J* = 1.67 Hz, 1 H), 4.15 (t, *J* = 7.35 Hz, 2 H), 3.85 (s, 3 H), 1.81 – 1.72 (m, 2 H), 1.24 (br. s, 14 H), 0.85 (t, *J* = 6.70 Hz, 3 Hz); ^{13}C NMR (100 MHz, $(CD_3)_2SO$, ppm): **δ** 136.5, 123.6, 122.3, 48.8, 35.8, 31.3, 29.4, 28.9, 28.8, 28.7, 28.4, 25.5, 22.1, 14.0; IR ν_{max} (neat) /cm^{-1}: 2923, 2854, 1479, 1299, 1163, 1026, 815, 742, 651, 622

Synthesis of Tri(1-butyl Pyridin-1-ium) Hexanitratodysprosate, MIL10

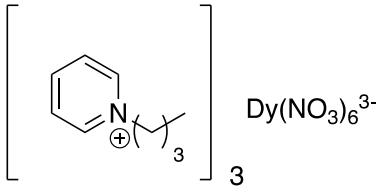

To a 100 mL round bottom flask, Pyridine (3.955 g, 0.05 mol, 1 eq.) was added. Bromo-butane (6.851 g, 0.05 mol, 1 eq.) was then added and the resulting mixture was stirred and heated under reflux conditions at 90 °C for 5 hours. The reaction mixture was monitored by ^{1}H NMR, once complete the resulting mixture was allowed to cool to room temperature where silver nitrate (8.493 g, 0.05 mol, 1 eq.) was then added in acetonitrile where a yellow precipitate then formed. The precipitate was filtered and removed, and solvent was removed under vacuum. The mixture was then re-dissolved in acetonitrile (30 mL) and filtered twice where acetonitrile was then removed again under vacuum. Dysprosium nitrate (5.809 g, 0.016 mol, 0.33 eq.) was then added and the resulting mixture was dried under high vacuum at 80 °C for 4 hours. This yielded the title compound as a pale yellow liquid. (7.7917 g, 0.008 mol, 51 %)

^{1}H NMR (400 MHz, $(CD_3)_2SO$, ppm): **δ** 9.12 (d J = 5.51 Hz, 2 H), 8.64 – 8.58 (m, 1 H), 8.17 (t, J = 7.23 Hz, 2 H), 4.62 (t, *J* = 7.92 Hz, 2 H), 1.93 – 1.85 (m, 2 H), 1.27 (sext. *J* = 7.51 Hz, 2 H), 0.91 (t, *J* = 7.51 Hz, 3 H); ^{13}C NMR (100 MHz, $(CD_3)_2SO$, ppm): **δ** 145.5, 144.8, 128.1, 60.6, 32.7, 18.8, 13.3; IR ν_{max} (neat) /cm^{-1}: 3067, 2964, 1466, 1297, 1169, 1027, 815, 769, 742, 682

Synthesis of Tri(1-Decyl Pyridin-1-ium) Hexanitratodysprosate, MIL11

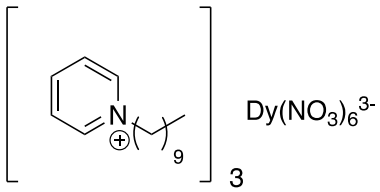

To a 100 mL round bottom flask, Pyridine (3.955 g, 0.05 mol, 1 eq.) was added. Bromo-decane (12.4615 g, 0.05 mol, 1 eq.) was then added and the resulting mixture was stirred and heated under reflux conditions at 90 °C for 24 hours. The reaction mixture was monitored by ^{1}H NMR, once complete the resulting mixture was allowed to cool to room temperature where silver nitrate (8.493 g, 0.05 mol, 1 eq.) was then added in a acetonitrile where a yellow precipitate then formed. The precipitate was filtered and removed, and the solvent was removed under vacuum. The mixture was then re-dissolved in acetonitrile (30 mL) and filtered twice where acetonitrile was then removed again under vacuum. Dysprosium nitrate (5.809 g, 0.016 mol, 0.33 eq.) was then added and the resulting mixture was dried under high vacuum at 80 °C for 4 hours. This yielded the title compound as a pale yellow liquid. (11.4412 g, 0.009 mol, 59 %)

^{1}H NMR (400 MHz, $(CD_3)_2SO$, ppm): **δ** 9.14 (d, *J* = 5.66 Hz, 2 H), 8.64 – 8.59 (m, 1 H), 8.17 (t, *J* = 7.08 Hz, 2 H), 4.62 (t, *J* = 7.08 Hz, 2 H), 1.9 (quin. 2 H), 1.22 (br. s, 14 H), 0.84 (t, *J* = 6.37 Hz, 3 H); ^{13}C NMR (100 MHz, $(CD_3)_2SO$, ppm): **δ** 145.5, 144.8, 128.1, 60.7, 31.3, 30.7, 28.9, 28.8, 28.7, 28.4, 25.4, 22.1, 14.0; IR ν_{max} (neat) /cm^{-1}: 2923, 2854, 1633, 1484, 1299, 1173, 1027, 815, 742, 682

Synthesis of Tri(1-Decyl,3-methylpyridin-1-ium) Hexanitratodysprosate, MIL12

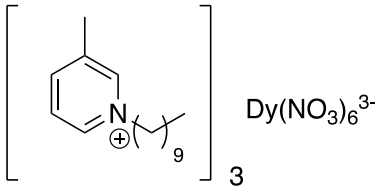

To a 100 mL round bottom flask, 3-Methyl pyridine (4.6565 g, 0.05 mol, 1 eq.) was added. Bromo-decane (12.4615 g, 0.05 mol, 1 eq.) was then added and

the resulting mixture was stirred and heated under reflux conditions at 90 °C for 24 hours. The reaction mixture was monitored by ^{1}H NMR, once complete the resulting mixture was allowed to cool to room temperature where silver nitrate (8.493 g, 0.05 mol, 1 eq.) was then added in acetonitrile where a yellow precipitate then formed. The precipitate was filtered and removed, and the solvent was removed under vacuum. The mixture was then re-dissolved in acetonitrile (30 mL) and filtered twice where acetonitrile was then removed again under vacuum. Dysprosium nitrate (5.809 g, 0.016 mol, 0.33 eq.) was then added and the resulting mixture was dried under high vacuum at 80 °C for 4 hours. This yielded the title compound as a pale yellow liquid. (9.8104 g, 0.008 mol, 49 %)

^{1}H NMR (400 MHz, $(CD_3)_2SO$, ppm): **δ** 9.05 (s, 1 H), 8.94 (d, *J* = 6.07 Hz, 1 H), 8.44 (d, *J* = 8.35 Hz, 1 H), 8.05 (m, 1 H), 4.55 (t, *J* = 7.59 Hz, 2 H), 3.33 (s, 4 H), 2.49 (br. s, 3 H), 1.23 (br. s, 12 H), 0.85 (t, *J* = 6.83 Hz, 3 H); ^{3}C NMR (100 MHz, $(CD_3)_2SO$, ppm): **δ** 145.8, 144.3, 142.0, 138.8, 127.4, 60.6, 31.3, 30.7, 28.9, 28.8, 28.7, 28.4, 25.4, 22.1, 17.9, 14.0;

IR ν_{max} (neat) /cm^{-1}: 2924, 2854, 1629, 1478, 1299, 1153, 1026, 814, 742, 686

6.2.2 Synthesis of DcILs

1,2-Bis-(3-methyl-1-pyridinium)ethane Dibromide, DcIL1

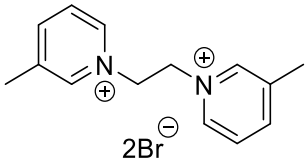

To a 100 mL round bottom flask, 3-Methyl Pyridine (4.656 g, 0.05 mol, 1 eq.) was added. 1-2 Dibromoethane (4.696 g, 0.025 mol, 0.5 eq.) was then added and mixed with 50 mL of acetonitrile. The resulting mixture was then heated to 80 °C under reflux for 24 hours. Acetonitrile was then removed under reduced pressure where the product was then dried under high vacuum.

This yielded the title product as a brown solid. (4.573 g, 0.01 mol, 48 %.)

^{1}H NMR (400 MHz, D_2O, ppm): δ 8.70 (s, 2 H), 8.59 (d, *J* = 6.13 Hz, 2 H), 8.51 (d, *J* = 7.97 Hz, 2 H), 8.00 (m, 2 H), 5.28 (s, 4 H), 2.50 (s, 6H)

^{13}C NMR (100 MHz, D_2O, ppm): δ 148.5, 144.6, 142.3, 141.7, 128.8, 60.6, 18.2

HRMS (ESI): Theoretical 293.0648, Found 293.0646 $(M - Br^-)^+$

1,5-Bis-(3-methyl-1-pyridinium)pentane Dibromide, DcIL2

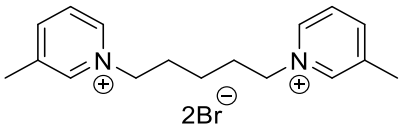

To a 100 mL round bottom flask, 3-Methyl Pyridine (4.656 g, 0.05 mol, 1 eq.) was added. 1-5 Dibromopentane (5.748 g, 0.025 mol, 0.5 eq.) was then added and mixed with 50 mL of acetonitrile. The resulting mixture was then heated to 80 °C under reflux for 24 hours. Acetonitrile was then removed under reduced pressure where the product was then dried under high vacuum.

This yielded the title product as an off-white solid. (4.593 g, 0.01 mol, 44 %.).

^{1}H NMR (400 MHz, D_2O, ppm): δ 8.71 (s, 2 H), 8.64 (d, *J* = 6.28 Hz, 2 H), 8.37 (d, *J* = 7.95 Hz, 2 H), 7.95 (m, 2 H), 4.58 (t, *J* = 6.36 Hz, 4 H), 2.56 (s, 6 H), 2.09 (quin. *J* = 7.16, 16.73, 4 H), 1.42 (m, 2 H)

^{13}C NMR (100 MHz, D_2O, ppm): δ 146.6, 144.2, 141.8, 140.5, 128.0, 61.7, 30.5, 22.6, 18.1

HRMS (ESI): Theoretical 257.2012, Found 257.2010 $(M - 2Br^- + H)^+$

1,10-Bis-(3-methyl-1-pyridinium)decane Dibromide, DcIL3

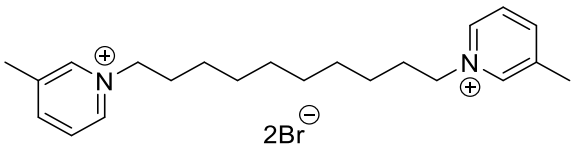

To a 100 mL round bottom flask, 3-Methyl Pyridine (4.656 g, 0.05 mol, 1 eq.) was added. 1-10 Dibromodecane (7.500 g, 0.025 mol, 0.5 eq.) was then added and mixed with 50 mL of acetonitrile. The resulting mixture was then heated to 80 °C under reflux for 24 hours. Acetonitrile was then removed under reduced pressure where the product was then dried under high vacuum.

This yielded the title product as an off-white solid. (4.330 g, 0.01 mol, 35.6 %.)

^{1}H NMR (400 MHz, D_2O, ppm): δ 8.71 (s, 2 H), 8.65 (d, *J* = 6.90 Hz, 2 H), 8.36 (d, *J* = 7.89 Hz, 2 H), 7.93 (m, 2 H), 4.56 (t, *J* = 6.90 Hz, 4 H), 2.55 (s, 6 H), 2.00 (m, 4 H), 1.32 (m, 12H)

^{13}C NMR (100 MHz, D_2O, ppm): δ 146.4, 144.2, 141.8, 140.4, 127.9, 62.2, 31.0, 28.8, 28.5, 25.7, 18.2, 1.4

HRMS (ESI): Theoretical 327.2795, Found 327.2792 $(M - 2Br^- + H)^+$

1,2-bis(pyridinium)ethane Dibromide, DcIL4

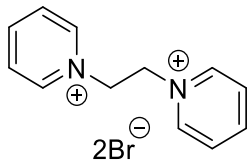

To a 100 mL round bottom flask, Pyridine (0.791 g, 0.01 mol, 1 eq.) was added. 1,2-Dibromoethane (0.939 g, 0.005 mol, 0.5 eq.) was then added and mixed with 50 mL acetonitrile. The resulting mixture was then heated to 80 °C under reflux for 24 hours. Acetonitrile was then removed under reduced pressure where the resulting product was then dried under high vacuum.

This yielded the title product as a white solid. (0.03 g, 0.002 mol, 42%)

^{1}H NMR (400 MHz, D_2O, ppm): δ 8.85 (m, 4 H), 8.70 (tt, *J* = 1.32, 6.08, 7.67, 2 H), 8.15 (m, 4 H), 5.36 (s, 4H)

^{13}C NMR (100 MHz, D_2O, ppm): δ 148.0, 145.2, 129.7, 60.7

HRMS (ESI): Theoretical 265.0335, Found 265.0335 $(M - Br^-)^+$

1,5-bis(pyridinium)pentane Dibromide, DcIL5

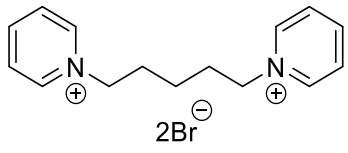

To a 100 mL round bottom flask, Pyridine (0.791 g, 0.01 mol, 1 eq.) was added. 1,10-Dibromopentane (1.1497 g, 0.005 mol, 0.5 eq.) was then added and mixed with 50 mL acetonitrile. The resulting mixture was then heated to 80 °C under reflux for 24 hours. Acetonitrile was then removed under reduced pressure where the resulting product was then dried under high vacuum.

This yielded the title product as a clear liquid. (0.63 g, 0.0018 mol, 36%)

^{1}H NMR (400 MHz, D_2O, ppm): δ 8.86 (m, 4 H), 8.57 (tt, *J* = 1.39, 6.41, 8.09, 2 H), 8.09 (t, *J* = 6.69 Hz, 4 H), 4.64 (t, *J* = 6.97, 4 H), 2.12 (quin. *J* = 7.81, 16.71, 4 H), 1.45 (m, 2 H)

^{13}C NMR (100 MHz, D_2O, ppm): δ 146.2, 144.7, 128.8, 61.9, 30.5, 22.6

HRMS (ESI): Theoretical 229.1699, Found 229.1699 $(M - 2Br^- + H)^+$

1,10-bis(pyridinium)decane Dibromide, DcIL6

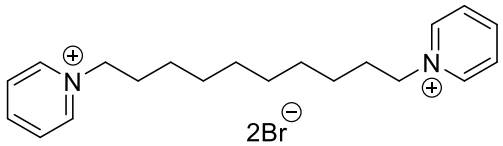

To a 100 mL round bottom flask, Pyridine (3.955 g, 0.05 mol, 1 eq.) was added. 1,10-Dibromodecane (7.500 g, 0.025 mol, 0.5 eq.) was then added and mixed with 50 mL acetonitrile. The resulting mixture was then heated to 80 °C under reflux for 24 hours. Acetonitrile was then removed under reduced pressure where the resulting product was then dried under high vacuum.

This yielded the title product as a white solid. (8.632 g, 0.018 mol, 75%)

^{1}H NMR (400 MHz, D_2O, ppm): δ 8.85 (m, 4 H), 8.56 (tt, *J* = 1.25, 6.05, 8.27, 2 H), 8.08 (t, *J* = 7.12, 4 H), 4.62 (t, *J* = 7.12, 4 H), 2.02 (m, 4 H), 1.33 (m, 12 H)

^{13}C NMR (100 MHz, D_2O, ppm): δ 146.0, 144.7, 128.7, 62.5, 32.6, 31.0, 28.8, 28.5, 28.2, 25.7

HRMS (ESI): Theoretical 299.2482, Found 299.2481 $(M - 2Br^- + H)^+$

6.2.3 XP Spectra

6.2.3.1 Pre and Post wear C1s spectra from tribological testing

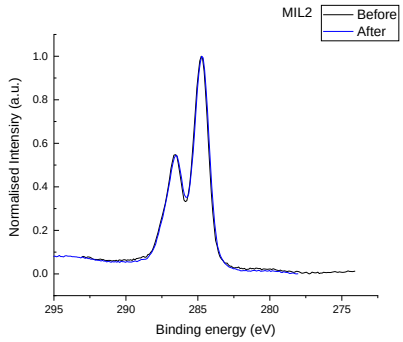

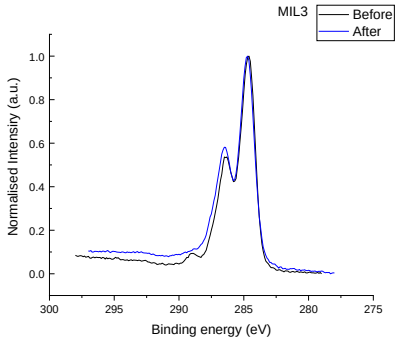

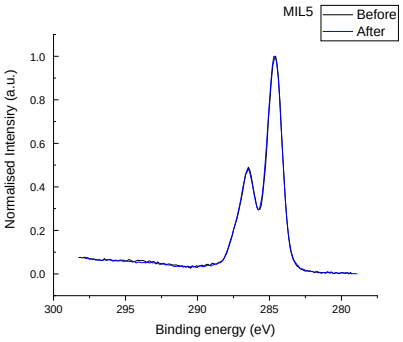

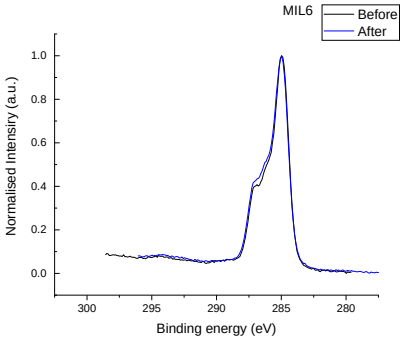

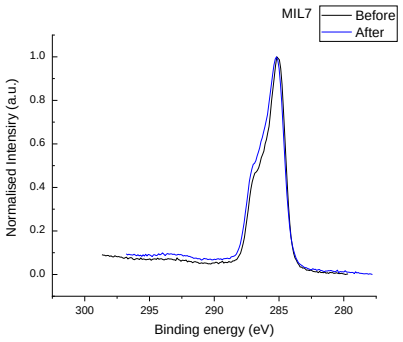

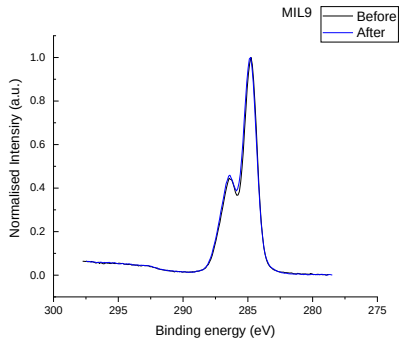

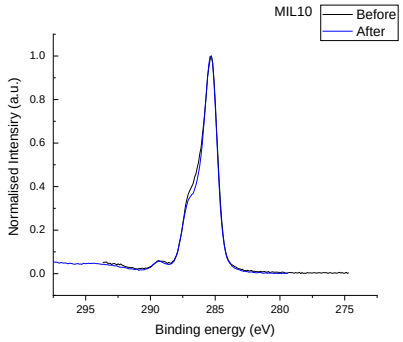

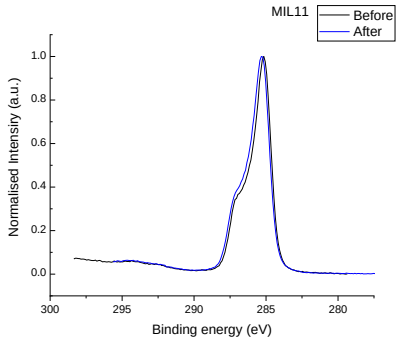

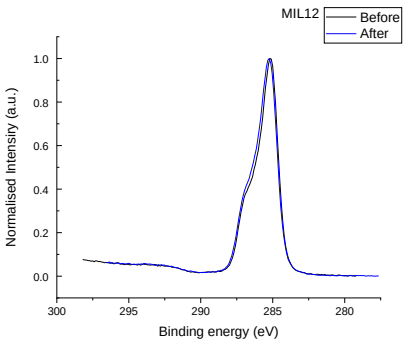

6.2.3.2 Pre and Post wear survey spectra from tribological testing

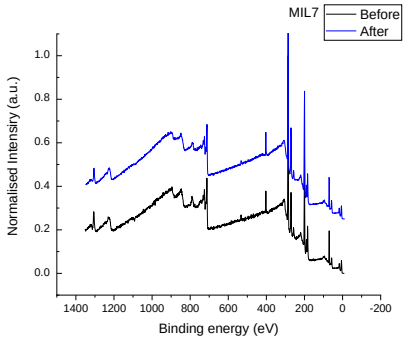

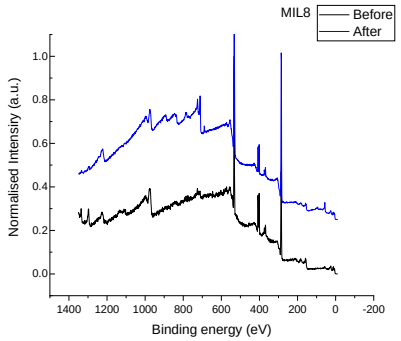

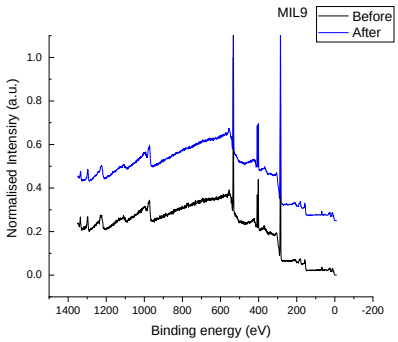

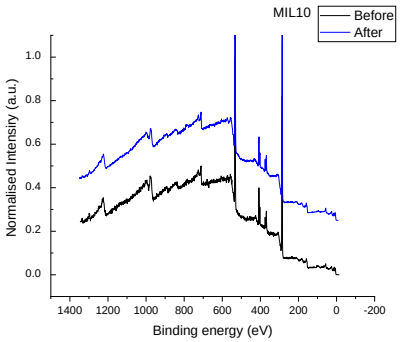

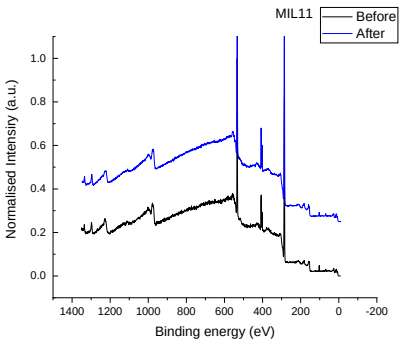

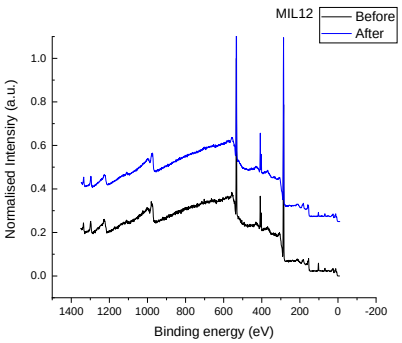

6.2.3.3 Pre and Post wear Oxygen 1s spectra from tribological testing